MID-TROPOSPHERIC FRONTOGENESIS AND POTENTIAL VORTICITY BEHAVIOR

by

LANCE F. BOSART

B.Sc., Massachusetts Institute of Technology (1964)
M.Sc., Massachusetts Institute of Technology (1966)

SUBMITTED IN PARTIAL FULFILLMENT OF THE
REQUIREMENTS FOR THE DEGREE OF DOCTOR OF PHILOSOPHY
at the
MASSACHUSETTS INSTITUTE OF TECHNOLOGY
May 1969

Signature of Author . . . . . .
Department of Meteorology, 1 May 1969

Certified by . . . . . .
Thesis Supervisor

Accepted by . . . . . .
Chairman, Departmental Committee on Graduate Students

MID-TROPOSPHERIC FRONTOGENESIS AND POTENTIAL VORTICITY BEHAVIOR

by

LANCE F. BOSART

Submitted to the Department of Meteorology on 30 April 1969 in partial fulfillment of the requirement for the degree of Doctor of Philosophy

ABSTRACT

Mid-tropospheric frontogenesis is investigated for a case study in which special three-hourly rawinsonde data are available. Isentropic analyses are generated by objective means. Detailed machine isentropic trajectories lead to the three-dimensional description of the velocity field in space and time accompanying the frontogenesis. Ertel potential vorticity calculations serve as a check on trajectories and as a means of delineating stratospheric from tropospheric air.

Miller's frontogenesis equation is applied in two and three dimensions to an intensifying mid-tropospheric baroclinic zone. Frontogenetical and frontolytical regions from the twisting, horizontal confluence, vertical shear of vertical velocity and ageostrophic contributions are delineated. Typical frontogenesis magnitudes are $2^{\circ}C\ (100\ km)^{-1}(3\ hrs)^{-1}$ and $2^{\circ}C\ (km)^{-1}(3\ hrs)^{-1}$ in two and three dimensions respectively.

Potential vorticity behavior is such to confirm previous observations of the extrusion of stratospheric air into the troposphere. Frictional rather than radiative effects are shown to be more important to the non-conservation of potential vorticity.

A synoptic sequence common to many occurrences of mid-tropospheric frontogenesis is described. Quasi-geostrophic reasoning is employed to explain the initial development of a thermally indirect circulation accompanying the early frontogenesis. Calculations suggest that the frontogenesis is playing a significant role in the downward momentum transport in mid latitudes. Mid-tropospheric frontogenesis seems to be a manifestation of the extrusion of stratospheric air into the

troposphere during which momentum, potential vorticity, ozone and radioactivity are transported downward and southward.

Thesis Supervisor: Frederick Sanders
Title: Professor of Meteorology

ACKNOWLEDGEMENT

The author is especially grateful to his advisor, Professor Frederick Sanders for his suggestions and encouragement throughout the course of this study. Thanks are also extended to Dr. Edwin F. Danielsen and Dr. Rainer Bleck of the National Center for Atmospheric Research for many stimulating discussions. Dr. Bleck in particular is cited for having made available machine routines for calculating isentropic trajectories. Fellow doctoral student Mr. John M. Brown is thanked for various contributions during the course of the study and for critically reading the final manuscript. Dr. John W. Kidson of the New Zealand Meteorological Service is cited for valuable programming assistance and fruitful discussions while he was a doctoral student at M.I.T. Professor Amos Eddy, now of the University of Oklahoma, is acknowledged for supplying the original objective analysis program. NCAR is further cited for having made available computer time necessary to complete this study. The author is indebted to the Marshall Space Flight Center for supplying the rawinsonde data in relation to the National Science Foundation Grant GP-1508. The aid of Mr. Orvel E. Smith in this connection is recognized.

Additionally, thanks are due to Miss Anna K. Corrigan and Mr. Edward Nelson for plotting chores, to Mr. Robert Crosby for programming assistance, to Miss Isabel Kole for drawing the figures and to Mrs. Jane McNabb for her patience in typing the manuscript.

Finally, the author's fiancee Miss Helen J. Haskell has his heartfelt gratitude for moral support during the completion of this study.

TABLE OF CONTENTS

LIST OF SYMBOLS

x, y, z	cartesian coordinates
x, y, θ	isentropic coordinates
x, y, p	pressure coordinates
s, n	natural coordinates
$\overline{(\ )}$	spacial mean value
$(\ )'$	departure from mean value
$\widetilde{(\ )}$	density weighted average
$(\ )_{\theta,p}$	quantity measured in x,y,θ or x,y,p space
$\underline{(\ )}$	vector quantity
$\hat{n}$	unit normal vector
t	time
u, v	horizontal velocity components
u_g, v_g	horizontal geostrophic velocity components
V	total wind speed, $\sqrt{u^2 + v^2}$
∇	three-dimensional gradient operator
∇_H	horizontal gradient operator

w vertical velocity in x,y,z space

ω vertical velocity in x,y,p space, $\equiv dp/dt$

B geographic wind direction

T temperature

R gas constant

c_p specific heat at constant pressure

κ $\equiv R/Cp$

g gravity

ρ density

α specific volume

Ψ Montgomery potential

f Coriolis parameter

ζ relative vorticity

η absolute vorticity vector

$\frac{\partial \theta}{\partial p}$ vertical stability measured over one kilometer

$P \equiv -g \frac{\partial \theta}{\partial p}(\zeta_\theta + f)$, Ertel potential vorticity

$\underline{F}$ vector sum of friction forces

$F \equiv \hat{n} \cdot \frac{d}{dx}\left(\nabla\Theta\right)$, frontogenesis function

l Prandtl mixing length

t_0, t_1 initial and final time of a trajectory

$\underline{s}_0, \underline{s}_1$ initial and final position of a trajectory

$\underline{v}_0, \underline{v}_1$ wind velocity at initial and final position of a trajectory

I. INTRODUCTION

1a. Statement of Problem and Goals

The purpose of this dissertation is to make use of an extraordinary data sample to complement and clarify earlier work with regard to the formation of intense baroclinic zones in the middle troposphere. Special three hourly rawinsonde data was available when a prominent example of the above phenomenon occurred. Initially the main problem was to process the data and develop an isentropic objective analysis routine. The basic goal is to derive and explain the three-dimensional velocity field in space and time during the intensification of the mid-tropospheric baroclinic zone. The primary tool to implement the goal is machine-calculated isentropic trajectories. Application is made to potential vorticity behavior and a form of Miller's (1948) frontogenesis equation to aid in the interpretations.

1b. Historical Background

Surface fronts were first postulated by the Bjerknes (1919) school to distinguish boundaries of air masses with different characteristics. Since then they have brought both joy and disillusionment to synoptic meteorologists searching for an infallible tool to forecast the weather. Yet, despite evidence to the contrary some meteorologists still insist that observed weather changes can be explained by frontal movements. Even today, one often observes fronts moved

about on surface maps like opposing armies in all the war games played in the various world capitals.

With the advent of good upper-air coverage baroclinic zones have been found in the middle and upper troposphere. For better or worse we are stuck with the name "front". However, what one means here are baroclinic zones of varying intensity. These zones are characterized by large vertical shears of the horizontal wind through an often deep stable layer. There is often a marked decrease in water vapor mixing ratio just below the base of the stable layer. The air in the zone is very dry and usually rich in ozone and radioactivity. In addition, potential vorticity values characteristic of stratospheric air are found in the zone.

It must be emphasized that these high tropospheric baroclinic zones are not rare occurrences. They are often found on the western sides of pronounced troughs and initially are located near the tropopause. As the zone moves to the south and southeast side of the trough it attains its greatest intensity between 500 mb and 600 mb. Air parcels themselves are streaming through the zone and are continually subjected to frontogenetical and frontolytical processes.

The concept of a tropopause is related to the above discussions. The tropopause, on the basis of scanty observations in the 1920's, was viewed as a thermal boundary or discontinuity. With the onset of the sounding era in the 1930's a major objective of the analysts was the location of the tropopause using preconceived ideas about the existence of discontinuity surfaces. Bjerknes (1932) postulated a continuous tropopause which extended from pole to equator. The

polar front was allowed to merge with the tropopause at high latitudes. Palmen (1933) proposed a multiple tropopause which was always in a state of continual flux. Its location was a function of the synoptic scale eddies. Unlike the continuous tropopause model this scheme allowes for mass transfer between the troposphere and stratosphere. Bjerknes and Palmen (1937) invoked a folded tropopause argument whereby the maximum gradient of potential temperature along the tropopause would be found in the vicinity of the fold. However, the boundaries of the polar frontal zone were not allowed to be contiguous with the fold.

1c. Recent Work

A renewed interest in mid-tropospheric baroclinic zones and fronts in general commenced in the late 1940's. Miller (1948) broadened the concept of frontogenesis to include sloping stable layers in the mid troposphere and emphasized the importance of considering frontogenesis as a three-dimensional process.

Sanders (1953) and Reed and Sanders (1953) observed the importance of the horizontal variation of vertical velocity across the flow leading to a thermally indirect circulation from case studies of intense frontogenesis at 500 mb. Newton (1954) made similar observations while also noting the significant contribution of the ageostrophic motions. Reed (1955) renewed the folded tropopause concept to account for the presence of very high potential vorticity air in a mid-tropospheric baroclinic zone. A stratospheric origin for this high potential vorticity air was noted. Additional support

for this reasoning came from Danielsen (1959) and Reed and Danielsen (1959). In addition, Danielsen (1959) in a detailed study of original rawinsonde traces showed the presence of many stable laminae which tended to persist in space and time. Isentropic trajectories established a stratospheric origin for many of these stable laminae, Danielsen (1961).

More recent work has tended to concentrate on putting quantitative estimates on the degree of stratospheric-tropospheric exchange in terms of potential vorticity, maxing ratio of water vapor, ozone and radioactivity changes. Staley (1960), from case studies, noted large negative individual potential vorticity changes within the baroclinic zone which he attributed to the vertical gradient of diabatic heating. Later work of Staley and Kuhn (1961), Staley (1965) and Staley and Jurica (1968) attenpted to show the importance of radiational cooling in the interpretation of individual potential vorticity changes. In this connection, Campana (1967) argued that diabatic effects were necessary to explain calculated potential vorticity increases in his case study.

Danielsen (1964) with the aid of potential vorticity and radioactivity measurements further investigated tropopause folding. He showed that these processes were consistent with the conservation of potential vorticity and that the air in the baroclinic zone of his case study was of stratospheric origin. Danielsen (1966a) and (1966b) reported on detailed trajectory calculations to resolve the three-dimensional structure of an intense cyclone and an associated stratospheric extrusion. Machine methods pioneered by Bleck (1968) were

utilized in the study. Danielsen and Diercks (1967) performed a numerical integration of the potential vorticity equation for a multilevel isentropic model. Given initial conditions favorable for tropopause folding by quasi-horizontal motions he was able to initiate folding west of the trough axis after twenty-four hours.

Paine (1966) in a case study attributed large negative individual potential vorticity changes along the lower boundary of a stratospheric extrusion to mixing produced by cumulonimbus clouds penetrating the stable layer from below. Like Kousky (1967), Paine found that potential vorticity changes due to radiational effects were small. Adler (1967) developed an equation representative of a mean potential vorticity more in keeping with what is measured on synoptic charts. Mean potential vorticity changes could then be interpreted in the light of diabatic effects, eddy mixing of potential temperature and eddy mixing of momentum. The latter two effects were found to be dominant for a particular case study. Danielsen (1967,1968) investigated stratospheric-tropospheric exchange based on radioactivity, ozone and potential vorticity. Positive correlations between potential vorticity, ozone and stratospheric radioactivity were noted. A model incorporating stratospheric mass inflow during tropopause folding and tropospheric air entering the stratosphere at low latitudes satisfying the above criteria was proposed. Subsynoptic scale mixing rather than diabatic effects were shown to be important to interpreting mean potential vorticity changes.

II. THEORETICAL BACKGROUND

2a. Adiabatic Assumption

In this study we will find it useful to work in isentropic coordinates in order to construct adiabatic trajectories. We will assume that the first law of thermodynamics for adiabatic flow may be written as:

$$\frac{d\theta}{dt} = 0 \qquad (2.1)$$

This states that potential temperature is conserved if one follows an air parcel. Fortunately, mid-tropospheric frontogenesis is generally associated with subsidence and relatively cloud free regions. Diabatic effects stemming from the release of latent heat and friction in the planetary boundary layer do not arise.

2b. Montgomery Potential

In isentropic coordinates the Montgomery potnetial, ψ, can be defined as:

$$\Psi = c_p T_\theta + g z_\theta \qquad (2.2)$$

Determination of the gradient of ψ on an isentropic surface enables one to calculate the geostrophic wind on that surface. Meteorologists have long scorned the Montgomery potential because rudimentary isentropic analysis in the 1930's showed that T_θ had to be measured to within $\pm$ 0.1°C in order to obtain a reliable estimate of the

geostrophic wind. Danielsen (1959) pointed out the flaw in this argument by noting that if Poisson's equation is used to relate T_θ to p_θ the latter leads directly to Z_θ. In this manner the error in the computed ψ up to the middle troposphere will be no worse than the error of the computed height of a constant pressure surface.

2c. Trajectory Concepts

Isentropic trajectories will be useful for describing the three-dimensional velocity field in space and time as well as in the interpretation of individual potential vorticity changes and frontogenesis calculations. Initially, in constructing trajectories the best one can do is to make use of the approximate kinematic relation:

$$D = \frac{V_1 + V_2}{2} \Delta t \qquad (2.3)$$

Here D is the total distance traversed by the parcel, V_1 is an average geostrophic velocity for the first half time period, V_2 an average geostrophic velocity for the second half time period and Δt the total time period.

The crudity of (2.3) led Danielsen (1961) to develop an equation which accounts for the change in kinetic energy of the parcel by giving it a deviation from its geostrophic path. Physically this change in velocity, and hence in kinetic energy, is a result of the horizontal pressure-gradient force acting on a parcel which has a non-geostrophic path. Danielsen's (1961) expression, which ignores diabatic effects, is:

$$\psi_f - \psi_i + \frac{V_f^2}{2} - \frac{V_i^2}{2} = \int_f^i \frac{\partial \psi}{\partial t}\, dt \qquad (2.4)$$

where $(\quad)_f$ is at the final time, and $(\quad)_i$ is at the initial time. The integral on the right can be approximated by the time difference between rawin observations in ψ at the initial, middle and final points of the trajectory.

Alternately, the observed winds themselves can be used to construct trajectories in an analogous manner to (2.3). The accuracy of this latter method increases measureably as the time between observations decreases. Bleck (1968) has developed machine methods of constructing dry and moist adiabatic trajectories based on (2.4) as well as for the case of just using the observed winds.

2d. Potential Vorticity

For frictionless, adiabatic motion following the parcel Ertel (1942) showed that

$$\frac{d}{dt}\left\{ \frac{\underline{\eta} \cdot \nabla \theta}{\rho} \right\} = 0 \qquad (2.5)$$

where the quantity in brackets is called potential vorticity and is conserved following the motion. For the case where the motion is neither frictionless nor adiabatic (2.5) [see e.g. Sanders (1967)] becomes:

$$\frac{d}{dt}\left[\frac{\underline{\eta} \cdot \nabla \theta}{\rho}\right] = \frac{1}{\rho}\left[\underline{\eta} \cdot \nabla\right]\frac{d\theta}{dt} + \frac{1}{\rho}\nabla\theta \cdot \nabla \times \underline{F} \qquad (2.6)$$

This expression tells us that potential vorticity is conserved following the motion of the parcel unless the gradient of diabatic heating has a component in the direction of the absolute vorticity vector or the curl of the friction force has a component normal to the isentropic surface. The usefulness of potential vorticity lies in an order of magnitude or more difference between values representative of the stratosphere and those representative of the troposphere. The conservative nature of the potential vorticity means that it can be used as a check on the accuracy of trajectories and more importantly as a means of delineating regions of stratospheric air from tropospheric air. For a broad discussion on the role of potential vorticity in the atmosphere see Danielsen (1968).

2e. Frontogenesis

Frontogenesis, after Miller (1948), can be defined by

$$F \equiv \hat{n} \cdot \frac{d}{dt}(\nabla\theta) = \frac{d}{dt}\left|\nabla\theta\right| \qquad (2.7)$$

If we are only considering the individual rate of change of $|\nabla_H\theta|$ we have (2.7) in component form:

$$F = \left|\nabla_H\theta\right|^{-1} \frac{\partial\theta}{\partial x}\left(\frac{\partial\theta}{\partial t}\frac{\partial x}{\partial x} - \frac{\partial x}{\partial\pi}\frac{\partial\theta}{\partial x}\frac{\partial x}{\partial t} - \frac{\partial y}{\partial\pi}\frac{\partial\theta}{\partial y}\frac{\partial x}{\partial t} - \frac{\partial z}{\partial\pi}\frac{\partial\theta}{\partial z}\frac{\partial x}{\partial t}\right)$$

$$+ \left|\nabla_H\theta\right|^{-1} \frac{\partial\theta}{\partial y}\left(\frac{\partial\theta}{\partial t}\frac{\partial y}{\partial x} - \frac{\partial x}{\partial\pi}\frac{\partial\theta}{\partial x}\frac{\partial y}{\partial t} - \frac{\partial y}{\partial\pi}\frac{\partial\theta}{\partial y}\frac{\partial y}{\partial t} - \frac{\partial z}{\partial\pi}\frac{\partial\theta}{\partial z}\frac{\partial y}{\partial t}\right) \qquad (2.8)$$

The first term on the right-hand side of (2.8) for the x-component for example, is the diabatic term. It arises from the variation of diabatic heating in the horizontal. The second and third terms are the contribution from horizontal confluence. These terms express the rate of frontogenesis or frontolysis due to the effects of the horizontal wind in concentrating or spreading the potential isentropes. The last term is the twisting effect and expresses the rate of frontogenesis or frontolysis due to the variation of adiabatic heating or cooling in the horizontal resulting in a tilt of the isentropic surfaces. In general, many meteorologists have regarded frontogenesis in this manner. Frontogenesis, defined by the individual rate of change of $|\nabla\theta|$ in three dimensions results in the following additional component to (2.8):

$$+|\nabla\theta|^{-1}\frac{\partial\theta}{\partial z}\left(\frac{\partial v}{\partial z}\frac{\partial\theta}{\partial y}-\frac{\partial w}{\partial y}\frac{\partial\theta}{\partial z}-\frac{\partial u}{\partial z}\frac{\partial\theta}{\partial x}+\frac{\partial w}{\partial x}\frac{\partial\theta}{\partial z}\right) \qquad (2.9)$$

The interpretation of the individual terms is similar to before. However, the second and third terms arise solely because of the ageostrophic motions. Substituting the thermal wind for geostrophic flow and the definition of potential temperature into these terms results in their sum being identically zero.

Another way to visualize frontogenesis is to consider

$$\frac{d}{dt}(\nabla\theta)=\frac{d}{dt}\left\{\nabla_H\theta+\frac{\partial\theta}{\partial p}\frac{\partial v}{\partial x}\hat{i}\right\} \qquad (2.10)$$

Noting the following identity

$$\left.\frac{\partial \theta}{\partial x}\right|_z = \left.\frac{\partial \theta}{\partial x}\right|_p + \frac{\partial \theta}{\partial p}\frac{\partial p}{\partial x} \tag{2.11}$$

we have

$$\frac{\partial}{\partial t}(\nabla\theta) = \frac{\partial}{\partial t}\left\{\nabla_p\theta + \frac{\partial \theta}{\partial p}\nabla p\right\} \tag{2.12}$$

or

$$\frac{\partial}{\partial t}(\nabla\theta) = \frac{\partial}{\partial t}\left\{-\frac{\partial \theta}{\partial p}\left(\nabla_\theta p - \nabla p\right)\right\} \tag{2.13}$$

But, within a mid-tropospheric baroclinic zone

$$\frac{\left.\frac{\partial x}{\partial t}\right|_z}{\left.\frac{\partial x}{\partial t}\right|_\theta} \approx 10^{-2} \tag{2.14}$$

Hence, to excellent approximation (2.13) becomes

$$\frac{\partial}{\partial t}\left\{-\frac{\partial \theta}{\partial p}\nabla_\theta p + \frac{\partial \theta}{\partial z}\hat{k}\right\} \approx \frac{\partial}{\partial t}(\nabla\theta) \tag{2.15}$$

or

$$-\frac{\partial \theta}{\partial p}\frac{\partial}{\partial t}(\nabla_\theta p) - \nabla_\theta p\,\frac{\partial}{\partial t}\left(\frac{\partial \theta}{\partial p}\right) - g\,\frac{\partial}{\partial t}\left(\rho\frac{\partial \theta}{\partial p}\right) \approx \frac{\partial}{\partial t}(\nabla\theta) \tag{2.16}$$

Thus, frontogenesis is likely in stable regions where the individual rate of change of the slope of the isentropes with respect to an isobaric surface is large and vice versa.

III. SYNOPTIC SITUATION: 19-20 FEBRUARY 1964

An initial investigation by Sanders (1967) established twenty-six cases of possible mid-tropospheric frontogenesis during the 1963-1964 winter season over the continental United States. These cases were gleaned from the regular 0000 GMT and 1200 GMT NMC facsimile 500-mb analyses. In order to qualify for inclusion among the sample a case had to meet the criterion of a $\nabla T \geq 16°C\ (5°\ lat)^{-1}$ at 500 mb. The case of 19-20 February 1964 had a maximum horizontal ∇T of $22°C(5°lat)^{-1}$.

At 1200 GMT on 18 February a weak 500-mb trough was located over the central United States while a small surface wave was appearing on the Florida Gulf coast. Cold air was beginning to stream out of Canada into the Northern Plains. At the same time cold advection through the 500-mb trough implied a rapid deepening. In the ensuing twenty-four hours the surface storm center deepened from 1000 mb to 984 mb and is located off the southeast New Jersey coast (fig. 3.1). At 500 mb on 1200 GMT 19 February two separate vorticity maxima are discernible (fig. 3.2). The downstream maximum is associated with the New Jersey surface storm and its related clouds and precipitation. A moderate baroclinic zone is embedded in the upstream vorticity maximum. Little, if any, surface weather is associated with this system except for some light cold core instability showers north of the jet.

By 0000 GMT on 20 February the baroclinic zone has increased

in intensity and moved eastward (fig. 3.4). Meanwhile, little change in intensity of the downstream surface storm is observed (fig. 3.3). The intensification aloft was accompanied by very little change in surface weather. Some light instability precipitation persisted in the cold core of the 500-mb vortex north of the jet. The air within and beneath the baroclinic zone was quite dry and relatively cloud free except for some low level stratocumulus clouds formed by daytime heating in an unstable air mass. The major point to note for now is the absence of any surface frontal structure beneath the intensifying baroclinic zone aloft.

IV. DATA REDUCTION

4a. Nature of Data

Rawinsonde data taken every three hours beginning 0000 GMT on the 19th of February and concluding with 0000 GMT on the 22nd of February was made available to me under National Science Foundation Grant GP-1508. The data project was directed by Mr. Orvel Smith of the George C. Marshall Space Flight Center, Huntsville, Alabama, under the auspicies of NASA. A total of thirty stations located in the southeastern United States participated in the project. Twenty three of these stations were Weather Bureau, two were Navy (Corpus Christi and Key West) and three were Air Force (Cape Kennedy, Grand Bahama and Eglin). In addition, two NASA stations (Marshall Space Flight Center and Mississippi Test Operations) cooperated in the venture.

The data is the best by far available for a case study of mid-tropospheric frontogenesis. Temperature, relative humidity and winds were evaluated for each pressure contact. The azimuth and elevation angle measurements were taken at the rate of ten times per minute. This basic data was transferred to IBM cards and a Herculean data reduction, processing and error checking program embarked upon. Most of the grisly details can be found in a report by Stuart, Watson and LaSeur (1967).

All of the pertinent data was stored on seven magnetic tapes. Unfortunately, each of the tapes contained machine errors from the

initial processing and this coupled with the inherent difficulty of trying to read "foreign" tapes on an IBM 360 made it extremely difficult to process the data.

4b. Vertical Smoothing of Observed Winds

Once the data was read the major problem became the elimination of spurious, and often large, oscillations in the u and v components of the observed winds. These oscillations were the result of critically small elevation angles for the balloons being approached above 500 mb. Strong and nearly uniform direction tropospheric westerlies were responsible for the relatively low altitude onset of the critically small elevation angles. An example of one of the worst cases of the above problem is shown in fig. 4.1. The solid line is the unsmoothed total velocity profile at Jacksonville for 2330 GMT on the 19th of February. Especially noticeable is the strong vertical wind shear through the baroclinic zone between 650 and 500 mb. The high frequency noise reaches unmanageable proportions near the jet level. A filter was needed which would eliminate as much of the spurious high frequencies as possible while retaining the genuine vertical wind shear associated with the baroclinic zone. Several filters with promising response characteristics for the elimination of high frequency oscillations were tested empirically. The filter that consistently minimized most of the errors is shown in fig. 4.2. The 31 points smooth over nearly ten minutes of the vertical sounding. Wave numbers $\geq$ 10 pressure contacts are passed essentially unchanged. Some geniune mesoscale oscillations will be

eliminated but this is consistent with synoptic scale potential vorticity measurements. The smoothed Jacksonville profile given by the dotted line in fig. 4.1 is derived from application of the filter depicted in fig. 4.2.

The filter was applied from the surface to the bursting altitude of the balloon. However, filtering was terminated when the balloon reached and remained below the critical 6° elevation angle. On the rare occasions when there were gaps in the vertical data profile a linear variation was assumed if the gap was less than one kilometer. For gaps greater than one kilometer but less than two kilometers a linear profile was assumed if the magnitude of the vertical wind shear was less than an arbitrary criterion of 10 m sec^{-1} per kilometer. Otherwise, the winds were terminated at the last reported level. The trend of the raw data at the end points was extrapolated through dummy points in a minor image manner as given by an example in fig. 4.3. Hence, the filter always operated on the same number of contact points.

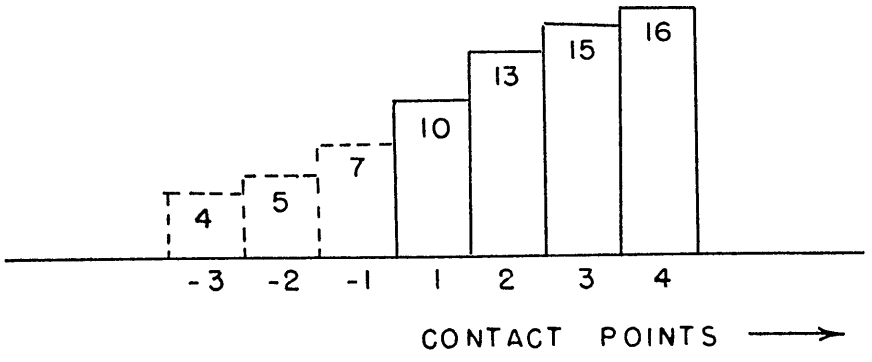

FIG. 4.3

It was recognized that the winds above 400 mb still contained too much noise in the extreme cases. Even heavier filters would be required to surpress these oscillations. Ideally, the filter should be a function of the elevation angle. This was not done in this case because the area of interest was well below the level where spurious oscillations still remained. Note that the Northern Hemisphere Data Tabluations (NHDT) winds for Jacksonville terminated just above 500 mb at 00 Z on 20 February.

The problems of wind errors in general have been discussed by deJong (1958), Danielsen (1959), Danielsen and Duquet (1967) and more specifically for the data in this case by Stuart, Watson and LaSeur (1967). With observations 10 times per minute and elevation angles $> 10°$ GMD-1 winds, with few exceptions, were accurate to $\pm$ 1° and $\pm$ 1 m sec^{-1} according to Danielsen and Duquet (1967). However, for elevation angles between 6° and 10° interference from ground reflected signals impairs these angle measurements. Danielsen and Duquet (1967) have shown that with the choice of appropriate filters mean wind profiles can be recovered for very low elevation angle cases which are comparable to those obtained by solving the balance equation from synoptic analyses of the geopotential fields. Simultaneous comparison of detailed temperature and wind profiles reveals much less variability in the former than in the latter. The variability in the wind profiles does not satisfy the thermal wind equation for the most part.

Some possibility exists that vertically propagating gravity waves of the type described by Danielsen and Duquet (1967) and Newell et al (1966) are present but they would be completely swamped by the

previously noted errors. Application of the previously described filter will minimize potential vorticity errors as in synoptic studies this quantity is primarily representative of mean conditions. Note that any basic ageostrophic component which extends over a finite depth will be retained after filtering.

V. MACHINE METHODS

5a. Generation of Isentropic Parameters

Pertinent meteorological parameters were calculated for each sounding at intervals of 2°C for virtual potential temperatures between 285° and 325°K. Outside of this range the quantities were calculated at isentropic levels separated by 5°C. For every station at the appropriate θ levels a modified version of a program described by Duquet (1964) computed the pressure in mb, the temperature and virtual temperature in °C, the relative humidity with respect to water and ice in percent, water vapor mixing ratio in g kg^{-1}, height in meters, u and v wind components in knots, wind direction in degrees, wind speed in knots, Montgomery potential in $cm^2\ sec^{-2} \times 10^5$, total energy in $cm^2\ sec^{-2} \times 10^5$, stability over a one-kilometer vertical distance in °C mb^{-1}, shear direction over one kilometer in degrees and shear magnitude over one kilometer in mb $(°lat)^{-1}$. The calculated parameters are self explanatory. The total energy is defined to be the left-hand side of (2.4). The wind shear vectors are useful in determining the pressure topography of the isentropic surface. In general the difference between the shear direction and geostrophic wind direction is less than 20° as Danielsen (1959) notes.

5b. Objective Analysis Techniques

Because of the large number of isentropic analyses that would have to be generated by hand it was decided to see if an objective

analysis procedure would be feasible. The author was fortunate to have spent some time with Dr. Amos Eddy who has recently developed a statistical objective analysis model for use with scalar data fields such that the weight curves are determined by the data themselves. See Eddy (1967a,b). Briefly, the way the scheme works is as follows. First, any latitudinal trend that exists is removed from the data. Second, a raw autocorrelation curve is determined from what is left. Third, a power density spectrum is determined from the raw autocorrelation curve and this spectrum is hanned. This amounts to a filtering to minimize truncation effects. Fourth, the power density spectrum is then integrated from the very long waves toward the shorter waves. The integration is halted if a specified percent of the variance has been obtained (98%) or the white noise level is reached. The rest of the spectrum is truncated and retransformed to give a smoothed autocorrelation curve. Fifth, a regression analysis based on the screening procedure is used to calculate an analyzed value and the fraction of the remaining variance at each grid point. To get the final analyzed value the previously removed trend value at each grid point is added back in and the results machine contoured. In the Eddy scheme the data determine their own statistics and hence autocorrelation curves whereas in Cressman (1959) type schemes the latter are artificially imposed. Also, the nature of the regression screening procedure enables the Eddy method to dub in highs and lows between grid points. Disadvantages, not confined to the Eddy approach alone, are the essentially two-dimensional approach and the assumptions of isotropy and homogeneity.

The scheme eventually used in this thesis differed from the original Eddy version in a number of ways. First, computer economy dictated working in grid coordinates rather than a latitude-longitude frame. This eliminated numerous trigonometric computations in the determination of separation distances for all pairs of stations making up the raw autocorrelation curve. The initial programming insight for this method came from Kidson (1968). The other major change involved the removal of the trend. Very large amplitude flow patterns existed at 500 mb on the 19 and 20 February. This suggested the removal of a two-dimensional, rather than a latitudinal trend. A simple Cressman (1959) analysis with a very large influence radius was used to generate a very smooth horizontal analysis in which the broad scale features were retained. To obtain the trend value at a given station a simple linear interpolation method was used based on the surrounding four grid points. If a station was located just outside the grid the trend value at the nearest grid point was assigned to that station.

5c. Pilot Objective Study

The initial study was confined to the analysis of Montgomery potential, pressure, % relative humidity, stability and the horizontal wind components on isentropic levels from 295°K to 315°K at 4°C intervals. Analyses were generated for the synoptic times of 00Z and 12Z on the 19 and 20 February. A 21 by 21 section of the NMC grid centered over the Northern Hemisphere was used (fig. 5.1).

All available data in blocs 70 through 80 in addition to ship radiosondes were used. Great care was taken in plotting to remove scattered errors from NHDT and teletype data sources. The availability of several different teletype circuits on microfilm allowed the significant levels to be included for those stations which only reported mandatory levels in the NHDT. The care taken in data pruning was reflected in the failure of any stations to be rejected on between group and within group variance limits of 3.5 standard deviations. The influence radius used in the simple Cressman analysis to remove the two-dimensional trend was five grid units or about 1200 nautical miles.

The smoothed autocorrelation curves generated from the pilot study were of interest. Encouragingly the statistics of a given quantity were relatively constant over the four time intervals. This fact will be used later to help justify using an average smoothed autocorrelation curve for a given scalar quantity to cut down on machine time. Table 1 below gives the range of zero lag smoothed autocorrelation values and the distance for the correlation to fall off to zero for appropriate parameters on isentropic surfaces ranging from $\theta = 295$ to $\theta = 315$ between approximately 900 mb and 300 mb overall. The table values were obtained for 180 stations in blocs 70-80. Zero lag variations in time were small but zero lag variations tended to decrease with increasing elevation reflecting the slow accumulation of errors. This was especially true of the relative humidity and was a reflection of motor-boating values with the assignment of estimated theoretical maximum values.

Table I

	ψ	Pres	% RH	$\partial\theta/\partial p$	u	v
Range of zero lag variations with increasing elevation	.97-.88	.95-.75	.75-.25	.90-.65	.90-.55	.90-.55
Distance in nautical miles to zero correlation	1000	1000	500	625	700	700

Figs. 5.2 through 5.5 show the objective analysis of ψ on $\theta = 303$ for the indicated times. The contour plotting on a polar stereographic background was done at NCAR using machine routines developed by Bleck (1968). Two dimensional smoothing using weights of 0.25, 0.50 and 0.25 was applied to cut down on wiggles near the southern boundary and in data poor regions. Clearly indicated is the large amplitude flow pattern and the double vorticity maximum trough over the southeastern United States that was noted earlier.

Recall from the definition of potential temperature that an isobar on an isentropic surface is also an isotherm on an isobaric surface. Hence, from the pressure field on all the isentropic surfaces we can recover the temperature field for any pressure surface merely by collecting on a single map the isobars from each of the isentropic surfaces which intersect this isobaric surface. This is done for the 500 mb surface between 00Z, 19 February and 12Z, 20 February in figs. 5.6 through 5.9. Immediately evident is the baroclinic zone over the lower Mississippi valley at 12Z, 19 February and its marked

intensification by 00Z, 20 February. The non intersection and packing of the isotherms derived entirely from this objective analysis procedure provided the green light for its use in a more detailed study using the three hourly data from 12Z, 19 February through 00Z, 20 February in the southeastern United States. The horizontal gradients derived from the objective analysis across the baroclinic zone and in the strong shear regions near the jet are only very slightly weaker than similar subjective analyses.

5d. Detailed Limited Area Objective Analysis

Reduction of the mesh length by a factor of three was carried out for the detailed analysis. Two grid intervals in the finer mesh (approximately 200 km) corresponds to the horizontal width of the baroclinic zone defined in the pilot study. The basic grid area is 28 by 31 on a polar stereographic projection as can be seen from fig. 5.10. The dark circles represent stations for which three hourly rawindonde data exist while the open circles indicate regularly reporting rawinsonde stations. I, J refer to grid coordinate directions and the numbers will be used later for cross-section references.

The essentially quasi-stationary nature of the statistics in table I suggested the use of averaged smooth autocorrelations based upon them for the detailed mesh calculations. However, judicious elimination of some of the less reliable Caribbean and Canadian stations along with a couple of United States Navy stations resulted in an improvement of the zero lag correlations. See, for example, History and Catalogue of Upper Air Data for the Period 1946-1960 (1963).

Additional improvement in the u,v statistics resulted when the highly filtered winds were used for the 30 stations in the southeastern United States. Fig. 5.11 shows the smoothed autocorrelation curves that are used in this detailed study. They are representative of the $\theta = 303$ surface which lies in the middle of the baroclinic zone and from our earlier discussion of table I are a slight overestimate in the lower regions of the zone and a slight underestimate in upper regions of the zone. The slight overestimate in zero lag values for u and v ensures good correspondence between objectively and subjectively analyzed jet stream maximums.

ψ, pressure, $\partial\theta/\partial p$, u and v are analyzed on the $\theta = 287$ through $\theta = 323$ surfaces at intervals of 4°C from 06Z, 19 February through 06Z, 20 February over the area indicated in fig. 5.10. These levels bracket the baroclinic zone which encompasses the $\theta = 291$ through $\theta = 315$ surfaces over that time period. The analysis procedure is as follows. Maps are generated on the relevant theta levels at the standard synoptic times as before. The trend for the off time analyses is obtained as a weighted linear combination of the standard time analyses. For example, the trend on a given theta level at 15Z is derived as a sum of the 12Z and 00Z final analyses weighted by 75% and 25% respectively. A procedure identical to before generates a final map which differs from the trend in regions under the influence of 15Z data. The same format is followed for 18Z and 21Z.

The presence of some high frequency noise in the form of small-scale wiggles made it necessary to apply a two-dimensional filter to the final analysis. The wiggles were probably induced by the finer

mesh size. Empirical testing established that the 25 point filter illustrated in fig. 5.12 was the most successful at eliminating the short wave noise while retaining the shape and the magnitude of the larger scale features. The ordinate and abscissa are given in inverse grid distances. The corresponding weights are given at the bottom of the figure. The source of the filter is Bleck (1965).

5e. Machine Trajectory Techniques

In this thesis trajectories are calculated both by the kinematical and energy balance methods described earlier. The resulting frontogenesis and potential vorticity changes following the parcel are calculated from both types of trajectories. Position differences between the two methods are at worst one grid interval for paths extending over 15-20 grid intervals. This is comparable with the maximum uncertainty of an individual trajectory path as will be discussed later. Further discussion will be based primarily on trajectories calculated by the kinematical method. The decision is aided by the suspected importance of the ageostrophic components coupled with the knowledge that the observed winds have been filtered both horizontally and vertically.

The energy balance machine method is well described by Bleck (1968). Some further elaboration on the kinematic method is in order. The trajectory defined by the path $\underline{r}(t)$ is related to the velocity field by

$$\frac{d\underline{r}(t)}{dt} = \underline{v}(\underline{r}, t) \qquad (5.1)$$

If the velocity field is known over a time interval (t_o, t) then trajectories can be constructed by integrating (5.1):

$$\underline{r}(t) = \underline{r}(t_o) + \int_{t_o}^{t} \underline{v}(\underline{r}(t'), t')\, dt' \qquad (5.2)$$

Numerical evaluation of (5.2) is unappealing with $\Delta t = 12$ hours but becomes feasible with $\Delta t = 3$ hours. The Bleck (1968) machine method as adopted for use in this case solves (5.2) by an iteration scheme which converges towards a point

$$\underline{r}_1 = \underline{r}_o + \int_{o}^{\Delta t} \underline{v}\, dt \qquad (5.3)$$

satisfying the equation

$$\left\{\underline{r}_o + \underline{v}(\underline{r}_o, t_o)\Delta t\right\} - \underline{r}_1 = \left\{\underline{r}_1 - \underline{v}(\underline{r}_1, t_1)\Delta t\right\} - \underline{r}_o \qquad (5.4)$$

The deviation between the point $\underline{r}_1$ and a straight-line forward displacement $\underline{r}_o + \underline{v}(\underline{r}_o, t_o)\,\Delta t$ equated in magnitude and direction to the deviation between the point $\underline{r}_o$ and the backward displacement $\underline{r}_1 - \underline{v}(\underline{r}_1, t_1)\,\Delta t$ yields a trajectory which satisfies (5.4). In actuality 6-hour trajectories centered at the grid points are constructed. The previously outlined procedure is applied both forward and backwards 3 hours in time from the grid point such that information in the wind field at t - 3, t and t + 3 hours is utilized. The curvature of the earth beneath the path is also included in the trajectory. This has an effect of a couple of tenths of a grid unit for paths extending over 15 to 20 grid units.

5f. Potential Vorticity Calculations

The statement of conservation of potential vorticity for frictionless, adiabatic motion expressed by (2.5) must be approximated by terms which can be calculated from synoptic maps. Taking the component of absolute vorticity in the direction of $\nabla\theta$, noting that θ changes most rapidly in the vertical and using the hydrostatic relation yields the excellent approximation

$$P = -g\frac{\partial\theta}{\partial p}\left(\zeta_\theta + f\right) \tag{5.5}$$

Actual soundings established that the average vertical depth of the baroclinic zone was nearly one kilometer. Hence $\partial\theta/\partial p$ is evaluated over a centered one kilometer interval (see Appendix II). Measuring $\partial\theta/\partial p$ over fixed θ intervals has the major disadvantage that the vertical sampling interval can vary by several orders of magnitude. Note that the above operation amounts to a vertical filtering of the temperature profile.

The absolute vorticity, $(\zeta_\theta + f)$, is measured on isentropic surfaces to insure the validity of (5.5). It is quite possible for the flow to be cyclonic on a pressure surface and anticyclonic on an isentropic surface which intersects that pressure surface. The difference between f measured in z coordinates and θ coordinates is of the order of 10^{-6} sec^{-1} and can be ignored. Unfortunately, in the meteorological literature the stability weighted absolute vorticity measured on a constant pressure surface is often called the potential vorticity. The difference between the expressions is given by

$$\zeta_\theta = \zeta_p - \nabla_p\theta \times \frac{\partial \underline{V}}{\partial\theta}\cdot\hat{k} \tag{5.6}$$

Where the isentropes slope strongly with respect to isobaric surfaces and ageostrophic motions are important the latter term can become very important. This seems to be the case during mid-tropospheric frontogenesis. For ease of computation a gravity weighted potential vorticity with units of °C $mb^{-1}sec^{-1}$ is used. In all cases ζ_θ is evaluated from

$$\zeta_\theta = \left(\frac{\partial v}{\partial x} - \frac{\partial u}{\partial y}\right)_\theta \qquad (5.7)$$

using centered differences.

5g. Frontogenesis Calculations

The frontogenesis equation expressed by (2.8) with the addition of the term given by (2.9) is perfectly general in x,y,z coordinates. In this thesis the diabatic term is initially ignored for reasons discussed earlier. This simplifies (2.8) and (2.9). The other terms are measured at the mid points of six-hour isentropic trajectories in an x,y,θ system. All terms on the right-hand side are measured instantaneously with the exception of the vertical velocity terms. At the end points of a trajectory ψ,p and θ are known and hence T_θ and Z_θ are obtainable. Thus w is a 6-hour average value centered at the mid point of a trajectory. In practice the calculated quantities are known in x,y,θ coordinates whereas to evaluate the terms in (2.8) and (2.9) deviatives in x,y,z space are required. The appropriate transformation of coordinate equations and the resulting frontogenesis equations for the two- and three-dimensional cases are given in Appendix I. Simple centered differences are used in the evaluation of all derivatives.

The calculated frontogenesis is compared with the observed frontogenesis which is the difference in the magnitude of the horizontal or three-dimensional gradient of potential temperature evaluated from the end points of six hour trajectories. Differences between observed and calculated values are due to the following reasons: (1) neglect of diabatic effects, (2) trajectory errors and (3) equating products of instantaneous values of horizontal velocity components and six hourly averaged vertical velocities with a six-hour difference in $|\nabla\theta|$ calculated from the end points of a trajectory.

VI. DISCUSSION OF FRONTOGENESIS CALCULATIONS

6a. Horizontal Description of Baroclinic Zone

Figs. 6.1 through 6.5 show the virtual potential temperature field on various pressure levels throughout the twelve-hour time period. Overall the baroclinic zone encompasses the θ = 291 through θ = 315 surfaces. Note the marked intensification of the zone between 12Z and 21Z with little change thereafter. The peak horizontal gradient of 16°C $(100\ km)^{-1}$ at 550 mb on 21Z compares favorably with stronger surface fronts and is among the most intense that the author has observed in the mid troposphere. The tendency for the θ = 311 and especially θ = 315 isotherms to "back up" during the intensification will turn out to be a reflection of the strong subsidence occurring on the warm boundary of the zone. More will be said later about the apparent downward propagation of the maximum horizontal gradient of temperature with time.

6b. Vertical Velocity Distribution Within Baroclinic Zone

Six-hour average vertical velocities centered at 12Z, 15Z, 18Z, 21Z and 00Z on θ = 295, 303 and 311 are given in fig. 6.6. The units are cm sec^{-1}. The x's mark the locations of centers of maximum ascent or descent with the appropriate magnitude next to the symbol. The θ = 295, 303 and 311 surfaces are representative of conditions in the lower, middle and upper regions of the baroclinic zone respectively. Descent is general throughout most of the zone with the strongest

subsidence occurring on the southern periphery or warm boundary of the zone, especially during the earlier time periods. A similar observation was made by Reed and Sanders (1953). The beginnings of ascent are visible at 21Z and more so at 00Z on the warm boundary of the zone. This behavior is in line with observations of Newton (1954).

6c. Frontogenesis in Two Dimensions

The evaluation of (2.8) without diabatic effects on $\theta = 303$ is portrayed in figs. 6.7-6.8. Fig. 6.7 describes the contribution from horizontal confluence and twisting while fig. 6.8 reveals the observed and calculated frontogenesis. Reference back to figs. 6.1 - 6.5 will aid in picturing the frontogenesis. The $\theta = 303$ surface falls approximately in the middle of the zone. Overall there is good agreement between the observed and calculated frontogenesis with respect to magnitude and sign. The exception is at 21Z where peak calculated values of 7°C $(100\ km)^{-1}$ $(3\ hrs)^{-1}$ are contrasted with observed values of 2°C $(100\ km)^{-1}$ $(3\ hrs)^{-1}$. Some reasons for this discrepancy can be seen from figs. 6.1 - 6.5. Between 450 mb and 550 mb the $\theta = 303$ surface lies in the middle of the maximum horizontal ∇T at 21Z with a somewhat weaker gradient at 00Z and a noticeably weaker gradient at 18Z. Trajectories whose midpoints lie in the peak horizontal ∇T region at 21Z will have a considerably larger calculated than observed frontogenesis value (recall the calculation procedure in section 5g).

Observed frontogenesis values ranged from 1°C - 3.5°C $(100\ km)^{-1}$

$(3\,\text{hrs})^{-1}$ on the $\theta = 303$ surface in the vicinity of the baroclinic zone. At 12Z and 15Z most air parcels whose midpoints lie within the zone are undergoing frontogenesis whereas by 21Z and 00Z a definite tendency exists for frontogenesis and frontolysis to occur in upstream and downstream regions of the zone respectively. Frontolytical values of the order of 2°C - 3°C $(100\text{ km})^{-1}$ $(3\text{ hrs})^{-1}$ are observed in downstream regions of the zone at 21Z and 00Z.

Quite evident from fig. 6.7 are the frontogenetical and frontolytical contributions of the twisting and horizontal confluence effects respectively in the vicinity of the zone through 15Z. Peak values approach 5°C $(100\text{ km})^{-1}$ $(3\text{ hrs})^{-1}$ and 2°C $(100\text{ km})^{-1}$ $(3\text{ hrs})^{-1}$ respectively. This is in accord with the findings of Reed and Sanders (1953) and physically represents a thermally indirect circulation with the strongest subsidence on the warm boundary. By 18Z the horizontal confluence and twisting effects are becoming frontogenetical and frontolytical respectively in downstream regions of the zone. Values are 5°C $(100\text{ km})^{-1}$ $(3\text{ hrs})^{-1}$ and 4°C $(100\text{ km})^{-1}$ $(3\text{ hrs})^{-1}$ respectively. However, the twisting effect is still very much frontogenetical in the upstream region of the zone reaching a value of 4°C $(100\text{ km})^{-1}$ $(3\text{ hrs})^{-1}$ whereas the horizontal confluence is essentially neutral. The trend established at 18Z is even more pronounced at 21Z and 00Z. Horizontal confluence is strongly frontogenetical throughout the entire zone reaching peak values of 5°C - 6°C $(100\text{ km})^{-1}$ $(3\text{ hrs})^{-1}$ in upstream regions. The twisting effect remains frontogenetical in upstream regions of the zone but becomes strongly frontolytical in downstream regions with peak values of 2°C - 4°C

$(100\ km)^{-1}\ (3\ hrs)^{-1}$ and $7°C\ (100\ km)^{-1}\ (3\ hrs)^{-1}$ respectively. The latter effect is associated with the beginning of ascent on the warm boundary of the zone as can be seen from fig. 6.6. Essentially similar behavior is exhibited on the other theta levels within the zone. However, horizontal confluence is neutral or slightly frontogenetical on $\theta = 311$ at 12Z and 15Z. The difference between the observed and calculated frontogenesis is less than on the $\theta = 303$ surface while the sign agreement remains excellent.

The following picture is suggested. Air parcels moving through the zone are continually undergoing frontogenesis in upstream regions and frontolysis in downstream regions. The horizontal variation of vertical velocity normal to the flow with the strongest subsidence on the warm boundary is associated with the early intensification of the zone. This effect becomes negative towards the end of the time period but the zone becomes embedded in a strongly confluent west-southwesterly flow which helps to maintain its intensity. Schematically the growth stage through 21Z is represented in fig. 6.9a and the nearly steady state or slight weakening stage in fig. 6.9b. The baroclinic zone is represented by the rectangular box. The solid vertical line separates the upstream and downstream regions. The solid horizontal line separates initial and final time values during the period illustrated in the schematic. C and T refer to horizontal confluence and twisting respectively while superscripts refer to the sign of the contribution.

Diabatic effects have been ignored until now. Assuming all other errors are negligible a rough measure of the horizontal

diabatic contribution can be obtained from an area average of the observed minus calculated frontogenesis. This operation yields values on the order of 0.1 to 0.3°C $(100\ km)^{-1}(12\ hrs)^{-1}$. The effect is frontolytical during the early growth of the baroclinic zone through 18Z with some suggestion for a frontogenetical contribution in downstream regions from 18Z through 00Z. However, the uncertainties in the above area average measurement turn out to be of the order of the measurement itself (see Section 8a).

6d. Frontogenesis in Three Dimensions

Frontogenesis evaluated in three dimensions on $\theta = 303$ without diabatic effects from (2.9) is described in figs. 6.10 and 6.11. The terms in (2.9) are $10^3 - 10^5$ times those in (2.8). The ageostrophic and $\partial w/\partial z$ contributions are depicted in fig. 6.10 while the observed and calculated frontogenesis is shown in fig. 6.11. Encouragingly the observed and calculated frontogenesis compare favorably with each other and with the previous results for the two-dimensional case with regard to sign. As before, intensification from 12Z through 18Z is generally noted throughout the zone with the largest positive values in the upstream or entrance region of the zone. Observed frontogenesis values range from 1°C to 4°C $(km)^{-1}(3hrs)^{-1}$ from 12Z through 00Z. Peak calculated values are somewhat larger ranging up to 12°C $(km)^{-1}(3\ hrs)^{-1}$ at 21Z over a very small area just downstream from the mid point of the baroclinic zone. Calculated downstream frontolytical values reach 6°C to 7°C $(km)^{-1}(3\ hrs)^{-1}$ at 21Z compared to observed values of 1°C to 2°C

$(km)^{-1}(3\ hrs)^{-1}$. The large discrepancies between calculated and observed values at 21Z and to some extent at 00Z are for the same reasons discussed in the previous two-dimensional case.

The following picture suggests itself. At 12Z the ageostrophic contribution is frontolytical in upstream regions of the zone becoming slightly frontogenetical in downstream regions. Characteristic values are on the order of 1°C - 3°C $(km)^{-1}(3\ hrs)^{-1}$. By 21Z and 00Z this contribution has become strongly frontogenetical throughout the zone with peak values approaching 11°C $(km)^{-1}$ $(3\ hrs)^{-1}$. The $\partial w/\partial z$ contribution is frontogenetical throughout most of the zone at 12Z and 15Z with characteristic values of 1°C - 3°C $(km)^{-1}(3\ hrs)^{-1}$. Frontolytical contributions of 5°C $(km)^{-1}$ $(3\ hrs)^{-1}$ are just showing up in the exit region at 15Z. These are more noticeable at 18Z. By 21Z and 00Z the frontogenetical and frontolytical contributions of $\partial w/\partial z$ approach 5°C $(km)^{-1}(3\ hrs)^{-1}$ and 9°C $(km)^{-1}$ $(3\ hrs)^{-1}$ in the entrance and exit regions of the zone respectively. Renewed inspection of fig. 6.6 discloses the frontogenetical and frontolytical regions of $\partial w/\partial z$ for $\theta = 303$. Quite similar behavior is noted on other theta levels except that the $\partial w/\partial z$ and ageostrophic effects are comparable on $\theta = 311$ at 12Z and 15Z. Initially, three-dimensional frontogenesis appears to be associated with $\partial w/\partial z < 0$ whereas by 21Z the ageostrophic effects are becoming dominant.

Comparison of figs. 6.1 through 6.6 and cross sections of vertical velocity through midstream regions of the baroclinic zone given in fig. 7.3 reveals the apparent downward propagation

of the maximum horizontal temperature gradient between 12Z and 21Z with little change thereafter. The halt of the downward propagation between 21Z and 00Z is in good agreement with broad-scale features which show the beginnings of ascent on the warm boundary in downstream regions of the baroclinic zone by 21Z. Between 12Z and 21Z the maximum horizontal temperature gradient descends from about 450 mb to 550 mb or about 4.5 cm sec^{-1}. Sanders (1967) computed an average descent of 5 cm sec^{-1} over a 36-hour period in another case study. However, lack of adequate vertical velocities prevented him from showing that the downward propagation was for any other reason than simple vertical advection.

Overall, figs. 6.1 through 6.6 and 7.3 suggest that in addition to simple advection air parcels are descending relative to the zone particularly in upstream regions prior to 21Z. By 00Z there is some suggestion of ascent of air parcels relative to the zone in downstream regions. As in the two-dimensional case air parcels passing through the zone are generally undergoing frontogenesis and frontolysis in upstream and downstream regions respectively. This is illustrated schematically for $\theta = 303$ in fig. 6.12. F, A and SW refer to frontogenesis, ageostrophic and $\partial w/\partial z$ contributions respectively. Superscripts denote the sign of the contribution. Otherwise, the conventions are identical to those in fig. 6.9.

An attempt is made to evaluate the vertical diabatic term in a similar manner to the horizontal case. The result yields a value of approximately 0.5 - 1.0°C $(km)^{-1}(3\ hrs)^{-1}$ with an estimated uncertainty of nearly the same magnitude. The vertical diabatic term

is seemingly frontolytical and frontogenetical in the upstream and downstream regions of the baroclinic zone respectively.

6e. Relation Between Frontogenesis in Two and Three Dimensions

When a baroclinic zone forms in the mid troposphere ζ_p normally increases. At the same time ζ_θ usually decreases and $\partial\theta/\partial p$ increases. These latter changes are consistent with the conservation of potential vorticity. All three changes are consistent when $\nabla \cdot v_p < 0$ and $\nabla \cdot v_\theta > 0$. Hence, in the following identity

$$\nabla \cdot \underset{\sim}{V}_p = \nabla \cdot V_\theta + \frac{\partial \underset{\sim}{V}}{\partial \theta} \cdot \nabla \theta_p \qquad (6.1)$$

the last term on the right must be negative and dominant. Furthermove, this term arises solely from ageostrophic motions because where the vertical wind shear is geostrophic the last term on the right of (6.1) is zero.

Figs. 6.13 - 6.15 trace the positions of trajectories which encompass the baroclinic zone on the $\theta = 295$, $\theta = 303$ and $\theta = 311$ surfaces respectively from 12Z through 00Z. The enclosed area at each time is given in relative units. Divergence is visible on $\theta = 295$ and $\theta = 303$, especially from 18Z through 00Z.

On $\theta = 311$ there is small divergence throughout. Our previous results have established the importance of horizontal confluence, particularly in the downstream regions of the baroclinic zone, from 18Z through 00Z. Horizontal convergence on a pressure surface is related to horizontal confluence in natural coordinates by:

$$\nabla \cdot \underline{V}_p = \frac{\partial V}{\partial s} - V \frac{\partial B}{\partial n} \qquad (6.2)$$

where B is the geographical wind direction. The first term on the right is a stretching or shrinking effect resulting from speed changes along the streamlines. The second term is the confluence or diffluence effect. In our case the speed maximums are in the vicinity of the center of the baroclinic zone. Hence, in downstream regions the horizontal confluence will be a slight underestimate of the horizontal convergence and vice versa. Consequently, for this case the horizontal convergence will increase with time and will be particularly important in downstream regions of the zone. Consistency of (6.1) with the observations is then achieved when the importance of the ageostrophic motions of 00Z is recalled from the earlier discussion of three-dimensional frontogenesis.

6f. Depiction of Baroclinic Zone in Time Sections

Time sections at a given station provide another means of viewing the intensification of the baroclinic zone. Fig. 6.16 depicts sections at Lake Charles (LCH) and Mississippi Test Operations (MTO). Time increases from right to left. Vertical wind profiles are indicated where the elevation angle of the balloon remains above 6 degrees. LCH is typical of conditions during the early intensification stages of the zone. A definite stable layer appears between 06Z and 09Z above 450 mb and reaches peak strength at 12Z. Between 12 and 15Z subsidence of the stable layer and warming is indicated as the winds veer following the trough passage. Note the

dry air within the stable layer. The apparent mixing ratio increase near 400 mb after 12Z is not genuine but rather is a reflection of the warming as the limiting relative humidity of the instrument is reached in the dry air. MTO is typical of conditions just before peak strength of the baroclinic zone. Data is available for this station every 1 1/2 hours. The features are quite similar to the LCH case. Vertical wind shears approaching 60 to 80 knots per kilometer at 15Z and 1630Z are evident. The zone is strongest at 15Z and 1630Z in the vicinity of 500 mb. Again subsidence and warming associated with the trough passage between these times is visible. The zone partially maintains itself through 21Z as it gradually sinks toward 600 mb. The relative coldness between 1330Z and 1630Z just below the base of the stable layer is consistent with cold advection from geostrophic conditions as represented by the backing of the winds with height. The presence of the stable layer in WNW flow at LCH and MTO is attributable to the frontogenetical contribution of the twisting term in upstream regions of the baroclinic zone as was noted earlier.

Fig. 6.17 can best be described as a time section cross section. Charleston (CHS), Jacksonville (JAX), Cape Kennedy (COF) nad Miami (MIA) are oriented approximately north-south near 80°W. Observe the strengthening of the stable layer in WSW flow without any trough passage after 18Z at the three northernmost stations. This lends support to the earlier noted frontogenetical contribution of horizontal confluence at 21Z and 00Z in downstream and midstream regions of the zone. Pronounced cooling at JAX and to a lesser extent at CHS is

noted below the base of the stable layer with its onset. The nearly 5°C cooling of the 750 mb - 650 mb layer at JAX between 18Z and 21Z can be mostly explained by geostrophic cold advection associated with increased vertical wind shear and backing winds.

An interesting feature of the JAX time section is the presence of a nearly dry adiabatic layer from the base of the stable layer to the surface from 21Z to 03Z. This occurs just before sunset so an explanation based only on daytime heating of the lower layers of the atmosphere is only a partial answer. Cooling just below the base of the layer contributes to a steepening of the lapse rate in the lowest levels. There is also the suggestion of an upward transport of water vapor from the sudden ascent of the 1 g kg^{-1} isoline of mixing ratio from 21Z through 03Z. Richardson number, Ri, values range from 0.3 to 0.7 beneath the stable layer at this time where

$$Ri \equiv \frac{\frac{g}{\bar{\theta}} \frac{\partial \bar{\theta}}{\partial z}}{\left(\frac{\partial \bar{u}}{\partial z}\right)^2} \qquad (6.3)$$

Such values are marginal for instability and are indicative of the vigorous mixing taking place from the surface to the base of the stable layer.

Further to the south a somewhat different picture is presented. At both COF and MIA, especially at MIA the moisture distribution associated with the stable layer between 800 mb and 900 mb from 12Z to 18Z suggests that this layer is the remains of a cold front which passed 6-12 hours earlier (recall fig. 3.3). However, the dry stable layers which appear at COF near 700 mb and MIA near 750 mb

after 00Z bear resemblance to the previously discussed stable layers at JAX and CHS.

VII. DISCUSSION OF POTENTIAL VORTICITY CALCULATIONS

7a. Horizontal and Vertical Potential Vorticity Distributions

Fig. 7.1 shows a Northern Hemisphere winter cross section of potential vorticity calculated from Petterssen's (1950) composite cross sections of absolute vorticity and potential temperature obtained from 18 individual sections at 20° longitude intervals around the hemisphere. The stability was computed over a vertical depth of one kilometer. Observe the large gradient of potential vorticity at the tropopause. Comparison with mean winter North America potential temperature and tropopause cross sections as given by Willett and Sanders (1959) suggests that potential vorticity values of 100 are probably stratospheric while values of 200 or more are definitely stratospheric.

Fig. 7.2 shows the horizontal distribution of potential vorticity on θ = 303 at 15Z, 18Z, 21Z and 00Z. Note the slow eastward progression of the blob of high potential vorticity stratospheric air associated with our baroclinic zone. The cellular structure of the blob is repeated at other theta levels and is consistent with potential vorticity distributions depicted by Danielsen (1968).

More information about potential vorticity distributions can be gleaned from cross sections. Fig. 7.3 depicts a slice through the central region of the baroclinic zone at five time periods. The I and J values refer to the coordinates described in fig. 5.10.

The thin dashed lines are the potential isentropes ranging from θ = 291 to θ = 315 at intervals of 4°K. The thin solid lines are potential vorticity in °C mb^{-1} sec^{-1} $\times$ 10^{-7} at intervals of 100 units while the dotted lines are vertical velocity in cm sec^{-1} at intervals of 2 units. Fig. 7.4 is identical to fig. 7.3 except that the thin solid and dotted lines represent u and v in m sec^{-1} respectively.

The marked intensification of the baroclinic zone and the steepening of the isentropes between 12Z and 21Z is clearly visible. Little change is observed between 21Z and 00Z. Recall the corresponding distributions of temperature on constant pressure surfaces from figs. 6.1 - 6.5. Descent during the intensification stages is very general. Ascent on the warm boundary by 00Z is consistent with the frontolytical contribution of the twisting term in downstream and midstream regions of the zone noted earlier. The frontogenetical contribution of the twisting term between 12Z and 21Z is only partially visible because the cross sections do not slice through upstream regions of the zone.

At 12Z the potential vorticity distribution is essentially horizontal with only a small indication of a tongue like extrusion between I = 17 and I = 21. However, a pronounced tongue develops by 21Z and 00Z in conjunction with the intensification of the stable layer. The 100 isoline extends as far southward as MIA (I = 23 to 24) at 00Z on θ = 303. Hence, the stable layer at MIA after 00Z (fig. 6.11) is probably a southward extension of the baroclinic zone. The 200 isoline sinks from just above 500 mb at 12Z to nearly 650 mb to 21Z

and 00Z. This corresponds to a downward advection of stratospheric air at the rate of 5-6 cm/sec in excellent agreement with the mean descent calculated from trajectories during the intensification of the zone.

The increasing vertical wind shear with time in fig. 7.4 is consistent with the intensification of the zone. Shear magnitudes exceed 30 m $sec^{-1}km^{-1}$ at 21Z while values of 20 m $sec^{-1}km^{-1}$ are common over a wide region of the zone. Observe the gradual shift of the flow from WNW to WSW from 12Z to 00Z as the zone moves around the bottom of the trough and becomes embedded in the confluent WSW flow.

7b. Interpretation of Potential Vorticity Changes

Figs. 7.2 and 7.3 suggest potential vorticity growth through 21Z at all levels within the zone followed by a marked decrease in mid and upper regions of the zone by 00Z. The extreme errors in relative vorticity measurements are probably of the order of 10-20 % (see Section 8a). Potential vorticity errors will arise from the product of stability and absolute vorticity. Yet an upper error bound of 10% appears reasonable for this case because the dense wind data are filtered horizontally and vertically and the stability itself is an average over a one-kilometer depth. Incorporating this limit the growth in fig. 7.2 expressed as a departure from the mean appears to be only marginally significant at best. The decrease could perhaps be real.

Interpretation of potential vorticity changes is a tricky

business. The latent heat contribution to the diabatic effect is negligible because of the pronounced descent within the zone. Radiation is another matter. Staley (1965) and Staley and Jurica (1968) have calculated radiational cooling rates of 3-5°C day^{-1} near the bases of very strong inversions in the mid troposphere characterized by a rapid decrease in mixing ratio just below the base of the stable layer. However, caution is required in application of this argument to the present case. Very often the stable layer is embedded in dry tropospheric air. This is particularly true in the early growth stages when the zone is located west of the trough axis and in WNW flow aloft. An example is presented in a skew T-log p plot in fig. 7.5. A trajectory on θ = 303 near 72235 (JAN) at 18Z passes very near 72226 (MGM) at 21Z and 72208 (CHS) at 00Z. Note the remarkable consistency of the base of the stable layer. Tropospheric air beneath the stable layer at JAN and MGM is quite dry and this is typical for soundings in the vicinity of mid and upstream regions of the zone through 21Z. At CHS and JAX (not shown) the moist layer extends up close to the base of the stable layer. Near the Atlantic coast residual low level tropospheric moisture exists despite the passage of a cold front associated with the Nantucket low as the flow aloft remains south of west.

Wagner (1961) has investigated the effect of the time constant of radiosonde sensors on the measurement of temperature and humidity discontinuities in the atmosphere. His results for the lithium chloride element are valid because most of the elements in February 1964 were still of that type. The temperature sensor had a time

constant ranging from 2-3.5 sec while the lithium chloride sensor had a non-linear time constant which reached 40 sec at -15°C. At the latter temperature the reported top of a moist layer could be as much as 700 feet too high for average ascent rates of 1000 ft/min. The magnitude of the cooling in Staley's calculation is inversely proportional to the height difference between the top of the moist layer and the base of the stable layer. The humidity sensor error would then lead to an overestimate of the radiative cooling at the base of the layer.

Fig. 7.6 indicates the track of the potential vorticity maximum (solid line) and two close trajectories (dashed lines) on the θ = 303 surface. The slow movement of the maximum between 15Z and 21Z is coincident with the time of apparent potential vorticity growth as well as the maximum rate of frontogenesis. Such behavior is expected if diabatic and mixing process are contributing to frontogenesis and potential vorticity growth in the upstream region of the baroclinic zone. Yet the discrepancy between the 12-hour displacement of the maxima and the air parcels is not very significant. Because of the separation of observing stations potential vorticity is representative of the larger scale mean motions. Potential vorticity distribution on the sub synoptic scale can be considerably different than that on the synoptic scale. The presence of many small stable layers in a given sounding as described by Danielsen (1959) is evidence for this. Hence, the mean potential vorticity distribution will be dependent upon the degree of organization of the fine scale distribution. For example, the mean potential

vorticity could remain the same or even increase at the same time as the peaks of the small-scale maxima are eroded by mixing if the large-scale motion is such to bring these peaks closer together in the vertical. The strong frontogenesis through 21Z could be a means for accomplishing this.

Adler (1967) has derived the following average potential vorticity equation in x,y,z space.

$$\frac{d\bar{P}}{dt} \equiv \frac{D}{Dt}\left[\nabla\tilde{\theta}\cdot\bar{\alpha}\tilde{q}_a\right] = \nabla\frac{d\tilde{\theta}}{dt}\cdot\bar{\alpha}\tilde{q}_a$$

$$-\nabla\left[\frac{\nabla\cdot\bar{\rho}\widetilde{v'\theta'}}{\bar{\rho}}\right]\cdot\bar{\alpha}\tilde{q}_a - \bar{\alpha}\nabla\tilde{\theta}\cdot\nabla\times\left[\bar{\alpha}\frac{\partial}{\partial x_i}\left(\bar{\rho}\widetilde{u_i'u_k'}\right)i_k\right] \tag{7.1}$$

where the Einstein summation convention is used. Her the squiggly bar, ~, is a density weighted average of the form

$$\tilde{A} = \frac{\overline{\rho A}}{\bar{\rho}} \tag{7.2}$$

along with the usual convention

$$u_i = \tilde{u}_i + u_i' \tag{7.3}$$

where the prime denotes the deviation from the average. The left-hand side of (7.1) is not exactly the average potential vorticity but is rather a product of averaged quantities. In synoptic studies $\nabla\tilde{\theta}\cdot\alpha\tilde{q}_a$ is what is calculated and for convenience will be called the average potential vorticity. The terms on the right-hand side of (7.1) reflect the contributions of diabatic heating, eddy entropy mixing and eddy momentum mixing respectively.

By recalling the importance of the vertical versus horizontal gradient of diabatic heating and replacing the absolute vorticity vector by its vertical component we have the following approximation for the first term on the right-hand side of (7.1)

$$\nabla \frac{d\tilde{\theta}}{dt} \cdot \bar{\alpha} \hat{q}_a \cong \bar{\alpha} (\zeta + f)_z \frac{\partial}{\partial z} \left(\frac{d\tilde{\theta}}{dt} \right) \qquad (7.4)$$

Since $(\zeta + f)_z$ is usually > 0 heating above and cooling below will produce a positive potential vorticity change. Similarly for positive vertical wind shear the neglected terms involving horizontal components of absolute vorticity require that heating to the west and/or north and cooling to the east and/or south will produce potential vorticity increases.

Molecular conduction will not effect $d\tilde{\theta}/dt$ except very close to the ground. Latent heat release is negligible within the baroclinic zone but will play a role in the cold core of the trough just north of the zone. A rough measure of the right-hand side of (7.4) can be obtained by equating it to the left hand side of (7.1). This is done for $\theta = 303$ along the path of the potential vorticity maximum from 21Z to 00Z (recall fig. 7.2). The potential vorticity change from the mean value over this interval is about 80×10^{-7} °C $mb^{-1} sec^{-1}$. The average absolute vorticity at 500 mb in this region is 24×10^{-5} sec^{-1} for a temperature of about -30°C. Therefore

$$\frac{\partial}{\partial z} \left(\frac{d\tilde{\theta}}{dt} \right) \approx -2.5\,^{\circ}C\,(1\,km)^{-1}\,(3\,hrs)^{-1}$$

This compares favorably with the mean diabatic magnitude of $0.5 - 1.0°C\ (km)^{-1}(3\ hrs)^{-1}$ obtained for three dimensional frontogenesis. The region beneath the potential vorticity maximum on $\theta = 303$ is not characterized by marked stable layers or moisture inversions during this interval. Estimated radiational cooling rates of $1\text{-}2°C\ (km)^{-1}(day)^{-1}$ for the mid troposphere are probably valid in this region. Clearly, a cooling of this magnitude cannot account for the diabatic change.

Latent heat release below 400-500 mb is one possible explanation. Between 21Z and 00Z the area bounded by the western Carolinas, extreme northern Georgia and Alabama and eastern Tennessee was reporting numerous light rain showers with occasional TCU's and small CB's visible. The convective activity was typical of that which accompanies the passage of a cold trough. Rainfall amounts in this region for the 6-hour period ending 00Z were of the order of 0.05" to 0.15". This corresponds to a latent heat release for the 850 mb - 500 mb layer of about $1°C(3\ hrs)^{-1}$. Such a value is not negligible.

By ignoring spacial variations of $\bar{\rho}$ and considering vertical derivatives only Adler (1967) approximated the entropy mixing term as follows:

$$-\nabla\left[\frac{\nabla\cdot\bar{\rho}\,\widetilde{v'\theta'}}{\bar{\rho}}\right]\cdot\bar{\alpha}\tilde{q}_a = -\bar{\alpha}\left(\zeta+f\right)_z\frac{d^2}{dz^2}\left(\widetilde{w'\theta'}\right) \qquad (7.5)$$

where w' is the deviation from the mean vertical wind speed. Thus from (7.1) $\bar{P}$ will decrease where the absolute vorticity is positive and when $d^2/dz^2(\widetilde{w'\theta'}) > 0$. Unfortunately, obtaining quantitative

information can be obtained from scaling arguments. Consider

$$\frac{\partial \Theta}{\partial t} = -\frac{\partial}{\partial z}\left(\overline{\Theta' w'}\right) \sim \frac{\Theta}{T} \approx \frac{\Theta W}{L} \sim T \approx \frac{L}{W} \qquad (7.6)$$

For a perfect $\widetilde{\theta' w'}$ correlation the following time scales for turbulent flow would perhaps be valid

L (m) \ W (cm sec^{-1})	10	1
100	20 min	2 min
1000	200 min	20 min

Fig. 7.7

In the real atmosphere $\widetilde{\theta' w'}$ correlation is probably more of the order of 10-20%. In this case our time scales would have upper and lower bounds of 1000-2000 min and 10-20 min respectively with a probable range of 100-200 minutes. Clearly turbulent mixing operates on time scales relevant to the interpretation of $\bar{P}$ changes.

Fig. 7.8 is a skew T, log p plot of soundings at MSFC, 72311 (ATH) and 72317 (GSO) at 18Z, 21Z and 00Z respectively. A trajectory on θ = 295 passes near these stations from 18Z through 00Z. The θ = 295 surface approaches the base of the stable layer marking the low tropopause with increasing time. The rise of the tropopause, particularly between 21Z and 00Z, would be expected if convective cloud tops from below were penetrating the base of the layer and mixing with the air above. Convective activity in this

region was established earlier. A similar argument was used by Paine (1966) to explain negative $\bar{P}$ changes in the lower regions of a stable layer situated on top of an unstable layer. Except where the lapse rate is superadiabatic $\widetilde{w'\theta'}$ will generally be negative. A large positive curvature, $d^2/dz^2(\widetilde{w'\theta'}) > 0$, and hence a negative $\bar{P}$ change, would be expected in the vicinity of $\theta = 303$ and just above at GSO at 00Z.

The last term on the right of (7.1) to good approximation becomes

$$-\bar{\alpha}\nabla\bar{\theta}\cdot\nabla\times\left[\bar{\alpha}\frac{\partial}{\partial x_i}\left(\bar{\rho}\,\overline{u_i'u_h'}\right)i_h\right] \approx$$

$$-\bar{\alpha}\frac{\partial\theta}{\partial p}\left[\left(\frac{\partial}{\partial x}\left\{\frac{\partial}{\partial x}\left(\overline{u'v'}\right)+\frac{\partial}{\partial y}\left(\overline{v'^2}\right)\right\}\right.\right.$$

$$\left.-\frac{\partial}{\partial y}\left\{\frac{\partial}{\partial x}\left(\overline{u'^2}\right)+\frac{\partial}{\partial y}\left(\overline{u'v'}\right)\right\}\right)$$

$$\left.+\left(\frac{\partial}{\partial x}\left\{\frac{\partial}{\partial z}\left(\overline{v'w'}\right)\right\}-\frac{\partial}{\partial y}\left\{\frac{\partial}{\partial z}\left(\overline{u'w'}\right)\right\}\right)\right] \qquad (7.7)$$

Initially this looks pretty grim, but the units of $\sec^{-2}$ inside the brackets offer a clue. The first term on the right of (7.7) is like an eddy diffusion of vorticity whereas the second term arises from the horizontal variation of the vertical convergence of vorticity by the eddies. Again, we can only postulate the effect of (7.7) indirectly. Individual positive $\bar{P}$ changes along trajectories ending in the vicinity of JAX on $\theta = 311$ at 00Z are of the order of 70×10^{-7} mb^{-1} sec^{-1} $(3\ hrs)^{-1}$. Taking into account the temperature and stability on $\theta = 311$ the right hand side of (7.7) becomes

$$\frac{d\zeta}{dt} \approx 3 \times 10^{-5}\ \text{sec}^{-1}\ (3\ \text{hrs})^{-1}$$

This cyclonic vorticity increase is certainly not unreasonable from an observational viewpoint. A physical process whereby eddy diffusion of vorticity could affect the above change might be envisioned as follows. Conservation of potential vorticity requires that air parcels gain relative anticyclonic vorticity on isentropic surfaces as they undergo a stability increase upon entering the baroclinic zone. Thus, a parcel may be required to switch from the cyclonic to anticyclonic side of the jet along a trajectory. Horizontal eddy diffusion of vorticity would act to lessen the anticyclonic relative vorticity increase south of the jet through a weakening of the gradient or a slight southward displacement of the jet axis relative to the parcel.

Extreme caution is required in attempting to obtain quantitative measurements of primed quantities from individual $\bar{P}$ changes along trajectories. The two factors in the product $(\zeta_\theta + f)\ \partial\theta/\partial p$ should be evaluated from similar scales of motion. This is another reason for the choice of a one-kilometer vertical sampling interval for stability calculations. Temperature perturbations due to gravity waves must be removed from the soundings. The ratio of the vertical depth for $\partial\theta/\partial p$ to the horizontal spacing of rawinsonde stations for $(\zeta_\theta + f)$ is of the order of 1/300 which is also of the order of the ratio of the vertical to horizontal scales of motion in the atmosphere. However, in the left side of (7.1) unavoidable errors still remain because a space-averaged product is not necessarily identical to the product of two space averaged quantities.

Individual potential vorticity changes for this case are probably not accurate to more than 20% to 40%. This figure was arrived at by comparing the previously discussed maximum trajectory error of one grid unit with actual $\bar{P}$ distributions. A rough way to visualize individual $\bar{P}$ changes is indicated in fig. 7.9 for θ = 303 and θ = 311. Machine techniques for carrying out this task are described by Bleck (1968). Vectors point from the end point of each trajectory to the nearest point where the potential vorticity is equal to the value at the starting point of the trajectory 6 hours earlier. The time listed below each diagram refers to the mid-time of a 6-hour trajectory.

In fig. 7.9 most of the vectors have a length within the maximum error radius of one grid unit and hence nothing can be said about the non-conservation of $\bar{P}$. The vectors over the Atlantic, Gulf and northern and western fringe areas probably reflect analysis uncertainties rather than any genuine non-conservation of $\bar{P}$. However, negative individual $\bar{P}$ changes are visible, especially on θ = 303, in the western Carolinas, eastern Tennessee and northern Georgia and Alabama where we previously observed local negative $\bar{P}$ changes, from 21Z to 00Z. Similarly, positive individual $\bar{P}$ changes from 18Z to 00Z on θ = 311 over northern Florida and southeastern Georgia and South Carolina are suggested in keeping with our prior observations. The "explosion" effect or individual positive $\bar{P}$ changes centered over northern Alabama on θ = 303 and 311 from 15Z to 21Z is associated with the time of maximum frontogenesis. Recall the discussion of fig. 7.6. However, this is not to imply that frontogenesis is the

result of diabatic or eddy mixing effects.

Perhaps the main point of this section is the importance of a mean synoptic potential vorticity. Individual and local changes of this quantity must then be interpreted in the light of diabatic and mixing effects. The evidence suggests that radiational effects play a minor role relative to other effects in contributing to $\bar{P}$ changes over the 12-hour period.

VIII METEOROLOGICAL IMPLICATION OF MID-TROPOSPHERIC FRONTOGENESIS

8a. Error Discussion

A feeling for how u, v errors effect the frontogenesis calculations can be obtained as follows. If the x axis is taken parallel to the isotherms then (2.8) and (2.9) become

$$F_{2D} = -\left(\frac{\partial v}{\partial y}\frac{\partial \theta}{\partial y} + \frac{\partial w}{\partial y}\frac{\partial \theta}{\partial z}\right)\frac{\partial\theta/\partial y}{|\nabla_H \theta|} \tag{8.1}$$

and

$$F_{3D} = -\left(\frac{\partial v}{\partial z}\frac{\partial \theta}{\partial y} + \frac{\partial w}{\partial z}\frac{\partial \theta}{\partial z}\right)\frac{\partial\theta/\partial z}{|\nabla\theta|} \tag{8.2}$$

Approximately

$$\frac{\partial\theta/\partial y}{|\nabla_H\theta|} \approx \frac{\partial\theta/\partial z}{|\nabla\theta|} \approx 1$$

$$\frac{\partial\theta}{\partial z} \approx 10^\circ C \ km^{-1}$$

$$\frac{\partial\theta}{\partial y} \approx 10^\circ C \times 10^{-2} \ km^{-1}$$

The following worst error estimates seem valid

$$\frac{\partial v}{\partial z} \approx 2 \ m \ sec^{-1} km^{-1} \ (10\% \ MAX \ \Delta v / km)$$

$$\frac{\partial w}{\partial z} \approx 1 \ cm \ sec^{-1} km^{-1} \ (10\text{-}20\% \ MAX \ \Delta w / km)$$

$$\frac{\partial w}{\partial y} \approx 1\text{-}2 \text{ m sec}^{-1} \times 10^{-2} \text{ km}^{-1} \left(10\text{-}20\% \text{ MAX } \Delta w / 100 \text{ km}\right)$$

$$\frac{\partial w}{\partial y} \approx 1 \text{ cm sec}^{-1} \times 10^{-2} \text{ km}^{-1} \left(10\text{-}20\% \text{ MAX } \Delta w / 100 \text{ km}\right)$$

Magnitudes of terms on the right-hand sides of (8.1) and (8.2) become respectively $1°C(100 \text{ km})^{-1}(3 \text{ hrs})^{-1}$, $1°C(100 \text{ km})^{-1}(3 \text{ hrs})^{-1}$, $2°C(\text{km})^{-1}(3 \text{ hrs})^{-1}$ and $1°C(\text{km})^{-1}(3 \text{ hrs})^{-1}$. These estimates represent upper bounds and range upwards to 30% of the average frontogenesis components calculated in chapter 6. Errors of this type are lessened with horizontal smoothing of the analyses and vertical filtering of the winds but are not eliminated.

An example of what can happen when teletype or NHDT data is substituted for every contact point data is given in figs. 8.1 and 8.2. The dashed line represents the teletype temperature report for Key West (EYW) and the NHDT temperature report for Grand Bahama Island (GBI) respectively. The dots indicate the detailed every contact point temperature profiles. Stable layers are poorly coded for transmission. Observe the pressure error of more than 20 mb near 800 mb at EYW. Temperature errors reach 2-3°C at given points.

Additionally, 100-mb layers in both soundings have reported mean temperatures more than 1°C different from the observed values. The coding rules requiring straight line temperature deviations of less than 1°C from the raw data are obviously violated. Errors of this magnitude are the most damaging in the principal regions of interest. Attempts to resolve the fine scale structure in a sounding without recourse to the original rawinsonde trace is tantamount to whistling

in the dark. Current technology makes it feasible for a master computer to process all raob data every 12 hours and then spit out the necessary information for teletype transmission. At the same time the processed detailed sounding can be stored for research uses, thus eliminating one of the super inefficient operations of the National Weather Records Center. Apparently economic and status quo factors stand in the way of achieving this goal.

Fig. 8.3 demonstrates the spacial and time continuity of stable laminae of the type first described by Danielsen (1959). The solid line represents the 15Z sounding from 72235 (JAN) and the dotted line the 18Z sounding from 72226 (MGM). A parcel on $\theta = 303$ passes very near JAN and MGM at 15Z and 18Z respectively. Observe the remarkable continuity from the base of the inversion at $\theta = 292$ through $\theta = 313$. Yet there is enough of a difference to demonstrate the effects of mixing and thermistor errors. Obviously, very noise $\bar{P}$'s will result when stabilities are calculated over vertical depths considerably less than one kilometer.

8b. Representativeness of the Calculations

Efforts to attach meteorological significance to the previous results must await a discussion of the representativeness of this particular case study. The downward transport of high potential vorticity stratospheric air is well documented for this case study. Danielsen's (1968) summary of detailed earlier case studies noted the same phenomenon and the excellent positive correlation between potential vorticity, ozone and radioactivity within air of

stratospheric origin. Hering (1966) and Newell (1965) have further summarized the excellent correlations between the above quantities. Unfortunately, radioactivity measurements are unavailable for this case. The only ozone station in the vicinity, Tallahassee, managed to take soundings at 12Z of the 19th, 20th and 21st. The ozonagrams depicted in Hering (1964) suggest some transport of mixing ratios of 0.2 - 0.5 μg/g from above 200 mb at 12Z on the 19th to below 300 mb at 12Z on the 21st. However, the results for a single station are not very conclusive. Overall, there is nothing about this case to suggest that any different result would have been obtained had detailed ozone and radioactivity measurements been available.

It is the author's contention that mid-tropospheric baroclinic zones of the type described in this paper are common occurrences during the winter season in mid latitudes. Recall from Chapter 3 that Sanders (1967) found 26 cases for the 63-64 winter season using relatively stringent criteria. Fig. 8.4 illustrates the 500 mb absolute vorticity calculated from observed winds from 12Z through 00Z. The 500-mb height contours at 12Z and 00Z are shown in figs. 3.2 and 3.4 respectively. The double vorticity maxima structure noted earlier is evident at 12Z and 00Z. A similar synoptic structure is observed in 14 of the above 26 cases, all of which primarily occur from the Rockies eastward to the Atlantic coast. However, this case is somewhat atypical in that the baroclinic zone reaches its greatest intensity in a confluent WSW flow after the upstream vorticity maximum has turned the bottom of the trough.

In the majority of the other cases with a double vorticity

maximum structure the baroclinic zone attains its peak intensity in a strong NW flow. An example of this type is given by Sanders (1967) for the case of 28-30 October 1963. The remnants of Hurricane Ginny developed into a major east coast extratropical storm at the same time as a strong baroclinic zone formed in NW flow upstream. The frontogenetical mechanism in these cases is mostly from cross-stream gradients of vertical velocity with the strongest subsidence on the warm boundary. In the current case the latter effect is important in initiating frontogenesis but horizontal confluence becomes important towards the later stages. In general, however, we cannot conceive of a motion field whereby mid-tropospheric frontogenesis can arise with the observed $\bar{P}$ distributions without the presence of dry stratospheric air, marked descent or the frontogenetical effect of the strongest subsidence on the warm boundary of the baroclinic zone.

Of further interest are the absolute vorticity patterns south of the jet axis in fig. 8.4. The quantity $(f - \partial u/\partial y)$, evaluated geostrophically, becomes negative across northern Florida and just offshore of the South Atlantic coast by 21Z and 00Z. The resulting inertial instability would lead to lateral mixing which would tend to reduce the anticyclonic shear. Perhaps this mechanism is also a factor in the previously noted $\bar{P}$ growth on θ = 311 in this area by 00Z. Less anticyclonic relative vorticity without a stability decrease would lead to a $\bar{P}$ increase.

8c. Mechanics and Dynamics of Frontogenesis

The development of horizontal confluence and a thermally direct circulation by 00Z in downstream regions of the baroclinic zone is in keeping with some of the classical theories of frontogenesis based upon quasi-geostrophic reasoning. Consider an ideal baroclinic zone in the mid troposphere oriented east-west and embedded in a horizontal deformation field. Quasi-geostrophic theory says that the transverse confluent north-south flow will tend to steepen the zone by virtue of the differential advection of temperature. However, the steepening will induce geostrophic imbalance because the pressure gradient force will exceed the Coriolis force. Cross-contour flow towards lower heights on a pressure surface will arise which from continuity considerations leads to the development of a thermally direct circulation. The latter counteracts the steepening tendency implied by the north-south geostrophic flow and allows for an increase in the vertical wind shear.

Namias and Clapp (1949) used the previous argument to explain the formation of jet streams. Sawyer (1956) used quasi-geostrophic theory to infer vertical motions in meridional planes normal to a frontal zone. No variation along the frontal zone was allowed. Eliassen (1962) extended Sawyer's (1956) results to the case where the actual wind rather than the geostrophic wind was used for advection. The y axis was taken normal to the isotherms with no variation along x parallel to the isotherms allowed. A Poisson type equation relating a stream function defined in terms of the departure from a geostrophic wind and the individual rate of change of pressure in the

yp plane to a forcing function was derived. Under most meteorological conditions this equation was elliptic and hence solvable. For the dry adiabatic case the forcing function simply became a measure of the vertical wind shear and horizontal confluence as follows:

$$Q = 2\left\{\frac{\partial u_g}{\partial p}\frac{\partial \alpha}{\partial y} - \frac{\partial u_g}{\partial y}\frac{\partial \alpha}{\partial p}\right\} \qquad (8.3)$$

Essentially, Eliassen's resultsimply that horizontal diffluence and confluence are associated with thermally indirect and direct transverse circulations respectively. Fig. 8.5 depicts an ideal cold front with the classic thermally direct transverse circulation. A positive Q implies a clockwise circulation and vice versa.

Poppe (1964) applied Eliassen's theory to obtain numerical results from a moderate mid-tropospheric baroclinic zone over Europe. Despite the limitations of the two-dimensional theory Poppe found that the derived vertical motions were consistent with a thermally direct transverse circulation. The results for this case study are quantitatively similar to Poppe's findings and Eliassen's qualitative results in downstream regions of the baroclinic zone towards the end of the time period. However, the limitations of the two-dimensional theory are readily seen. Considerable variation exists parallel to the isotherms such that gradients parallel to the zone are not always negligible compared to gradients normal to the zone. Also, Q in (8.3) does not include the effects of differential diabatic heating and mixing.

A fundamental question still remains: How does a stable layer

develop within a region of horizontal temperature gradient in conjunction with a thermally indirect circulation? Danielsen (1964, 1968) has argued that mid-tropospheric frontogenesis is really a manifestation of a stratospheric extrusion accompanied by tropopause steepening and folding. He has further shown that tropopause steepening and folding can be initiated by geostrophic motions. The argument is in agreement with synoptic observations of frontogenesis in strong NW flow. The tropopause is high and cold to the southwest of the jet axis and low and warm to the northeast. The rather large potential temperature gradient along the inclined tropopause enables folding to take place without the generation of superadiabatic lapse rates.

Fig. 8.6 shows the 200-mb, 300-mb and 400-mb charts for 19 February at 00Z and 12Z. The height contours are standard for these pressure levels. The greater westerly component at 200 mb versus 400 mb connotes tropopause steepening from geostrophic considerations as the shear vorticity maximum moves from Colorado to Texas between 00Z and 12Z. Not shown in fig. 8.6 are the observed winds. Some tendency exists for subgeostrophic flow at 200 mb in the NW flow. At 400 mb the flow is geostrophic with only the slightest hint of supergeostrophic flow. However, the evidence is rather flimsy as the differences are nearly in the noise level of the wind observations.

Schematically the following picture suggests itself. Initially a weak baroclinic zone exists embedded in NW flow (fig. 8.7a). The isotherms are parallel to the flow. Geostrophically, negative vorticity advection connotes moderate and weak descent at A and B

respectively. Fig. 8.7b is a NE-SW cross section through the zone.* The stronger descent at C versus A allowing for tropopause steepening arises from the argument used in fig. 8.7a. Air warming at C relative to D creates geostrophic imbalance as a result of a weakening of the pressure gradient force such that a NE ageostrophic wind component acts to steepen the tropopause locally. Eventually descent is induced on the warm boundary at F and then still later ascent on the cold boundary at G as a thermally indirect circulation tends to establish itself (fig. 8.7c). This picture is consistent with Danielsen's (1964,1968) arguments on tropopause steepening and folding from geostrophic considerations as well as with the qualitative reasoning in fig. 8.6.

Eliassen's (1962) scheme is used to derive the schematic shown in fig. 8.8. The format is identical to fig. 8.5. The cross section is aligned SW-NW such that u and v are positive in the SE and NE directions respectively. Convenience dictates taking $\partial v/\partial y = 0$. $\partial v/\partial p$ is taken < 0 to conform to qualitative and quantitative observations from figs. 7.3 and 8.6 respectively. Equation (8.3) then says that a center of negative Q is embedded within the baroclinic zone with the resulting thermally indirect circulation. In this example the transverse circulation acts to steepen the baroclinic zone and thus counteracts the tendency of the geostrophic (thermal) wind to flatten the isentropes. The situation is roughly comparable to a warm front at the surface.

---

* The author is indebted to John M. Brown, Dept. of Meteorology, MIT, for thoughtful suggestions and ideas for these schematic cross sections.

8d. Trajectory Aspects in Inadequate Data Regions

After 00Z the baroclinic zone moves out over the Atlantic eliminating any further hope of obtaining quantitative measurements. However, the zone does reach Bermuda (78016) between 12Z and 18Z on the 20th as the skew T - log p plots in fig. 8.9 reveal. The humidity distributions are given to the right of the temperature profiles. A dry stable layer encompassing θ = 297 through θ = 307 appears between 12Z and 18Z. A trajectory on θ = 303 satisfying energy considerations, (2.4), whose end point is 78016 at 18Z has a 00Z source between JAN and MGM. This is within the stratospheric air comprising the upstream region of the baroclinic zone. Similarly a trajectory on θ = 303 from 78016 at 12Z has a 00Z source jst east of GBI (78063) which is prior to the arrival of the zone at GBI by three hours. Average ω's are 240 mb/18 hrs and 0 mb/12 hrs respectively.

Dry stratospheric air cutting beneath a broad SW flow ahead of the trough axis is probably responsible for the presence of the dry stable layer at 18Z between two moist layers. A similar structure was noted earlier in the MIA time section (fig. 6.17). Danielsen (1966) and Paine (1966) showed that convective instability in a similar case resulted in overturning and mixing of stratospheric air with tropospheric air below. Light rain showers are observed at 78016 at 12Z and 18Z. However, there are no reports of Cb's or TCu's, only Cu and Sc. This is in agreement with the top of the moist layer at 750 mb at 18Z. Hence, the showery weather at 78016 is probably just a reflection of the passage of colder air over warmer water in

the wake of a vigorous disturbance. Station 78016 is by no means unique as ship reports in the area indicate the absence of convective activity. Evidently this region is too far removed from significant low- and middle-level upward motion capable of triggering the release of the convective instability.

8e. Role in the Atmospheric Momentum Budget

Priestley (1967) has suggested that surface fronts are capable of explaining a significant part of the average mid-latitude surface stress of 1 dyne-cm^{-2} through downward momentum transport. A similar possibility for mid-tropospheric baroclinic zones suggests itself. The equations of motion can be approximated as

$$u \approx u_g + \frac{1}{f} F_y - \frac{w}{f} \frac{\partial v}{\partial z}$$
$$v \approx v_g - \frac{1}{f} F_x + \frac{w}{f} \frac{\partial u}{\partial z} \qquad (8.4)$$

where the subscript g indicates that the component is measured geostrophically. Generally over the length of the baroclinic zone the effects of the horizontal advection terms tend to cancel such that du/dt and dv/dt can be approximated by w ∂u/∂z and w ∂v/∂z respectively. If frictional effects are ignored the contribution to nongeostrophic vertical momentum flux becomes

$$\rho \overline{wu} = -\frac{\rho w^2}{f} \frac{\partial v}{\partial z}$$
$$\rho \overline{wv} = \frac{\rho w^2}{f} \frac{\partial u}{\partial z} \qquad (8.5)$$

For evaluation purposes the following average values are chosen:

A = area of zone = 1200 km × 7°lat = 9.3×10^{5} km^{2}

Area of 30-40°N latitude band = 3.64×10^{7} km^{2}

$f(35°N) = 0.84 \times 10^{-4}$ sec^{-1}

ρ(500 mb, -20°C) = 0.6881×10^{-3} gm cm^{-3}

w(6 hr avg) = -4 cm sec^{-1} (range -2 to -21 cm sec^{-1})

$\partial \underline{v}/\partial z$(avg) = 15 m sec^{-1}km^{-1} (range 10-30 m sec^{-1}km^{-1})

With these values the downward momentum transport across 500 mb for the 12-hour period within area A is 1.97 dynes cm^{-2}. This is equivalent to an average surface stress of 0.05 dynes cm^{-2} for the 30°N - 40°N latitude band for the 12-hour period. Danielsen's (1968) results suggest the presence of anywhere from 3 to 5 regions of high potential vorticity air around the hemisphere for the mid-spring season between 30°N - 40°N on a daily basis. The evidence of many case studies implies that downward momentum transport through baroclinic zones is taking place in these regions. With the assumption of 4 such regions on a daily basis for the winter season the downward momentum flux across 500 mb within this latitude band would be equivalent to an average surface stress of 0.2 dynes cm^{-2}. Kidson's (1968) results suggest a vertically integrated horizontal momentum convergence of 16.6×10^{24} gms cm^{-2} sec^{-2} between 30°N - 40°N which is equivalent to an average surface stress of 0.88 dynes cm^{-2}. Clearly, the downward momentum and mass transport during a stratospheric extrusion is of some importance in the atmosphere.

An attempt is made to verify Danielsen's (1964) proposed model of trajectories in extruded stratospheric air. In the model the

air parcels fan out from their stratospheric source during the tropopause folding process. To the right of the jet facing downstream the air is supergeostrophic such that air parcels continually undergo anticyclonic turning as they descend and eventually reach the surface in NE, E and SE flow around a high. To the left of the jet axis facing downstream the air parcels curve cyclonically and descend until they reach the trough axis after which they begin to ascend. The results for the present case are inconclusive. Air parcels do curve cyclonically and descend in subgeostrophic flow north of the jet on theta levels comprising the baroclinic zone but soon escape out over the Atlantic. South of the jet trajectories establish slight anticyclonic curvature, principally in upstream regions of the zone one $\theta = 291$ through $\theta = 303$. The N and NE flow at Merida (76644) at these levels suggests further anticyclonic turing around the surface high in the western Gulf. Absence of Gulf of Mexico data makes this conclusion tentative.

Strong downward momentum flux implies a region of supergeostrophic flow within the baroclinic zone. Some suggestion of this behavior is noted in the 400-mb - 600-mb range in upstream regions of the zone in the vicinity of the northwest Gulf coast. Quantitative calculations imply the same thing but the degree of confidence is nowhere near as high as that of subgeostrophic flow in downstream regions of the zone north of the jet. Visual inspection of the 500-mb maps for the remainder of the double vorticity structure cases failed to disclose significant regions of supergeostrophic flow. In fiew of the small departure from geostrophy (recall Section 8a) necessary to

produce significant ageostrophic contributions this is not surprising.

Of the remaining 12 cases not associated with a double vorticity structure more than half feature baroclinic zones embedded in northerly flow immediately upstream from a pronounced 500-mb cutoff low over the southwestern U.S. The strongest flow is on the western sides of these cutoffs with 150 knot winds not uncommon at 300 mb and 200 mb. Additionally, this strong northerly flow at high levels is often super-geostrophic by 10 or 20 degrees.* With the presumed vertical velocity structure the ageostrophic contribution to the downward momentum flux must be of considerable importance.

Overall, there is the implication that the subtropical jet of winter is playing a significant role in these momentum considerations. Generally speaking the subtropical jet extends as WSW to W flow across Mexico and the southern U.S. to as far as 30°N between 70° and 80°W. See, e.g., Krishnamurti (1961a, 1961b). Observations of cirrus cloud bands streaming ENE out of the Pacific and across Mexico and the southern U.S. lend support to Krishnamurti's findings. Through the tilted trough-ridge mechanism there must be strong northward momentum flux at 200 mb across 20°N - 30°N in the mean winter season. Kidson's (1969) results suggest such behavior. When a pronounced cutoff low is present at 500 mb over the southwestern U.S. the subtropical jet is often quite intense with the jet axis whistling out of the Pacific to as far as 35°N along the Atlantic seaboard. Hence mechanisms exist for large-scale northward momentum flux at 300 mb and 200 mb immediately

---

* The author is indebted to John M. Brown, Dept. of Meteorology, MIT, for pointing out this fact to him several years ago.

downstream from regions where significant downward momentum transport is occurring. Further investigation is required to obtain quantitative estimates.

IX. CONCLUSIONS

9a. Summary

Mid-tropospheric frontogenesis has been investigated from a case study in which special three-hourly rawinsonde data was available. Isentropic analyses were generated by objective means. Detailed machine isentropic trajectories led to the three-dimensional description of the velocity field in space and time accompanying the frontogenesis. Potential vorticity calculations were made throughout the baroclinic zone to serve as a check on trajectories and as a means of delineating stratospheric from tropospheric air.

An already existing weak baroclinic zone prior to 12Z 19 February 1964 at 400 mb intensified markedly between 12Z and 21Z with very little change thereafter. At the same time the peak horizontal gradient slowly subsided from 400 mb to 550 mb by 00Z on the 20th. Air parcels streaming through the zone were continually undergoing frontogenesis and frontolysis in upstream and downstream regions respectively. Two-dimensional frontogenesis calculations reflected the initial importance of the horizontal gradient of cross-stream subsidence with the strongest sinking on the warm boundary. Later, as the intensifying zone entered a WSW flow horizontal confluence became dominant. Three-dimensional frontogenesis calculations reflected the initial importance of the vertical gradient of vertical velocity and the later importance of ageostrophic motions.

Potential vorticity behavior was such to confirm previous

observations of the extrusion of stratospheric air into the troposphere. The difficulties in attempting to infer mean synoptic potential vorticity changes were acknowledged. Turbulent rather than radiative effects were shown to be more important in the interpretation of potential vorticity changes over a 12-hour period. Potential vorticity decreases towards the end of the time period near the cold core of the 500-mb vortex were attributable to convective mixing from below along with some latent heat release. Individual potential vorticity changes following the trajectories were mostly within error tolerances such that nothing definite could be said about conservation or non conservation. However, a decrease along trajectories passing near the cold core towards the end of the time period was noted. Additionally there was some suggestion for inertial instability on the anticyclonic side of the jet at 500 mb towards the end of the time period leading to potential vorticity increases as the anticyclonic shear was lessened.

Mid-tropospheric frontogenesis was noted to be a relatively common occurrence during the winter season. In more than half the cases surveyed for a winter season an intensifying baroclinic zone was embedded in a 500-mb vorticity maximum in NW flow immediately upstream from a vorticity maximum associated with a pronounced surface storm. Similarly there was a tendency for baroclinic zones to intensify in strong northerly flow just west of a 500-mb cutoff low over the southwestern U.S. The present case was typical in the former respect but somewhat atypical in that the peak horizontal temperature gradient was achieved after the zone had turned the bottom of the trough.

Geostrophic negative vorticity advection in NW flow aloft was capable of initiating tropopause steepening and folding in a manner first suggested by Reed and Danielsen. Application of Eliassen's theory on vertical circulations in frontal zones supported the idea of a thermally indirect circulation associated with tropopause steepening and folding. The change over from a thermally indirect to direct circulation was controlled by the passage of the short-wave containing the baroclinic zone around the bottom of the long-wave trough. Furthermore, it appeared that these zones play a significant role in the downward momentum transport in the atmosphere during the winter season. Some interaction with the subtropical jet was suggested in this connection. Mid-tropospheric frontogenesis then arises as a consequence of the extrusion of stratospheric air into the troposphere during which potential vorticity, ozone, radioactivity and momentum are transported downward and southward.

9b. Suggestions for Further Work

Further research should delve into the manner in which tropospheric air enters the stratosphere. This may or may not occur at the same time as a pronounced stratospheric extrusion into the troposphere. Very warm 500-mb, 400-mb and 300-mb temperatures were observed over the Caribbean south of the very strong westerly jet along the Gulf coast. These temperatures were often more than three standard deviations warmer than mean winter season values given by Kidson (1968). Perhaps this is a result of the enhancement of the

Hadley circulation under mid-latitude forcing. A winter season case study of tropical motions accompanying the passage of a pronounced trough in lower middle latitudes with special emphasis on the role of the subtropical jet is in order.

Additional work could be done in an effort to better understand mixing processes. Perhaps the acceleration terms could be measured from the three-hourly data such that the sign or possible magnitude of the friction terms could be ascertained directly. Information on the magnitudes of the lateral and vertical eddy diffusion coefficients might follow. Also, further research on the relation between clear air turbulence (CAT) and stratospheric extrusions is required. Briggs and Roach (1963) have discussed this possibility. Unfortunately, this case was generally devoid of CAT reports. However, it would be erroneous to assume that CAT did not occur.

APPENDIX I

Miller's (1948) equation for frontogenesis in three dimensions with the neglect of diabatic effects can be expressed in x,y,z space as:

$$F = |\nabla\theta|^{-1}\frac{\partial\theta}{\partial x}\left(-\frac{\partial u}{\partial x}\frac{\partial\theta}{\partial x} - \frac{\partial v}{\partial x}\frac{\partial\theta}{\partial y} - \frac{\partial w}{\partial x}\frac{\partial\theta}{\partial z}\right)$$

$$+ |\nabla\theta|^{-1}\frac{\partial\theta}{\partial y}\left(-\frac{\partial u}{\partial y}\frac{\partial\theta}{\partial x} - \frac{\partial v}{\partial y}\frac{\partial\theta}{\partial y} - \frac{\partial w}{\partial y}\frac{\partial\theta}{\partial z}\right) \qquad \text{(I-1)}$$

$$+ |\nabla\theta|^{-1}\frac{\partial\theta}{\partial z}\left(-\frac{\partial u}{\partial z}\frac{\partial\theta}{\partial x} - \frac{\partial v}{\partial z}\frac{\partial\theta}{\partial y} - \frac{\partial w}{\partial z}\frac{\partial\theta}{\partial z}\right)$$

Our problem is to relate the above derivatives in x,y,z space to their counterparts in x,y,θ space for which we have measurements. If Q is any scalar quantity the appropriate transformation expression for the x coordinate is:

$$\left.\frac{\partial x}{\partial Q}\right|_z = \left.\frac{\partial x}{\partial Q}\right|_\theta - \left.\frac{\partial x}{\partial z}\frac{\partial z}{\partial Q}\right|_\theta \qquad \text{(I-2)}$$

For example

$$\left.\frac{\partial x}{\partial u}\right|_z = \left.\frac{\partial x}{\partial u}\right|_\theta - \left.\frac{\partial x}{\partial z}\frac{\partial z}{\partial u}\right|_\theta \qquad \text{(I-3)}$$

or

$$\left.\frac{\partial x}{\partial u}\right|_z = \left.\frac{\partial x}{\partial u}\right|_\theta - \left.\frac{\partial x}{\partial z}\frac{\partial z}{\partial\theta}\frac{\partial\theta}{\partial u}\right|_\theta \qquad \text{(I-4)}$$

$$\text{or} \quad \left.\frac{\partial u}{\partial x}\right|_z = \left.\frac{\partial u}{\partial x}\right|_\theta + \frac{gp}{RT}\,\frac{\partial \theta}{\partial p}\,\frac{\partial u}{\partial \theta}\,\left.\frac{\partial z}{\partial x}\right|_\theta \qquad \text{(I-5)}$$

All quantities on the right-hand side of (I-5) are known. Derivatives are evaluated as centered differences. Similar expressions exist for the other x,y derivatives of u,v and w. Also

$$\frac{\partial u}{\partial z} = \frac{\partial u}{\partial \theta}\,\frac{\partial \theta}{\partial z} = -\frac{gp}{RT}\,\frac{\partial u}{\partial \theta}\,\frac{\partial \theta}{\partial p} \qquad \text{(I-6)}$$

Similar expressions exist for v and w derivatives with respect to z.

$$\left.\frac{\partial \theta}{\partial x}\right|_z = -\frac{\partial \theta}{\partial z}\,\left.\frac{\partial z}{\partial x}\right|_\theta = \frac{gp}{RT}\,\frac{\partial \theta}{\partial p}\,\frac{\partial z}{\partial x} \qquad \text{(I-7)}$$

$$\frac{\partial \theta}{\partial z} = \frac{\partial \theta}{\partial p}\,\frac{\partial p}{\partial z} = -\frac{gp}{RT}\,\frac{\partial \theta}{\partial p} \qquad \text{(I-8)}$$

APPENDIX II

The vertical stability, $\partial\theta/\partial p$, is evaluated as a centered difference over one kilometer. Input data consists of p, T, θ and z at every contact point. The height of a given isentropic surface is known such that p, T and θ can be determined at z's $\pm$ 0.5 km from this level. For example, let the subscript k refer to conditions 0.5 km above the height of the given isentropic level. A machine search routine locates the two contact points which bracket the k level. Let the subscripts i and i-1 denote the upper and lower contact points respectively. Then

$$z_i = z_{i-1} + \frac{R}{g}\int_i^{i-1} T \, d(\ln p) \qquad \text{(II-1)}$$

Linear interpolation in p^K space allows

$$T_k = \left(\frac{T_i - T_{i-1}}{p_i^K - p_{i-1}^K}\right)\left(p_k^K - p_{i-1}^K\right) + T_{i-1} \qquad \text{(II-2)}$$

$$\therefore z_k - z_{i-1} = -p_{i-1}^K \frac{R}{g}\left\{\frac{T_i - T_{i-1}}{p_i^K - p_{i-1}^K}\right\}\int_k^{i-1}\frac{dp}{p}$$

$$+ \frac{R}{g}\left\{\frac{T_i - T_{i-1}}{p_i^K - p_{i-1}^K}\right\}\int_k^{i-1} p^{K-1}\,dp + \frac{R}{g}T_{i-1}\int_k^{i-1}\frac{dp}{p} \qquad \text{(II-3)}$$

This can be expressed as

$$z_{sh} - z_{i-1} = \frac{R}{g^{\kappa}} \left[p_{i-1}^{\kappa} \left\{ \frac{T_i - T_{i-1}}{p_i^{\kappa} - p_{i-1}^{\kappa}} \right\} - T_{i-1} \right] \ln \left(\frac{p_{sh}^{\kappa}}{p_{i-1}^{\kappa}} \right)$$

$$+ \frac{R}{g^{\kappa}} \left\{ \frac{T_i - T_{i-1}}{p_i^{\kappa} - p_{i-1}^{\kappa}} \right\} \left[p_{i-1}^{\kappa} - p_{sh}^{\kappa} \right] \qquad \text{(II-4)}$$

Let $$\Delta p_{up}^{\kappa} \equiv p_{sh}^{\kappa} - p_{i-1}^{\kappa} \qquad \text{(II-5)}$$

and noting $\ln(1 + x) = x$ for small x we have

$$\Delta p_{up}^{\kappa} = z_{sh} - z_{i-1} \left\{ \frac{p_{i-1}^{\kappa}}{\frac{-R}{g^{\kappa}} T_{i-1}} \right\} \qquad \text{(II-6)}$$

$$\therefore T_{sh} = \left\{ \frac{T_i - T_{i-1}}{p_i^{\kappa} - p_{i-1}^{\kappa}} \right\} \Delta p^{\kappa} + T_{i-1}^{\kappa} \qquad \text{(II-7)}$$

Hence, the virtual potential temperature is then determined from Poisson's equation

$$\Theta_{v_{sh}} = T_{sh} \left(\frac{1000}{p_{sh}} \right)^{\kappa} \qquad \text{(II-8)}$$

A similar procedure is used to get the pressure and virtual potential temperature at a level one half kilometer below the given isentropic level. Then the stability is easily calculated over the one-kilometer interval.

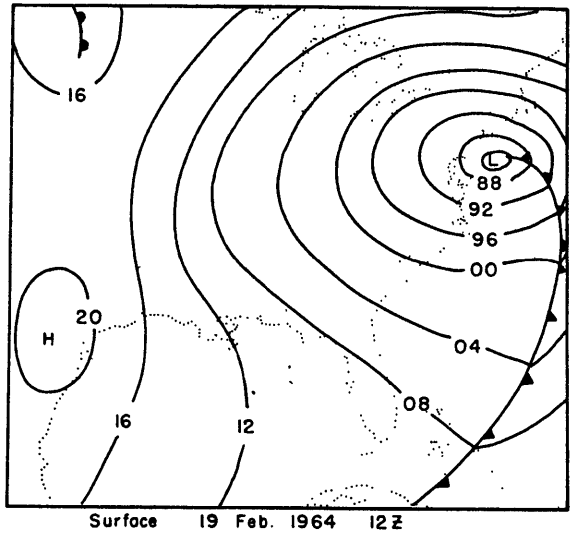

Surface 19 Feb. 1964 12Z

FIG. 3.1

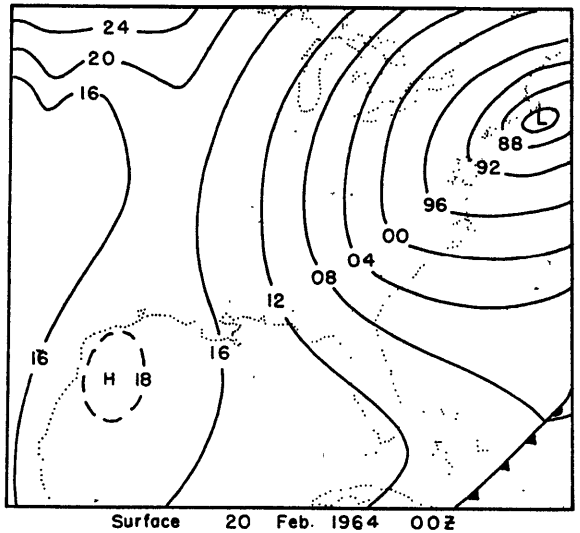

Surface 20 Feb. 1964 00Z

FIG. 3.3

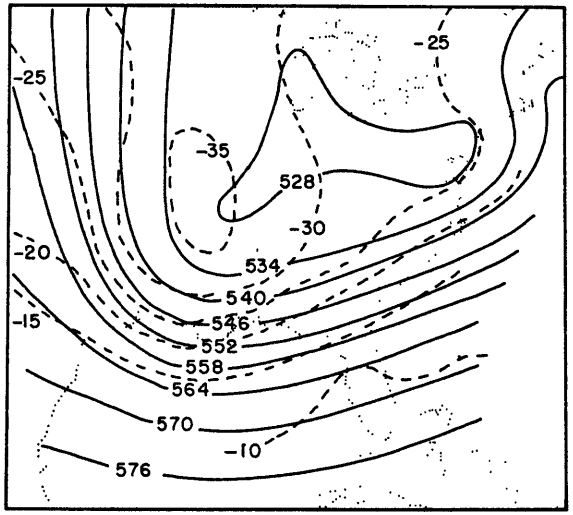

500 MB 19 Feb. 1964 12Z

FIG. 3.2

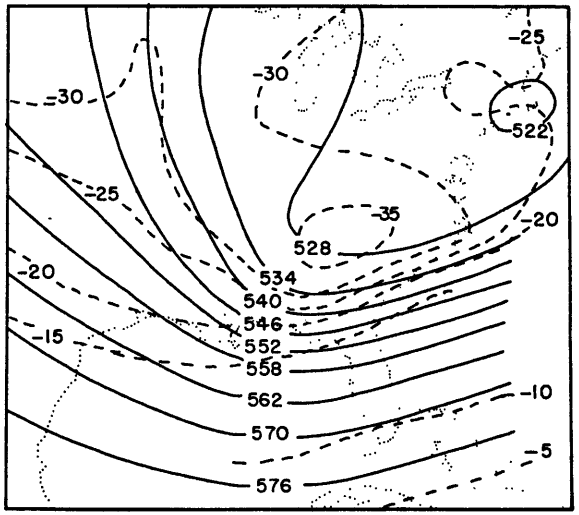

500MB 20 Feb 1964 00Z

FIG. 3.4

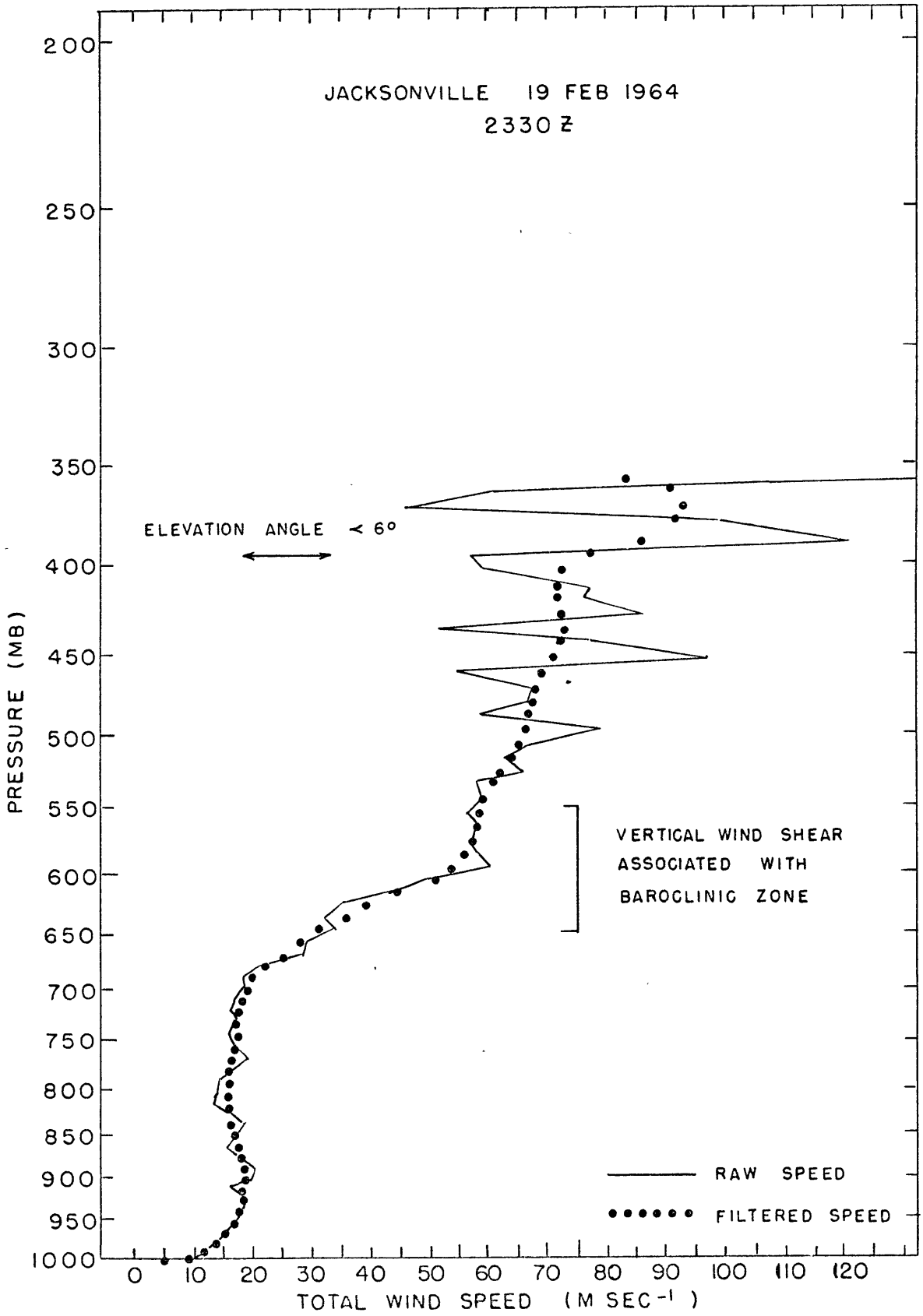
JACKSONVILLE 19 FEB 1964
2330 Z
ELEVATION ANGLE < 6°
VERTICAL WIND SHEAR
ASSOCIATED WITH
BAROCLINIC ZONE
RAW SPEED
FILTERED SPEED
PRESSURE (MB)
200
250
300
350
400
450
500
550
600
650
700
750
800
850
900
950
1000
0 10 20 30 40 50 60 70 80 90 100 110 120
TOTAL WIND SPEED (M SEC-1)

FIG. 4.1

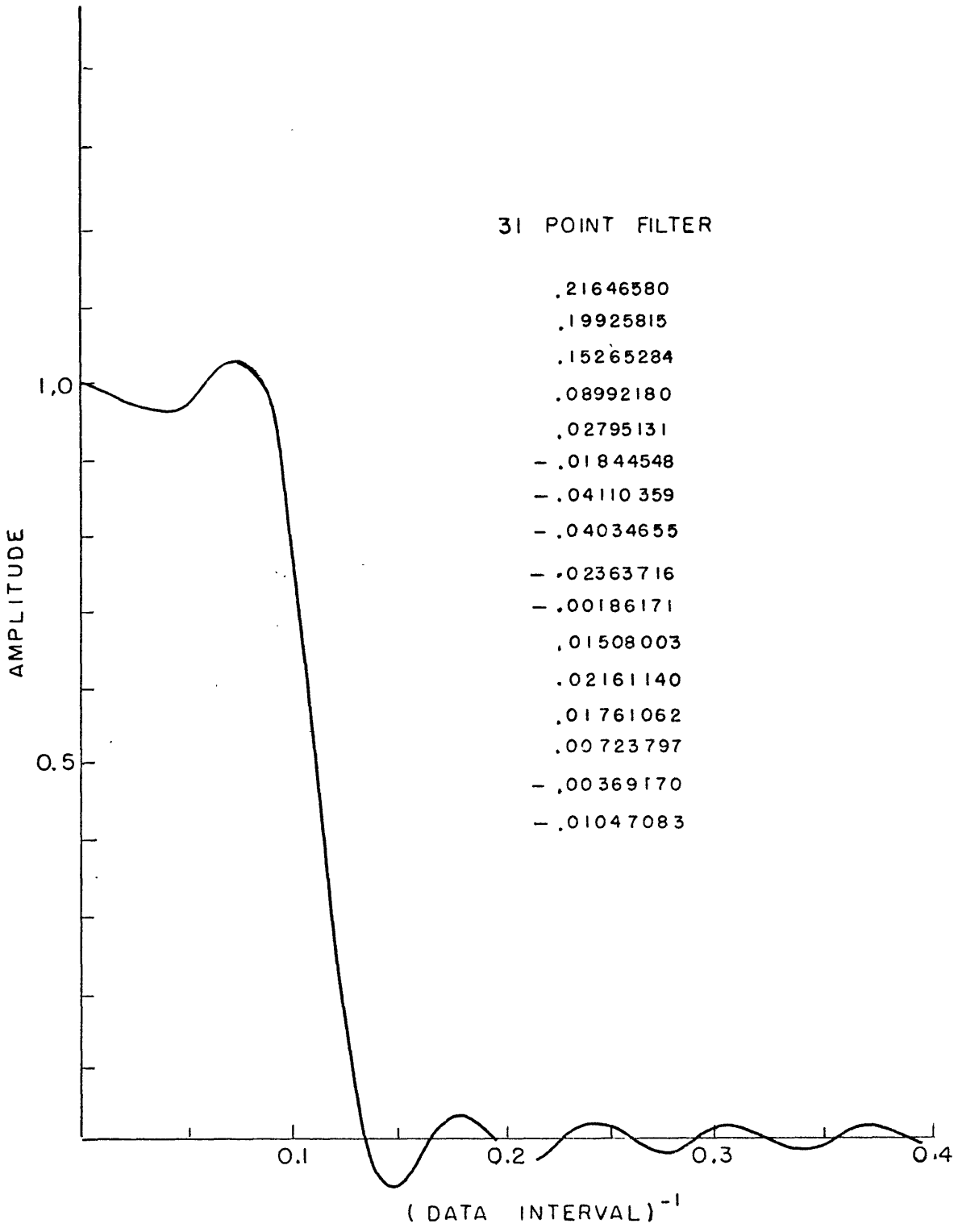
31 POINT FILTER
.21646580
.19925815
.15265284
.08992180
.02795131
-.01844548
-.04110359
-.04034655
-.02363716
-.00186171
.01508003
.02161140
.01761062
.00723797
-.00369170
-.01047083
1.0
0.5
AMPLITUDE
0.1
0.2
0.3
0.4
(DATA INTERVAL)$^{-1}$

FIG. 4.2

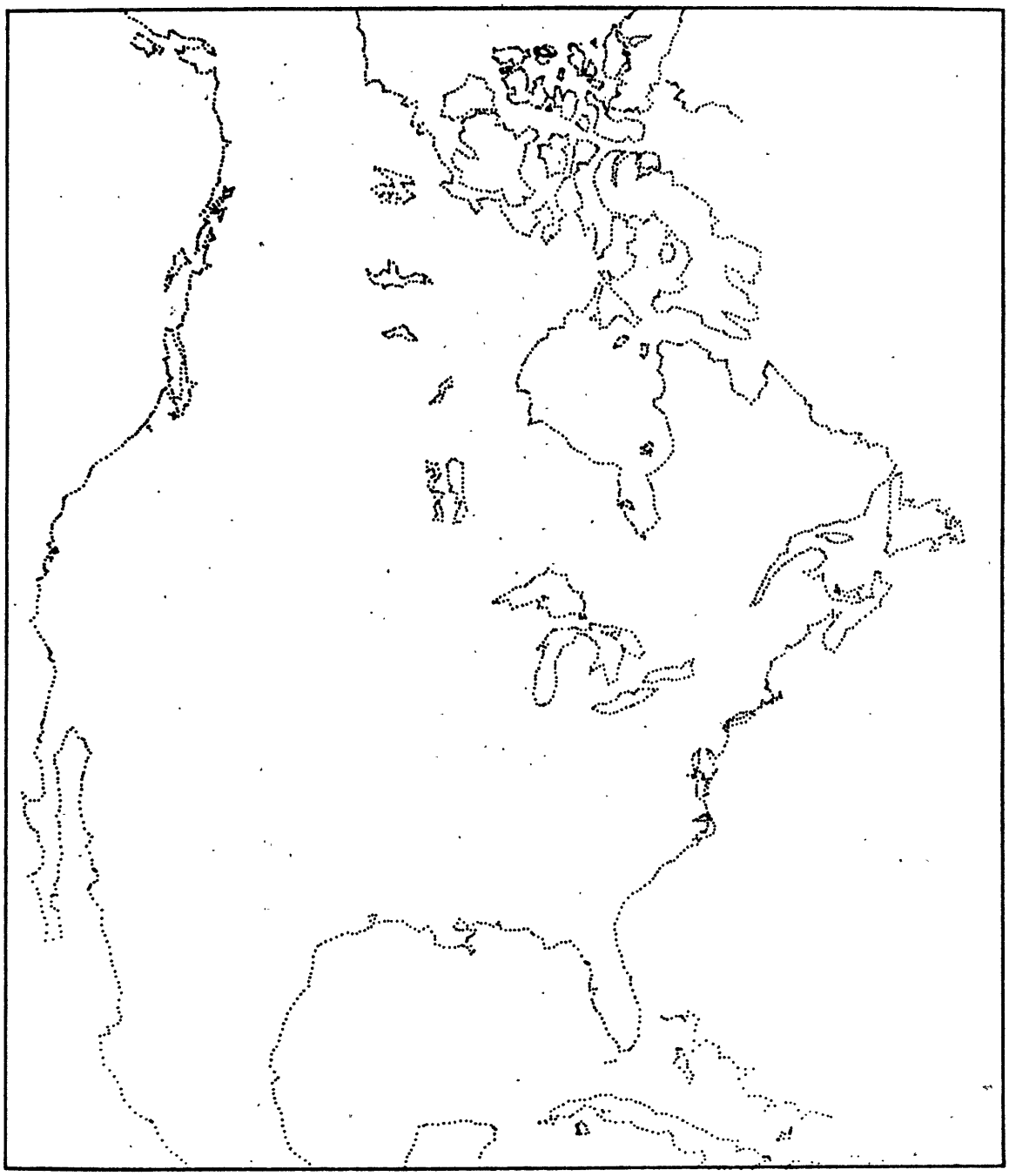

FIG. 5.1

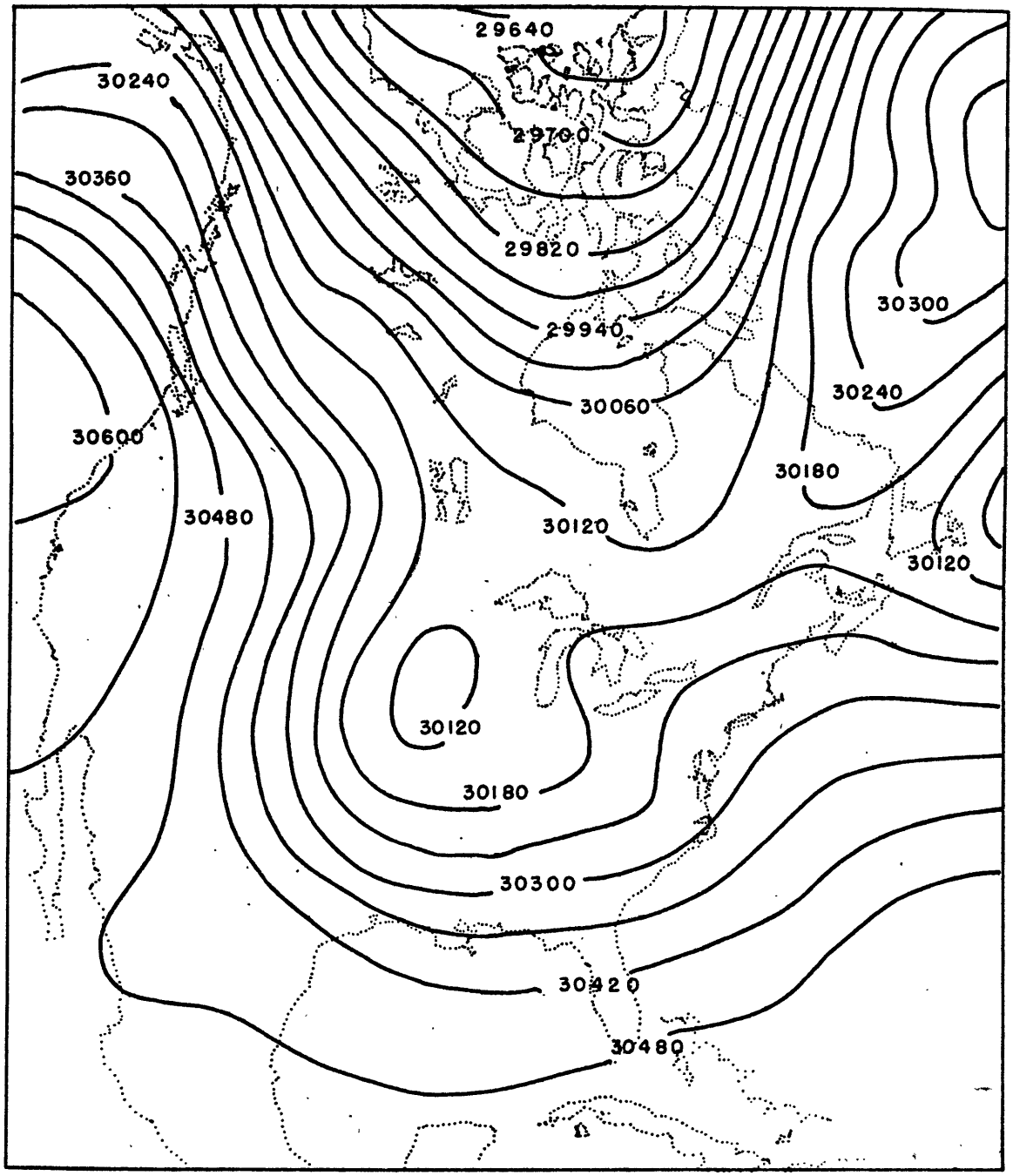

MONTGOMERY POTENTIAL X 10^5 cm^2 sec^{-2}

19 FEB 1964 00Z , θ = 303

FIG. 5.2

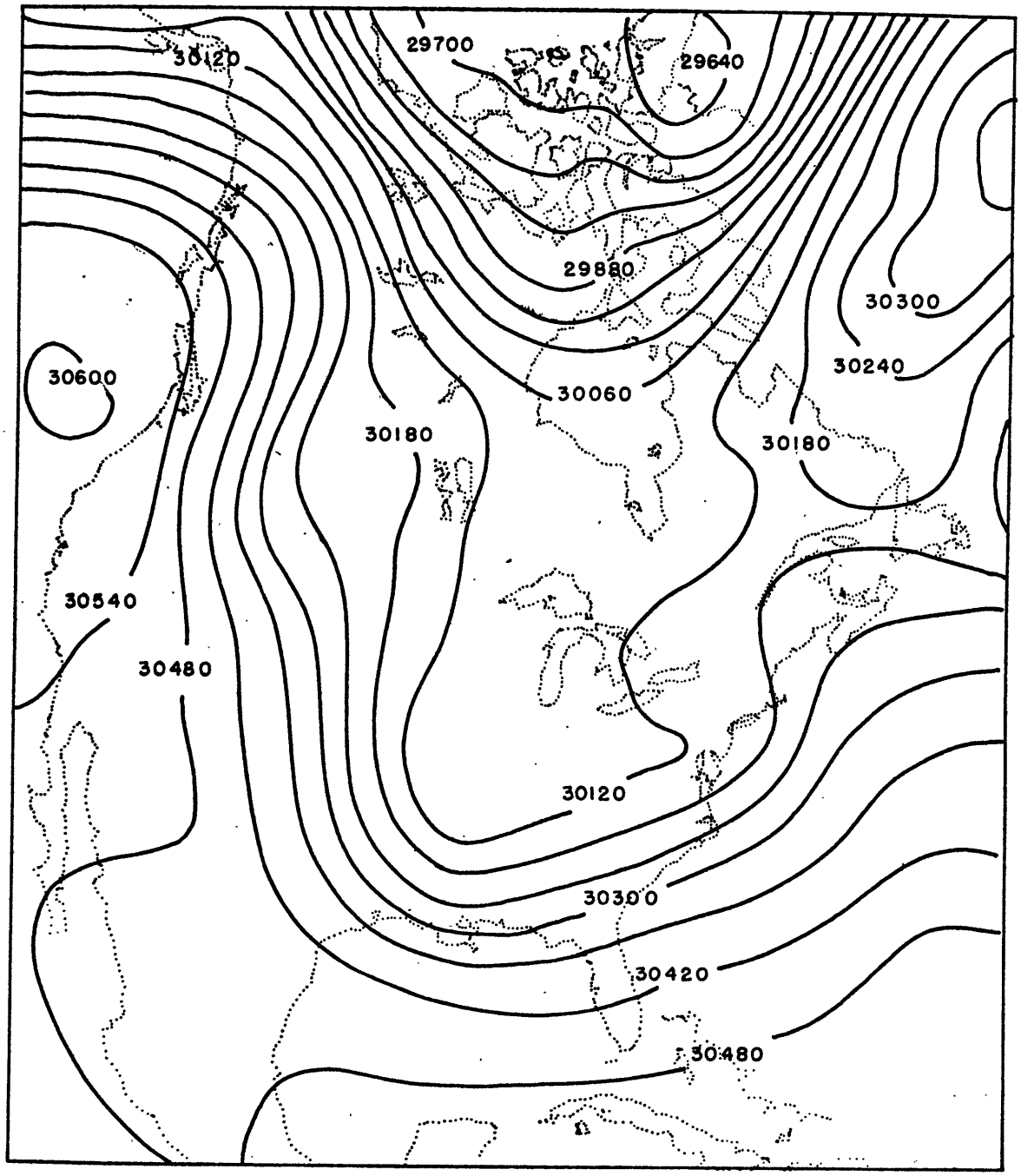

MONTGOMERY POTENTIAL X 10^5 cm^2 sec^{-2}

19 FEB 1964 12Z θ = 303

FIG. 5.3

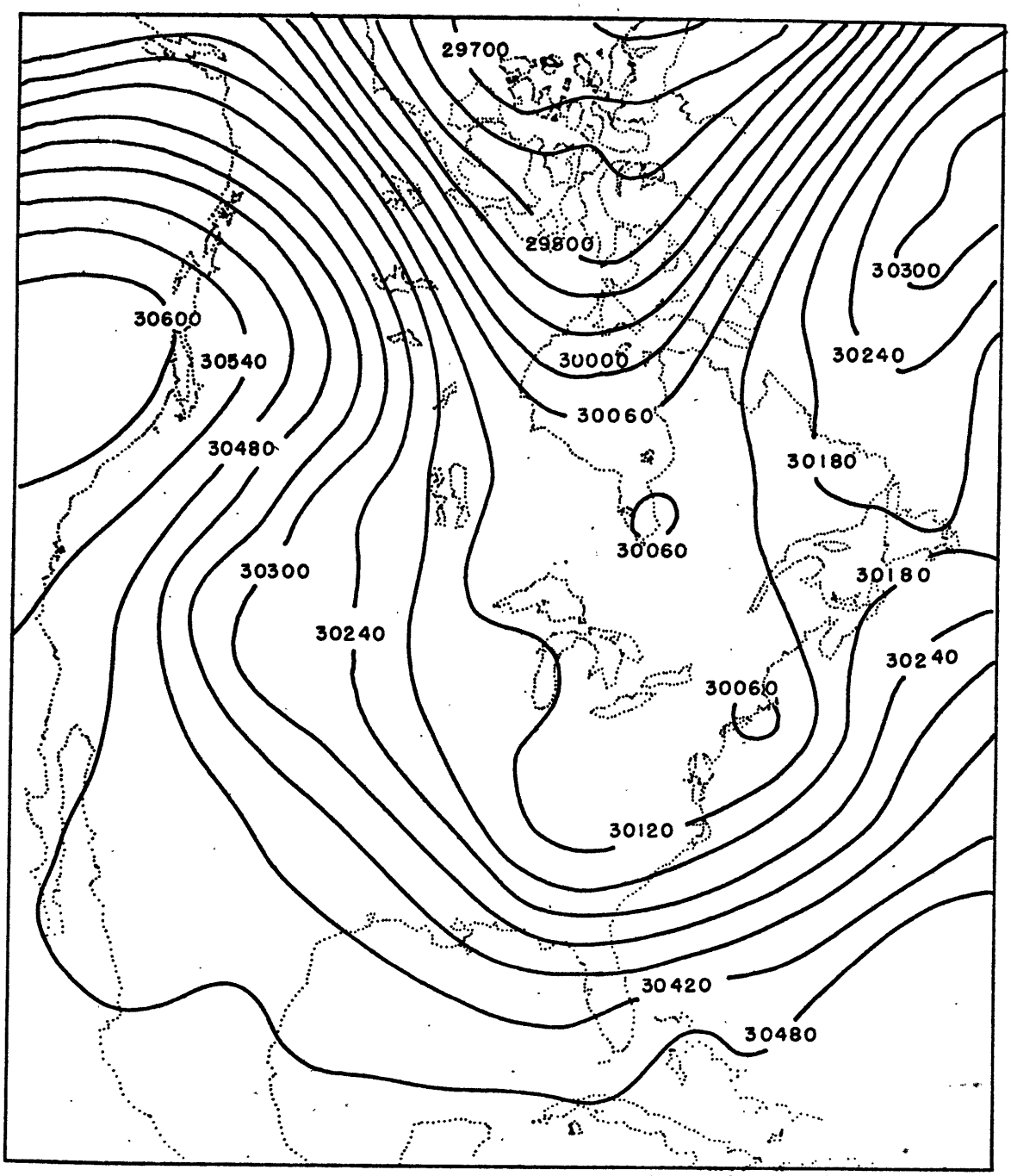

MONTGOMERY POTENTIAL X 10^5 cm^2 sec^{-2}

20 FEB 1964 00Z θ = 303

FIG. 5.4

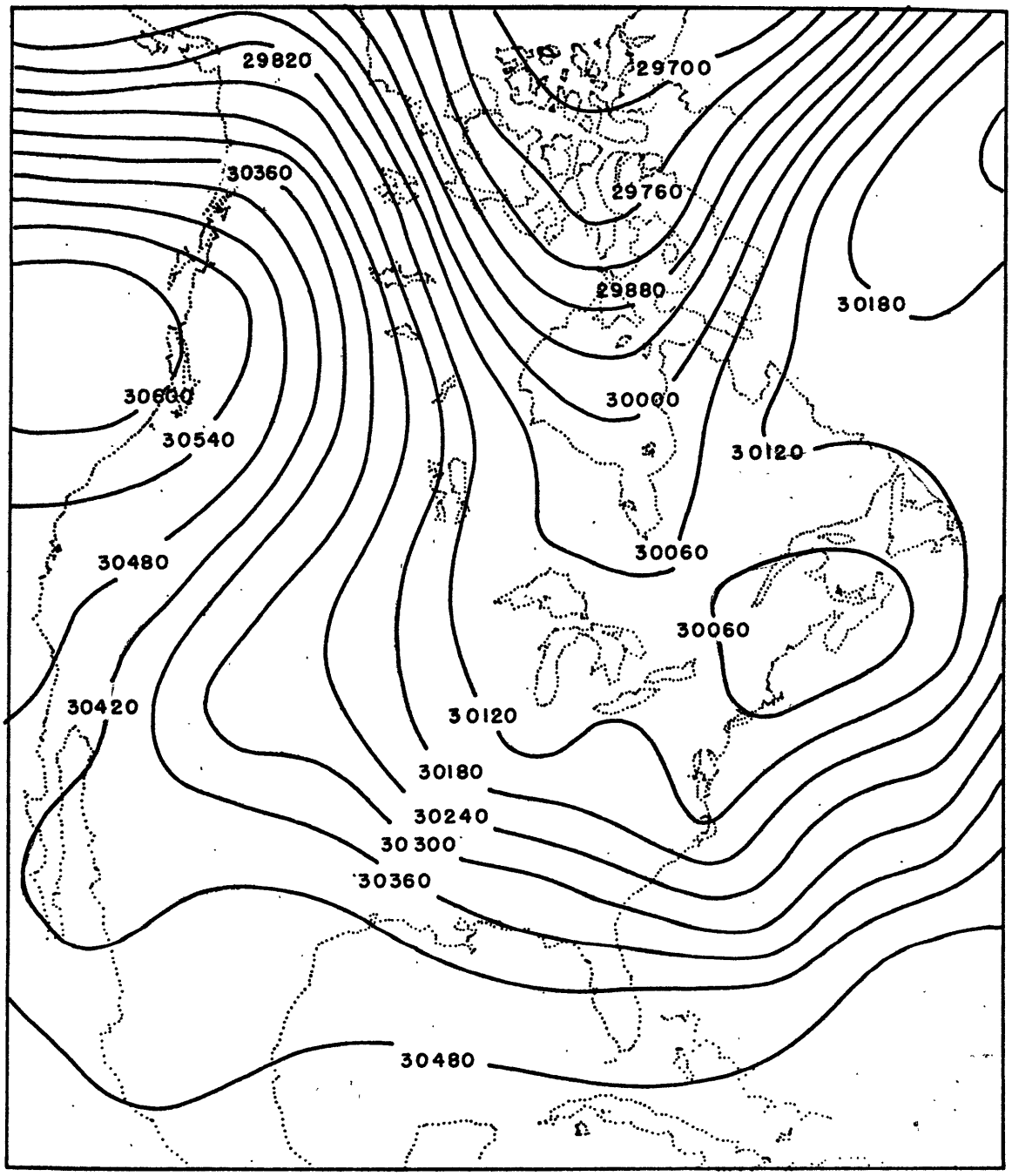

MONTGOMERY POTENTIAL X 10^5 cm^2 sec^{-2}

20 FEB 1964 12Z θ = 303

FIG. 5.5

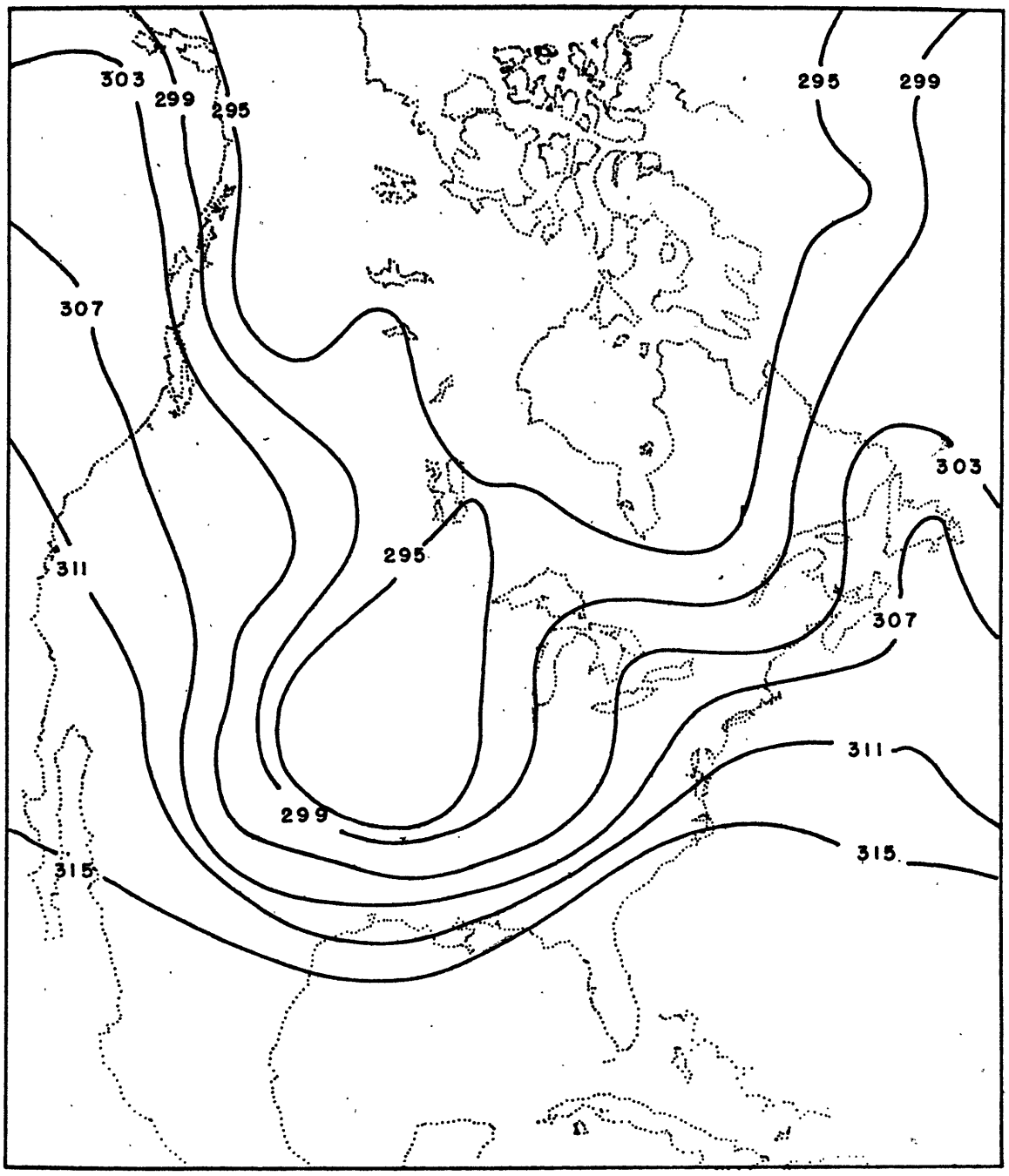

500mb TEMPERATURE 19 FEB 1964 00Z

FIG. 5.6

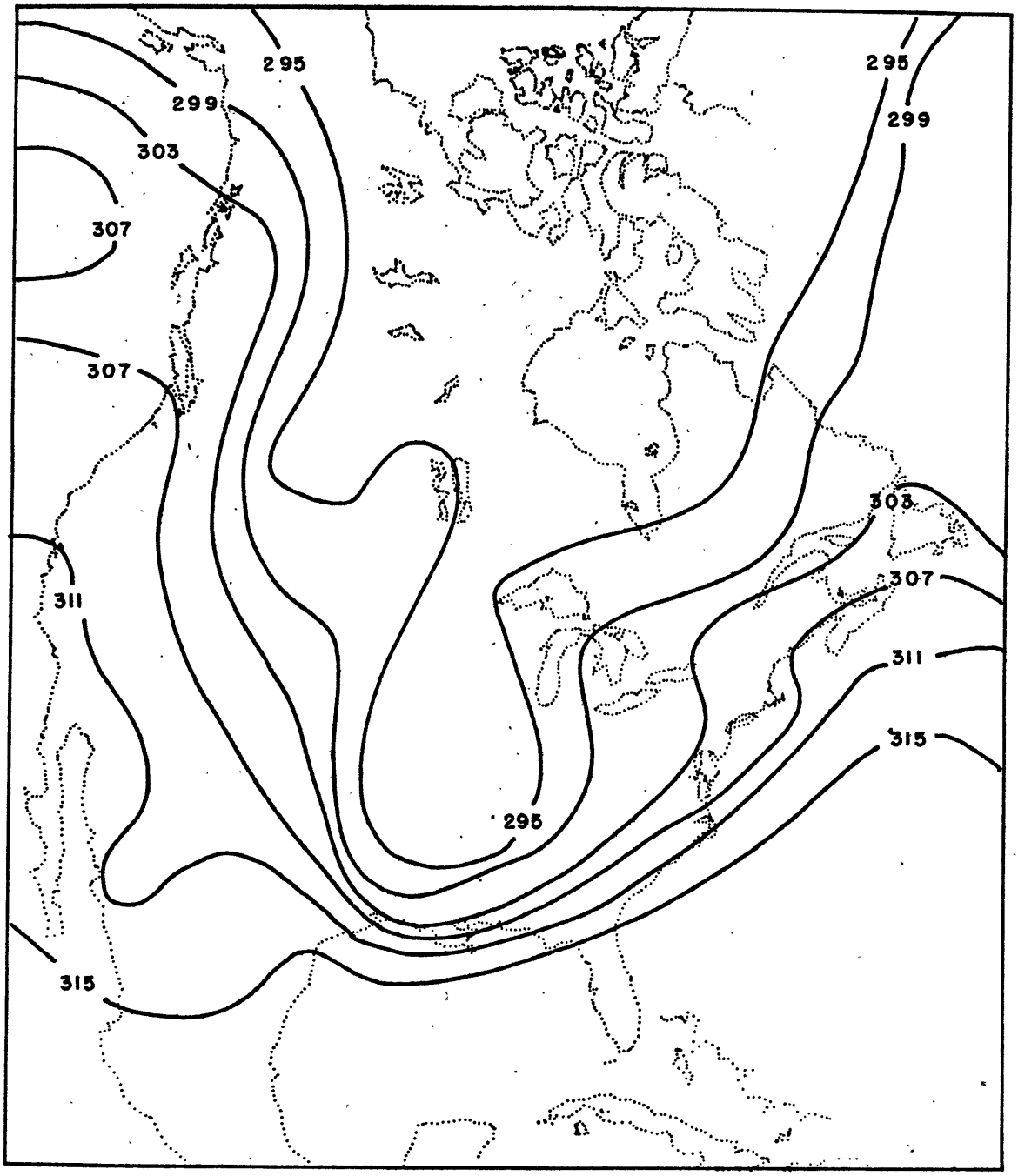

500mb TEMPERATURE 19 FEB 1964 12Z

FIG. 5.7

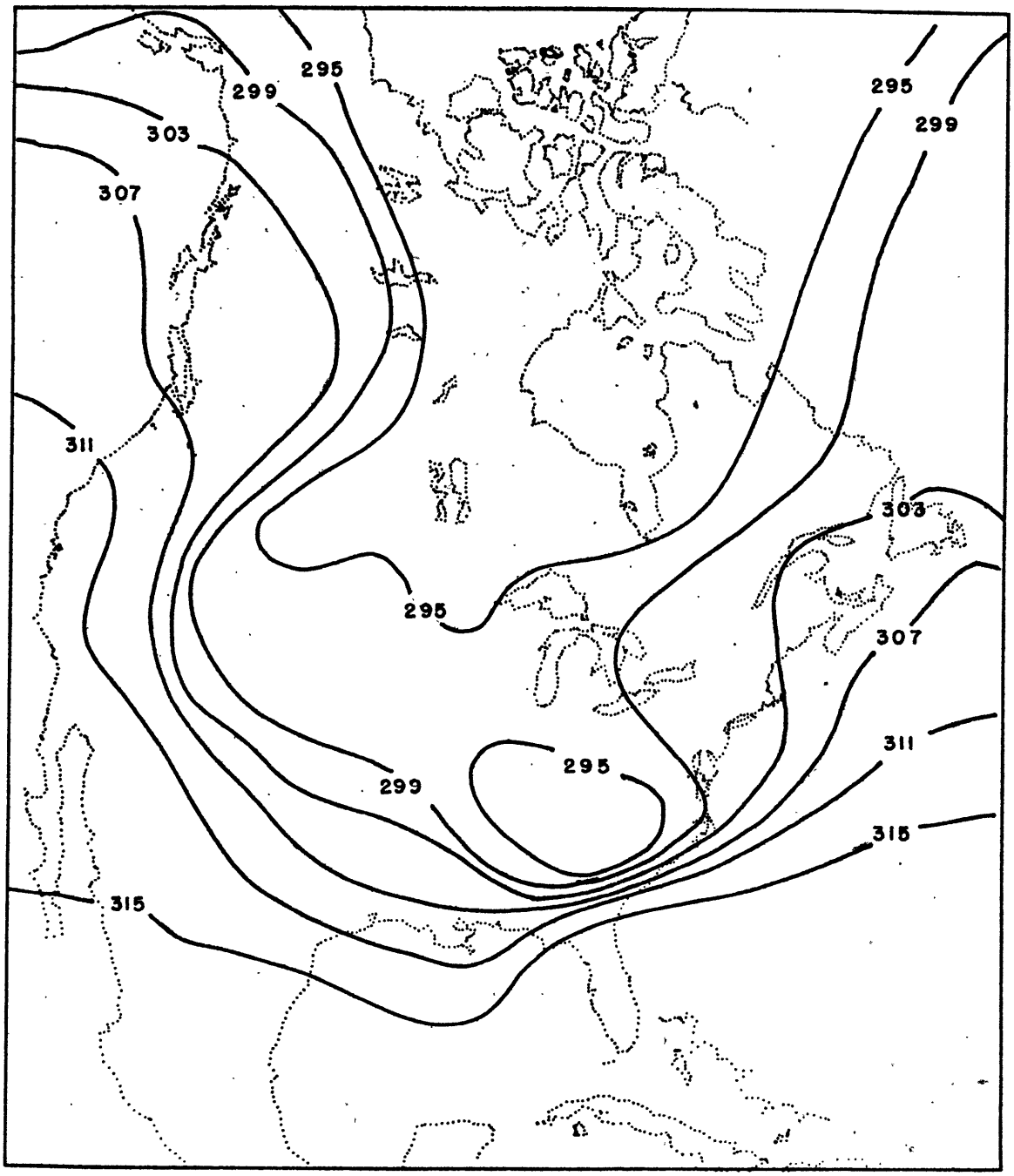

500mb TEMPERATURE 20 FEB 1964 00Z

FIG. 5.8

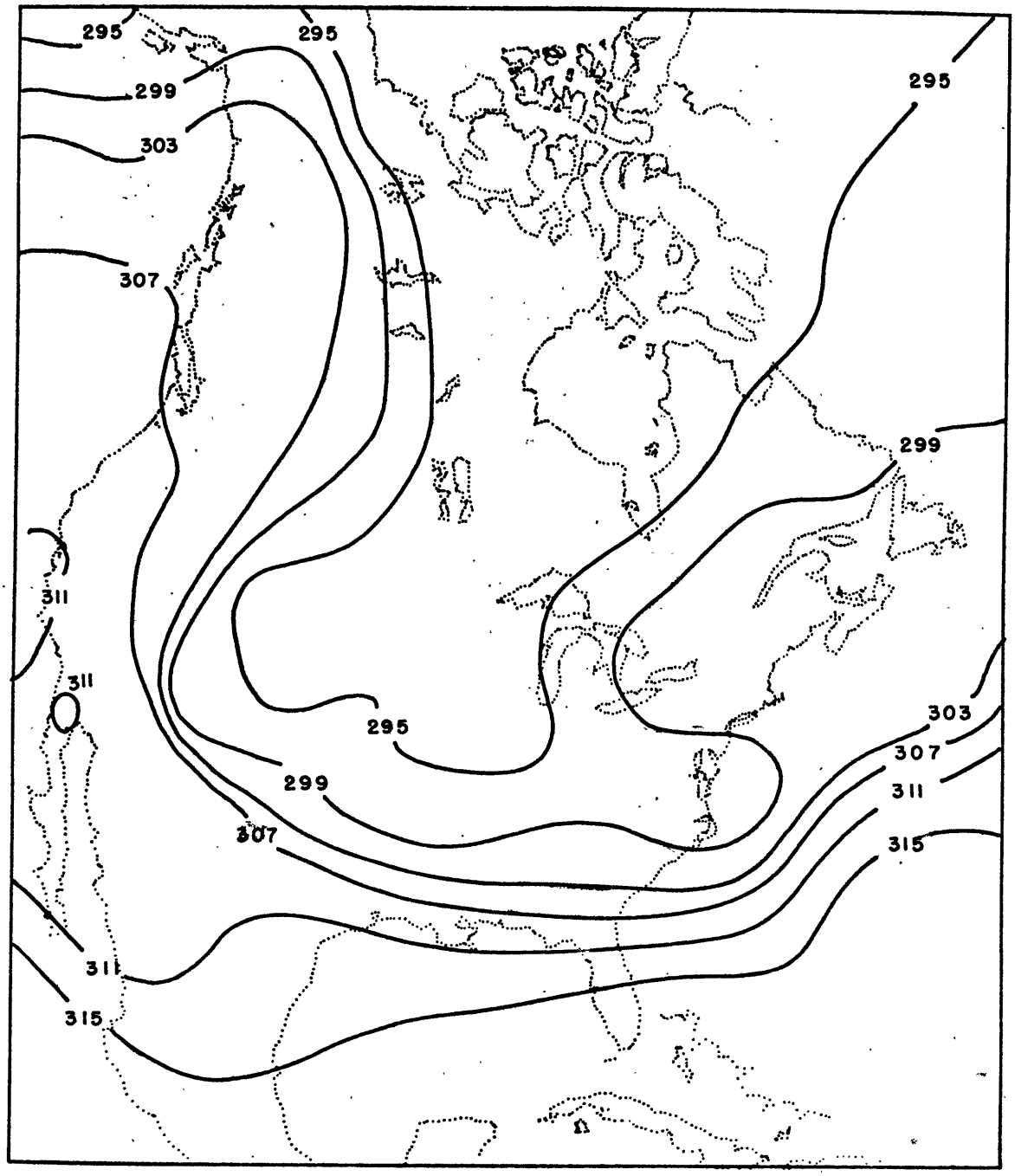

500mb TEMPERATURE 20 FEB 1964 12Z

FIG. 5.9

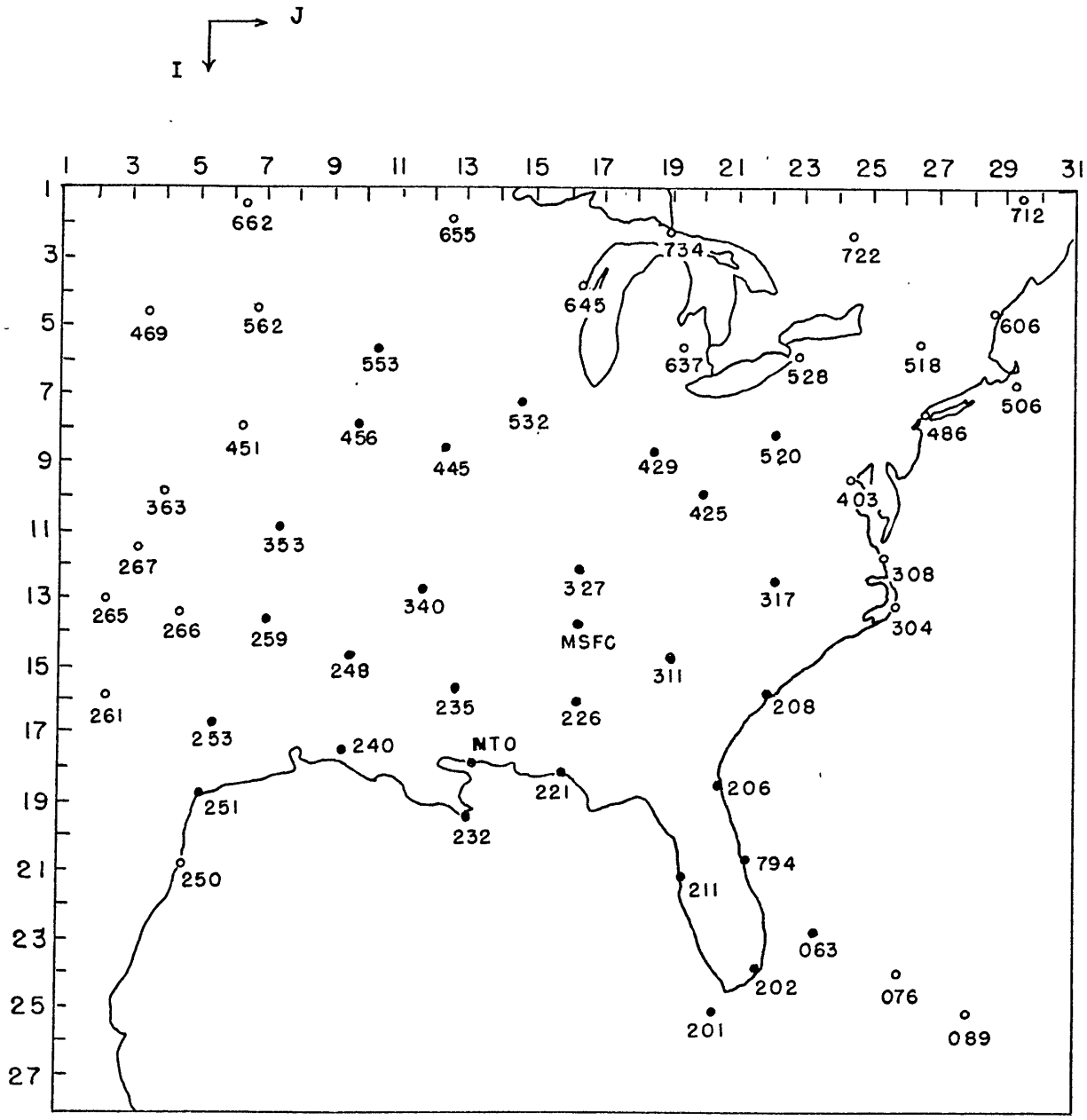
J
I
1 3 5 7 9 11 13 15 17 19 21 23 25 27 29 31
1 3 5 7 9 11 13 15 17 19 21 23 25 27
662
655
734
722
712
645
469
562
606
553
637
528
518
506
532
451
456
445
429
520
486
403
363
425
353
267
308
327
340
317
265
266
259
MSFC
304
248
311
261
235
226
208
253
240
NTO
221
206
251
232
794
250
211
063
202
076
201
089

FIG. 5.10

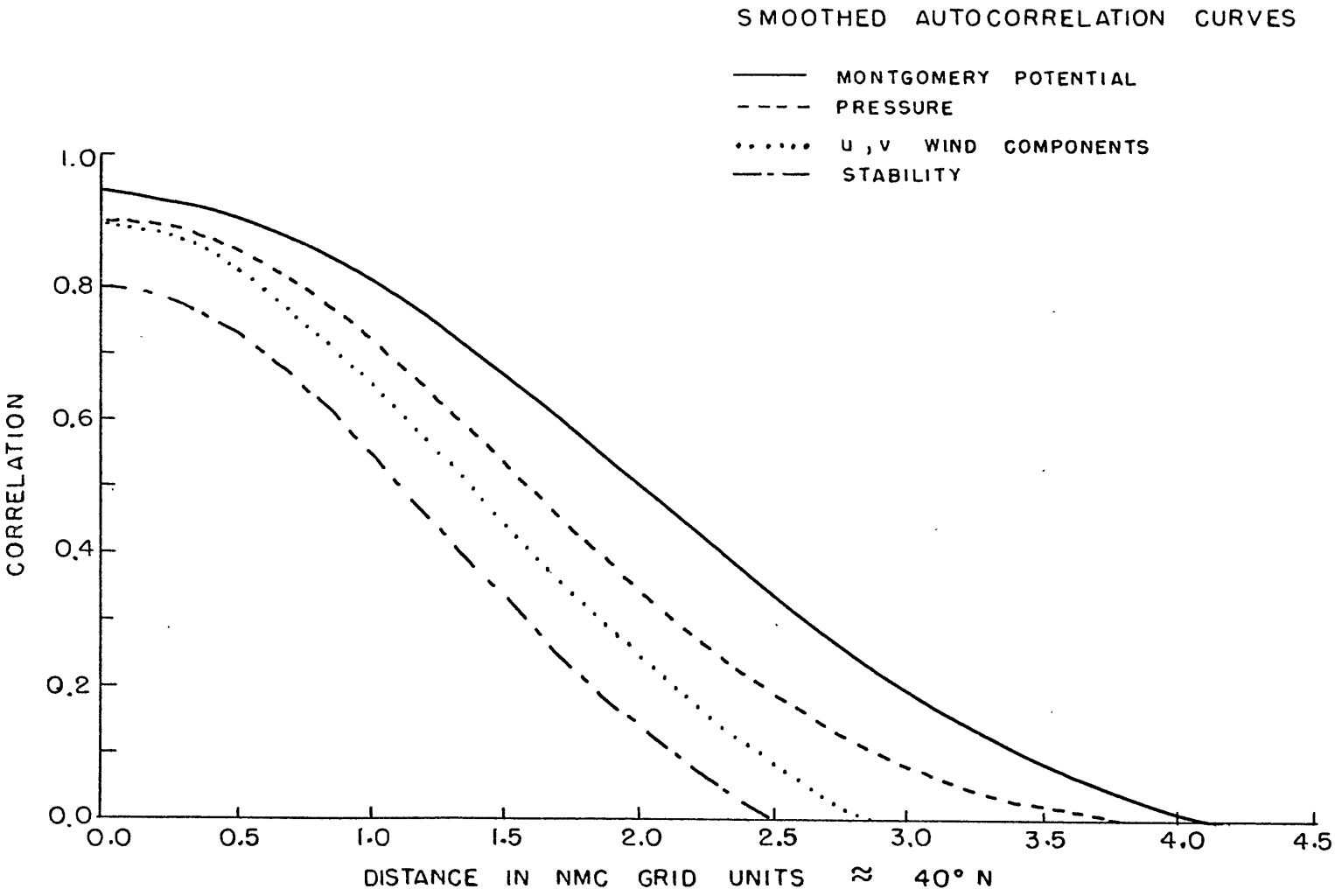
SMOOTHED AUTOCORRELATION CURVES
MONTGOMERY POTENTIAL
PRESSURE
U , V WIND COMPONENTS
STABILITY
CORRELATION
1.0
0.8
0.6
0.4
0.2
0.0
0.0
0.5
1.0
1.5
2.0
2.5
3.0
3.5
4.0
4.5
DISTANCE IN NMC GRID UNITS ≈ 40° N

FIG. 5.11

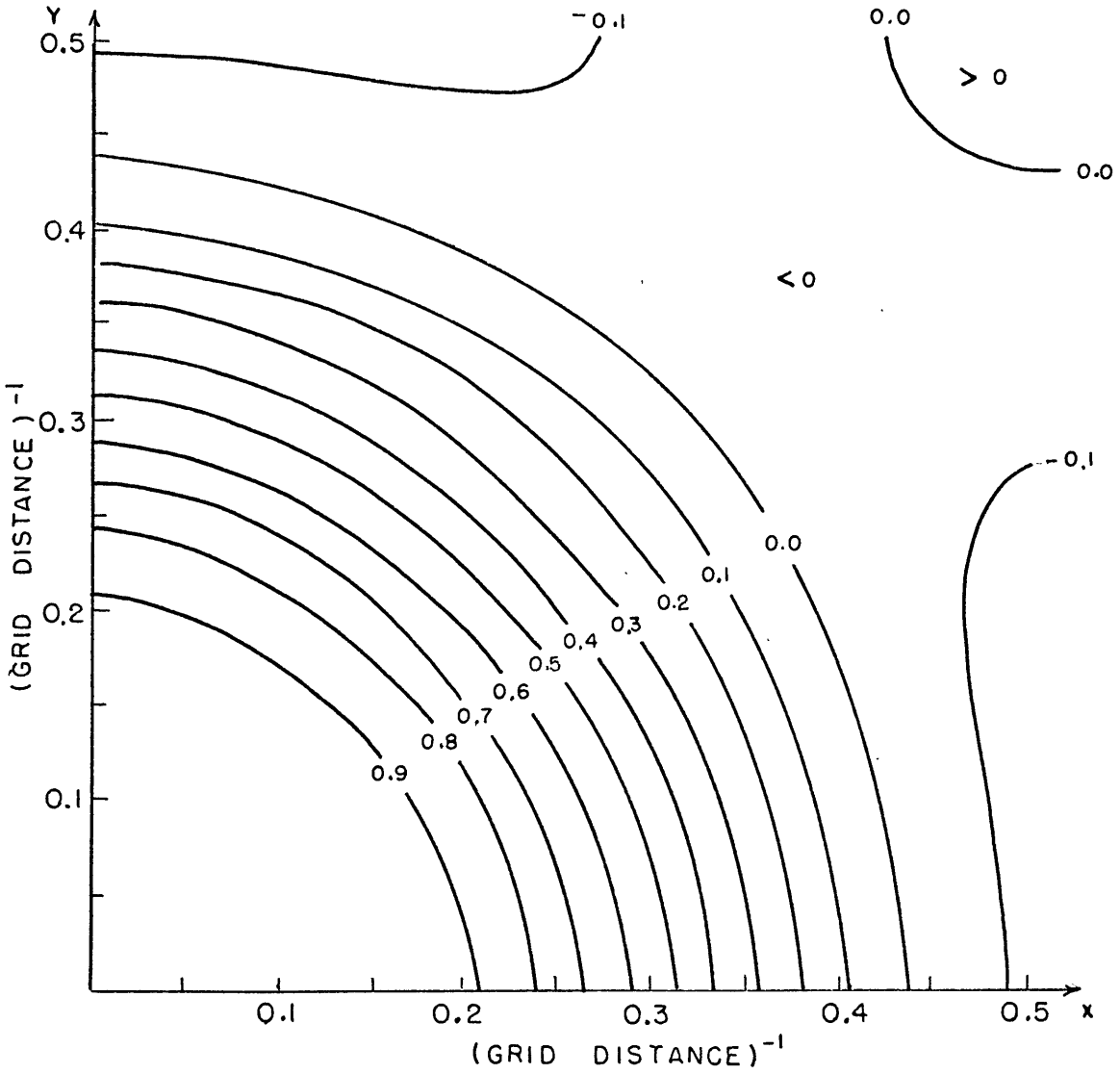

w_6	w_5	w_3	w_5	w_6
w_5	w_4	w_2	w_4	w_5
w_3	w_2	w_1	w_2	w_3
w_5	w_4	w_2	w_4	w_5
w_6	w_5	w_3	w_5	w_6

$w_1 = 0.279372$
$w_2 = 0.171943$
$w_3 = -0.006918$
$w_4 = 0.077458$
$w_5 = -0.024693$
$w_6 = -0.012940$

TWO DIMENSIONAL FILTER WEIGHTS AND DAMPING FREQUENCIES

FIG. 5.12

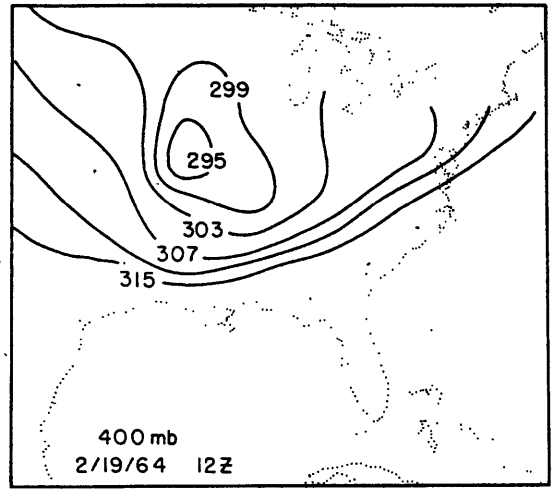

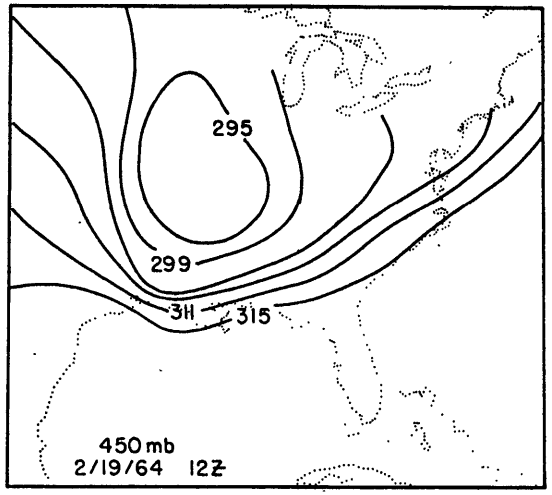

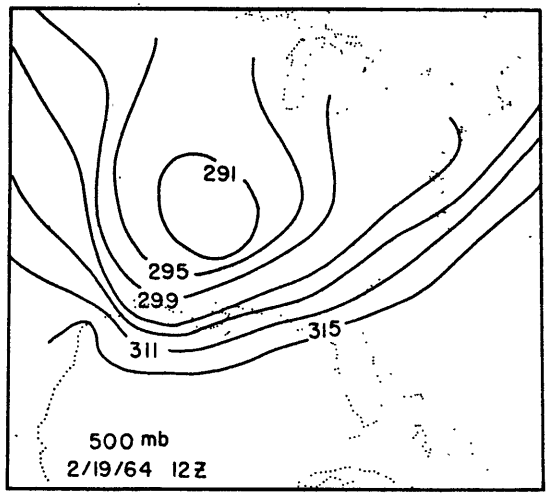

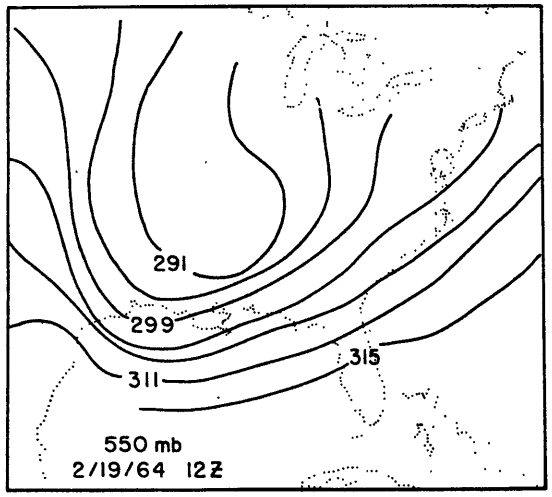

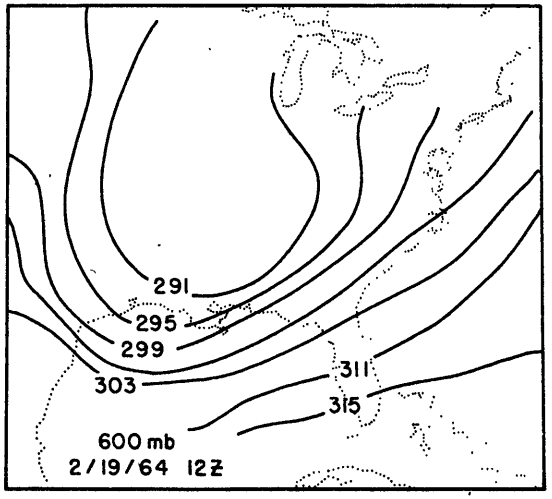

POTENTIAL TEMPERATURE ON CONSTANT PRESSURE SURFACE

(CONTOUR INTERVAL EVERY 4 °K)

FIG. 6.1

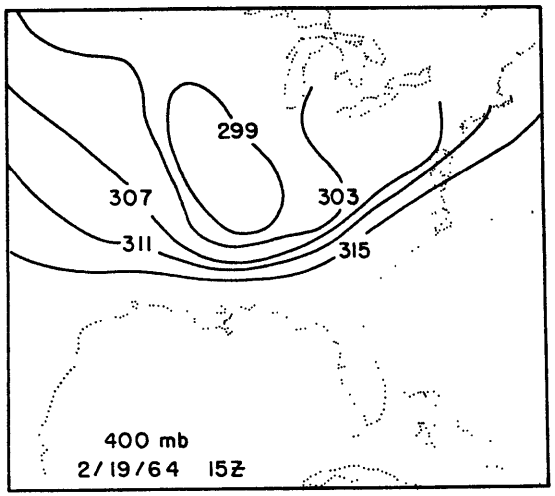

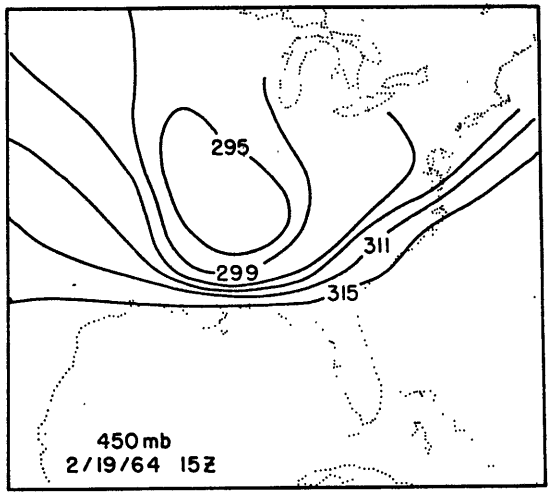

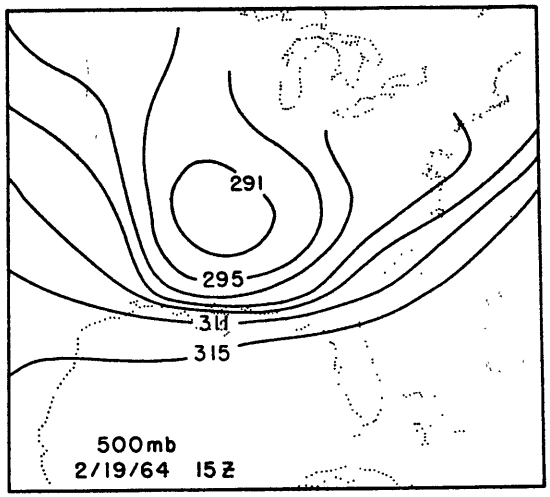

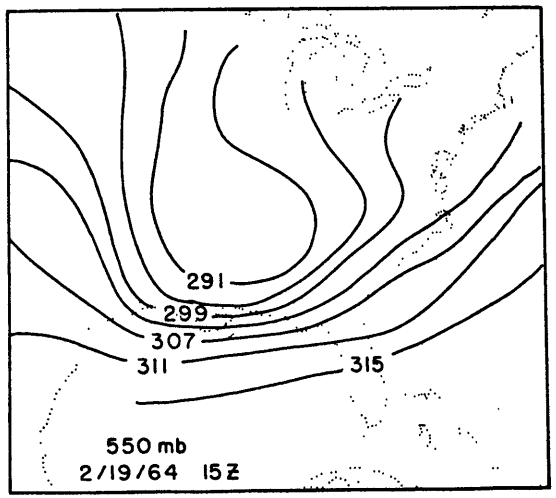

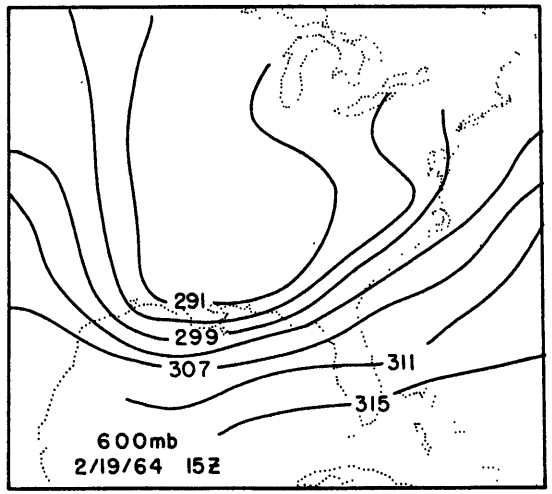

POTENTIAL TEMPERATURE ON
CONSTANT PRESSURE SURFACE

(CONTOUR INTERVAL EVERY 4 °K)

FIG. 6.2

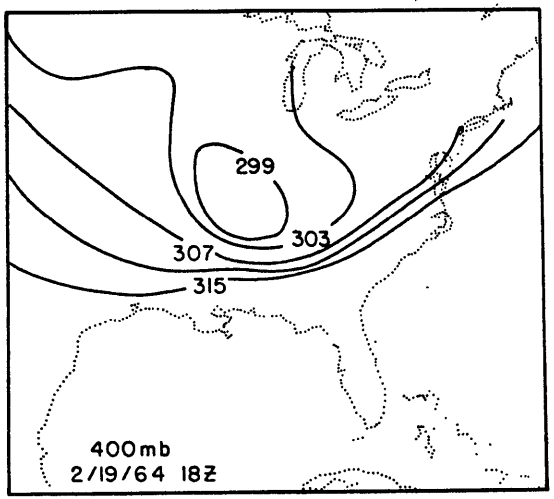

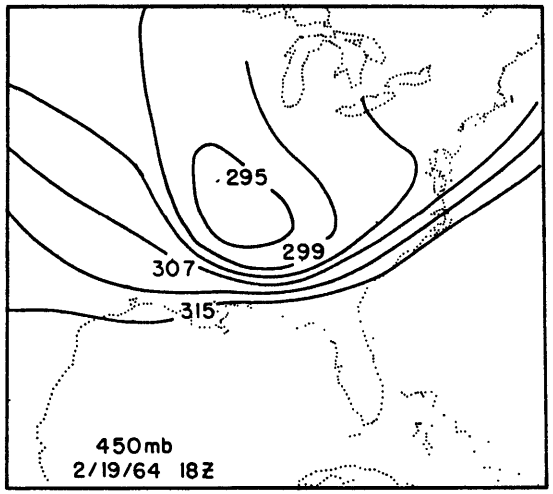

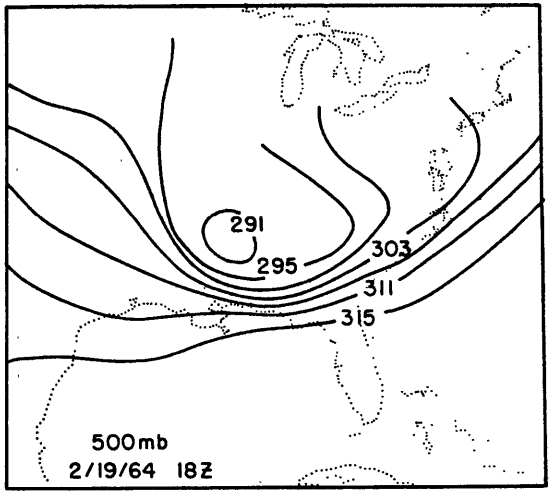

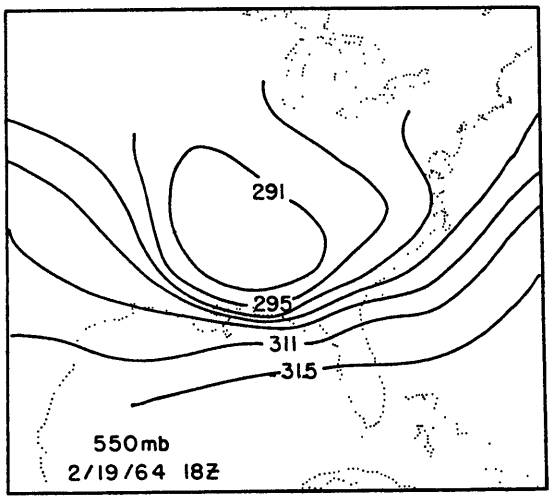

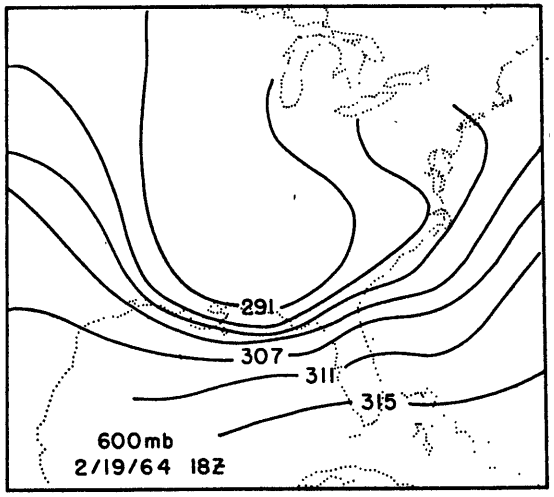

POTENTIAL TEMPERATURE ON
CONSTANT PRESSURE SURFACE

CONTOUR INTERVAL EVERY 4 °K

FIG. 6.3

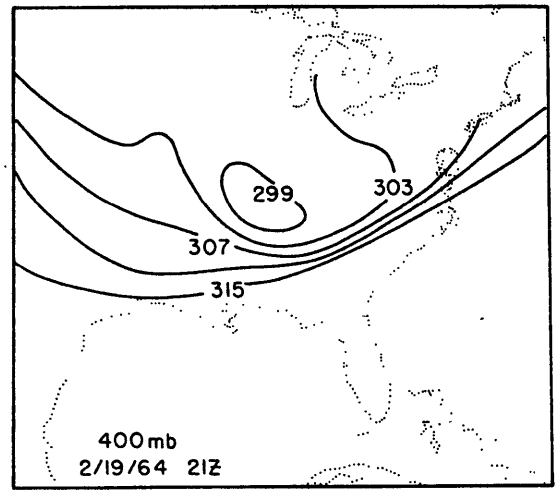

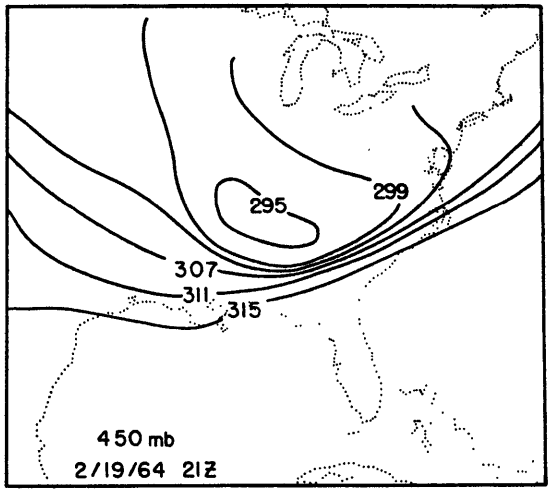

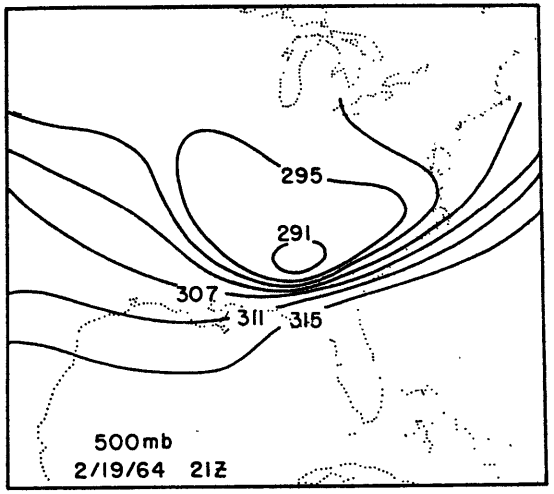

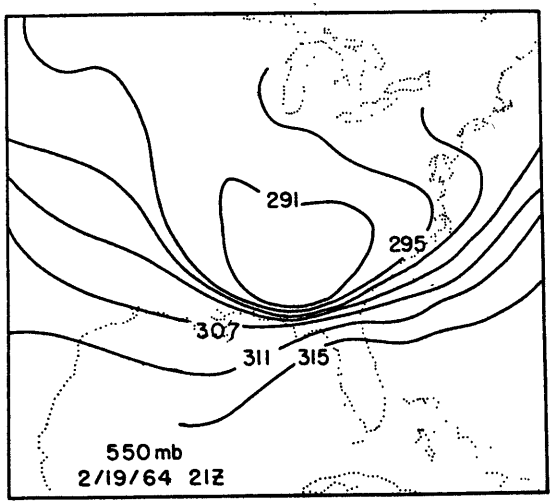

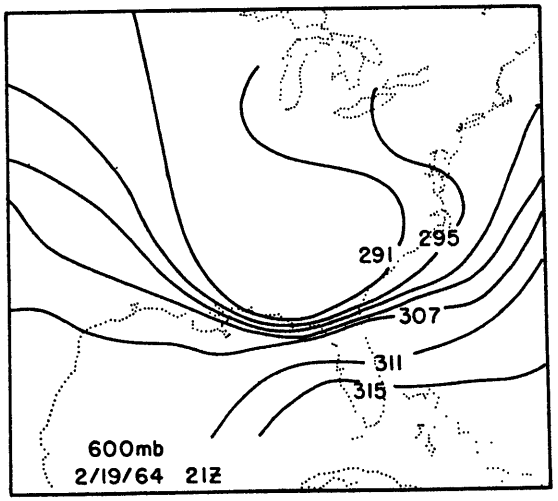

POTENTIAL TEMPERATURE ON CONSTANT PRESSURE SURFACE

(CONTOUR INTERVAL EVERY 4 °K)

FIG. 6.4

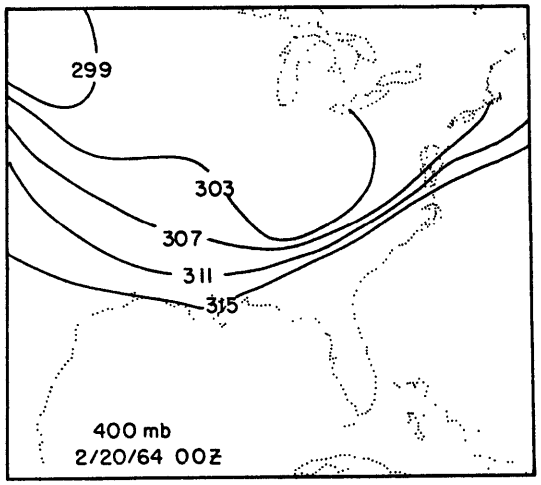

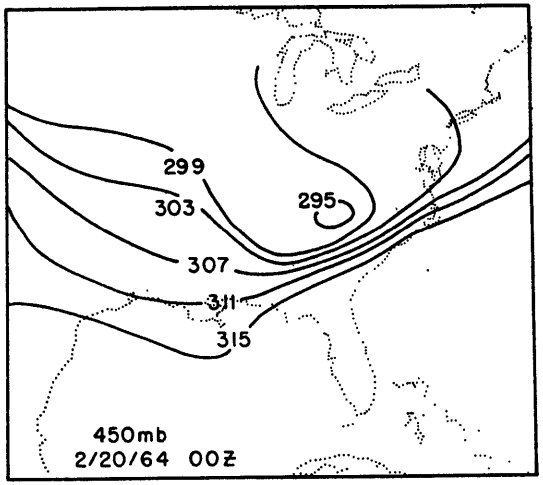

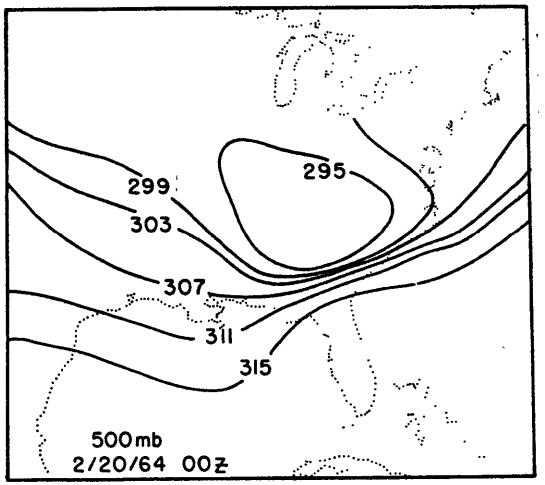

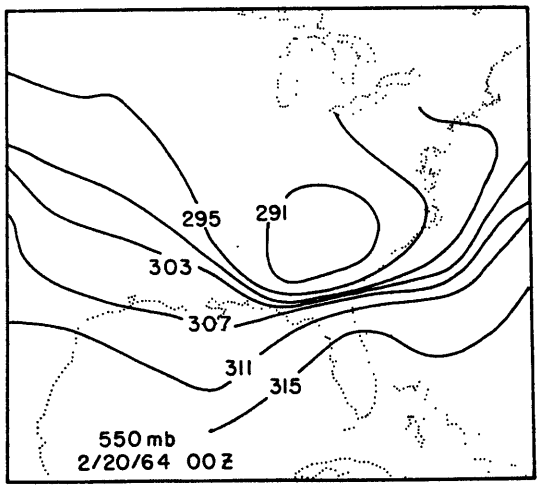

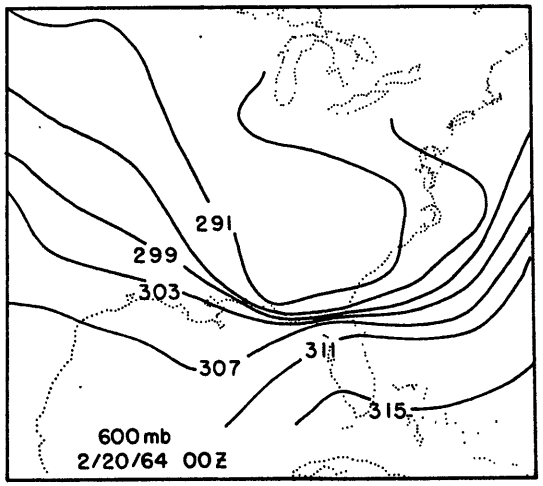

POTENTIAL TEMPERATURE ON
CONSTANT PRESSURE SURFACE

(CONTOUR INTERVAL EVERY 4 °K)

FIG. 6.5

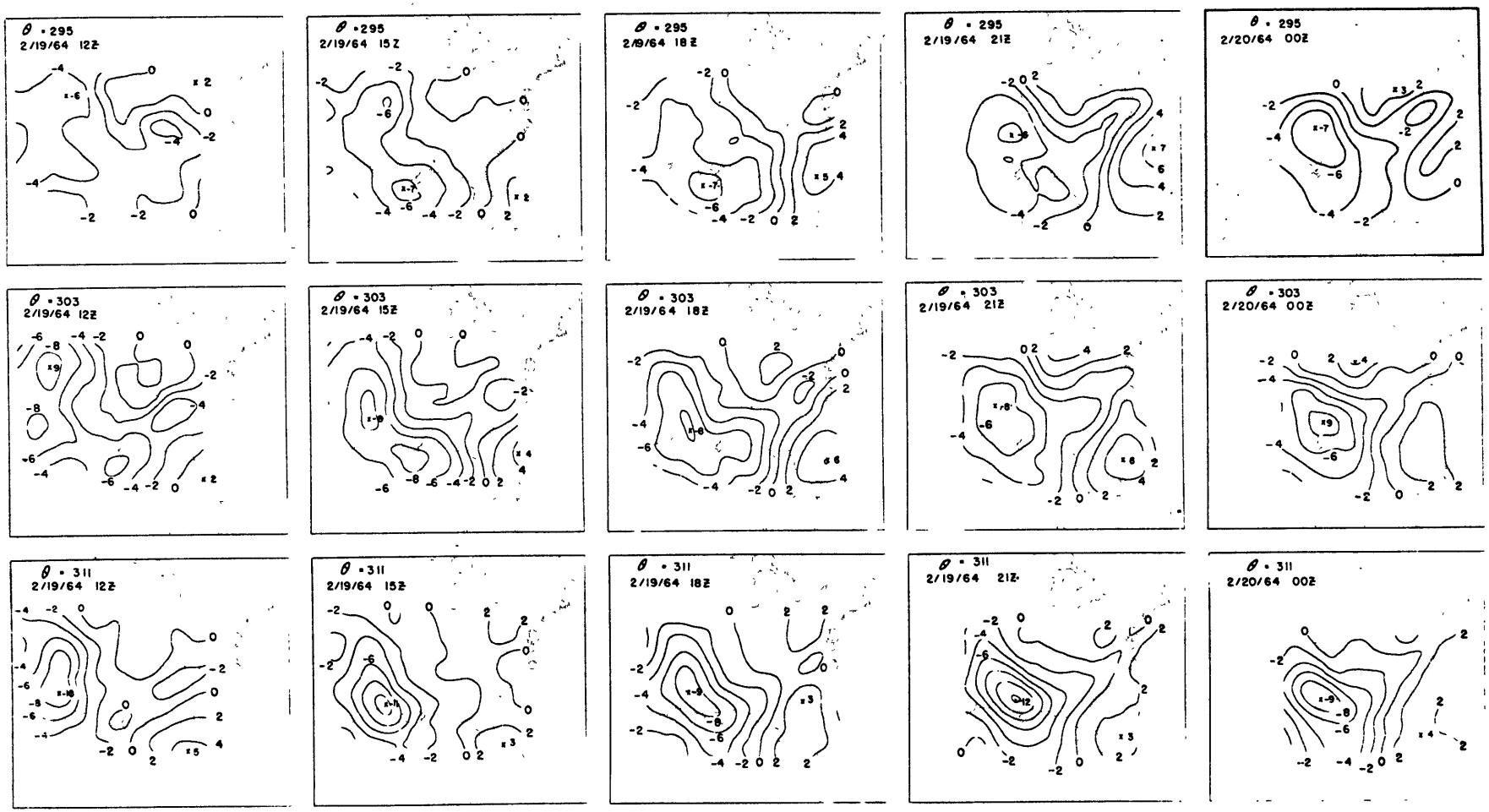

FIG. 6.6 6 HOUR AVERAGE KINEMATIC VERTICAL VELOCITIES IN CM SEC^{-1}

HORIZONTAL CONFLUENCE

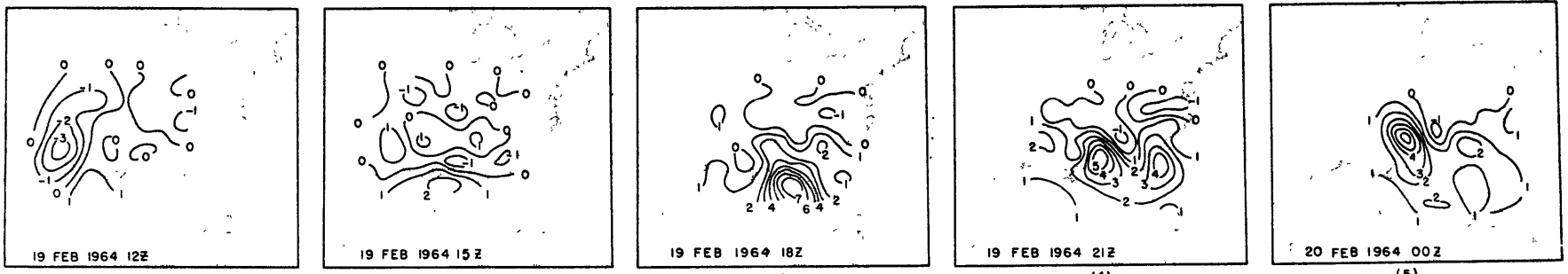

TWISTING

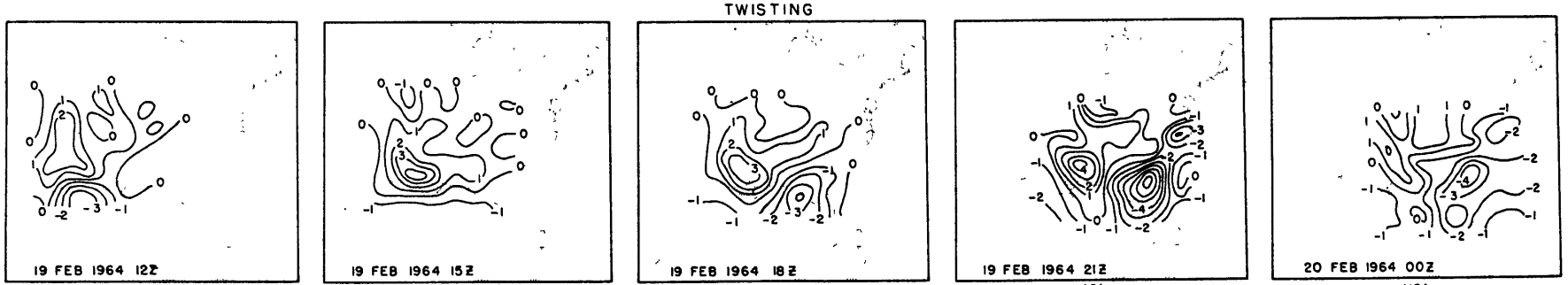

CONTRIBUTION OF HORIZONTAL CONFLUENCE AND TWISTING TO TWO DIMENSIONAL FRONTO-GENESIS BASED ON KINEMATIC TRAJECTORIES θ = 303 °K

UNITS: °C (100 KM)$^{-1}$ (3HRS)$^{-1}$

FIG. 6.7

CALCULATED FRONTOGENESIS

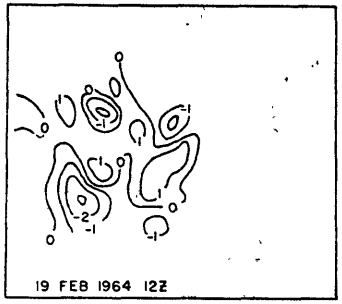

(1)

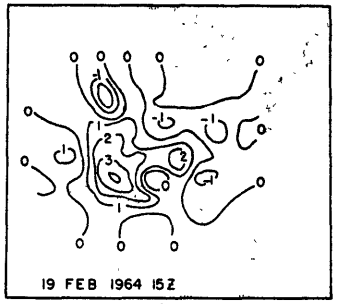

(2)

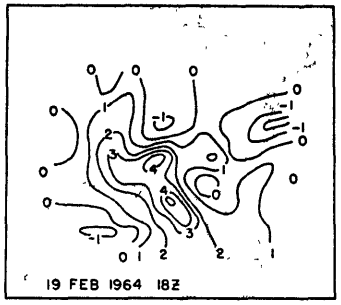

(3)

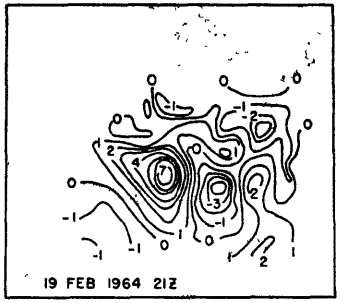

(4)

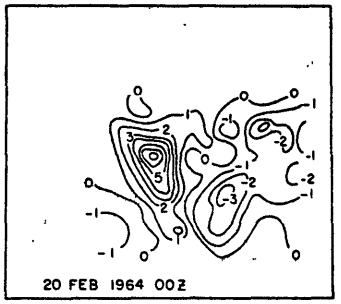

(5)

OBSERVED FRONTOGENESIS

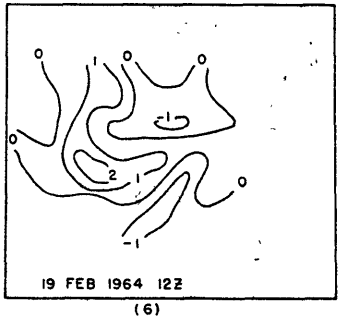

(6)

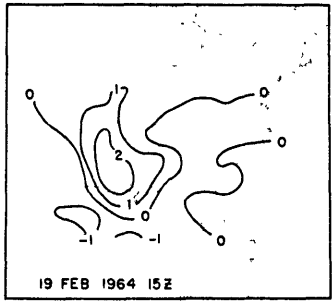

(7)

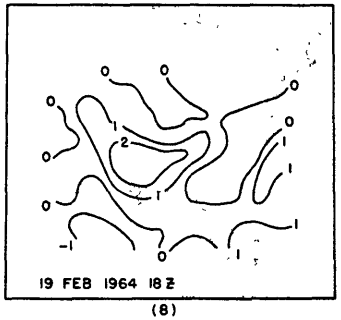

(8)

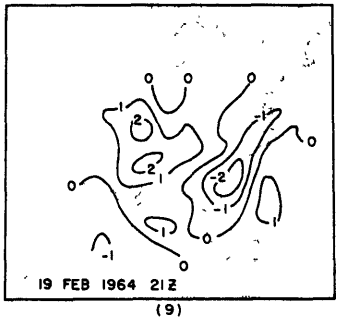

(9)

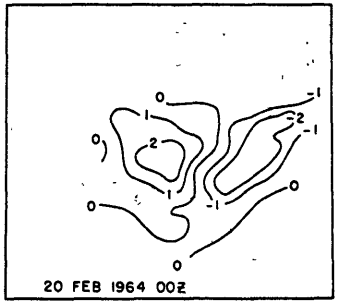

(10)

OBSERVED AND CALCULATED FRONTOGENESIS IN TWO DIMENSIONS BASED ON KINEMATIC TRAJECTORIES θ = 303 °K

UNITS: °C(100KM)$^{-1}$ (3HRS)$^{-1}$

FIG. 6.8

SCHEMATIC
TWO DIMENSIONAL FRONTOGENESIS

GROWTH STAGE

12Z – 21Z 2/19/64 , θ = 303

SLIGHT C^- MODERATE T^+	NEUTRAL C NEUTRAL T
LARGE C^+ MODERATE T^+	MODERATE C^+ LARGE T^-

FIG. 6.9a

QUASI – STATIONARY STAGE

21Z 2/19/64 – 00Z 2/20/64 θ = 303

LARGE C^+ MODERATE T^+	MODERATE C^+ LARGE T^-
LARGE C^+ SLIGHT T^+	SLIGHT C^+ MODERATE T^-

FIG. 6.9b

(SEE TEXT FOR EXPLANATION)

AGEOSTROPHIC CONTRIBUTION

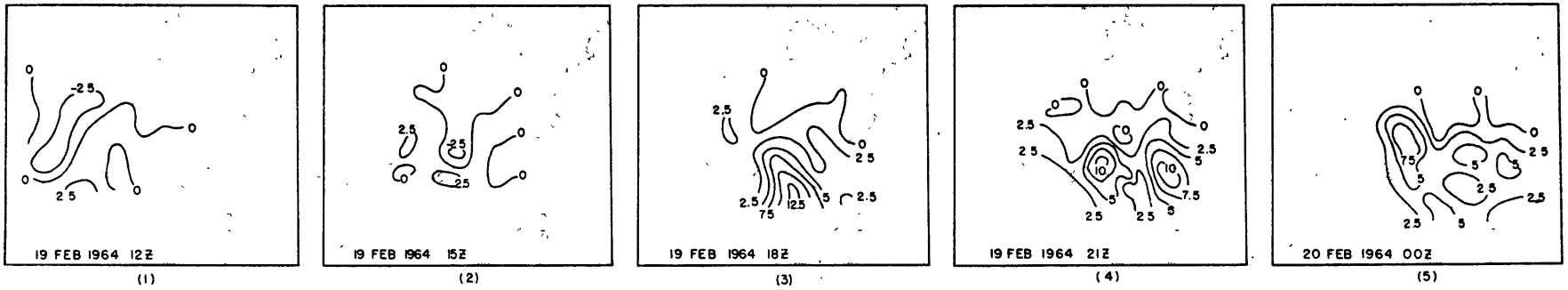

VERTICAL SHEAR OF VERTICAL VELOCITY CONTRIBUTION

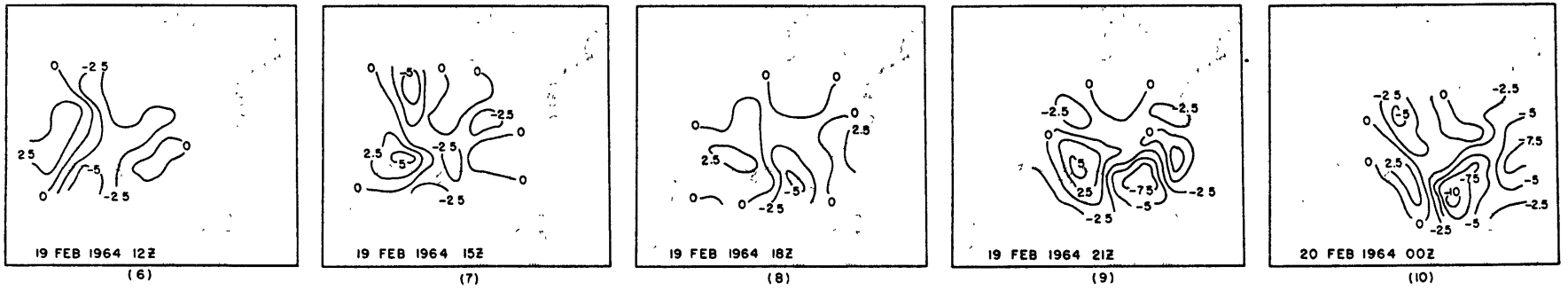

AGEOSTROPHIC AND VERTICAL SHEAR OF VERTICAL VELOCITY CONTRIBUTIONS TO THREE DIMENSIONAL FRONTOGENESIS ON θ = 303

UNITS: °C $(KM)^{-1}(3\,HRS)^{-1}$

FIG. 6.10

CALCULATED FRONTOGENESIS

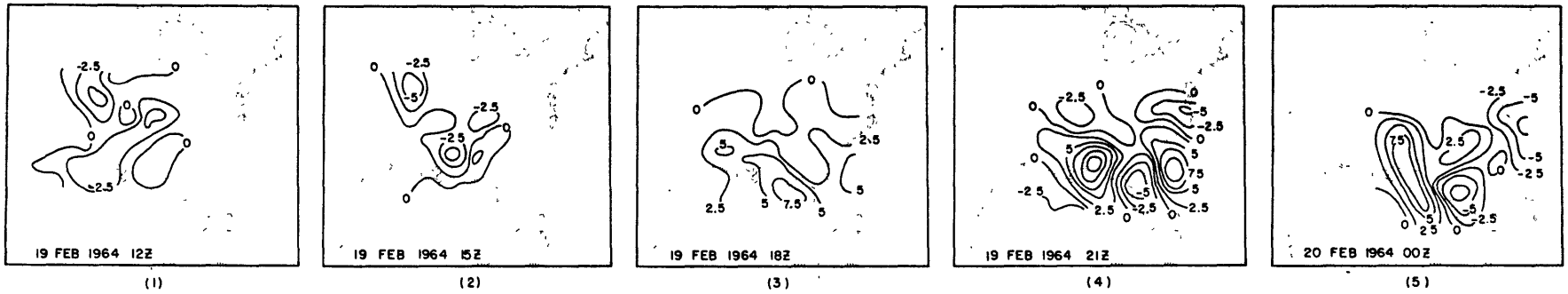

CALCULATED AND OBSERVED THREE DIMENSIONAL FRONTOGENESIS ON θ = 303 °K

UNITS : °C $(KM)^{-1}$ $(3HRS)^{-1}$

FIG. 6.11

SCHEMATIC

THREE DIMENSIONAL FRONTOGENESIS

$\theta \doteq 303$

2/19/64 12Z — 2/20/64 00Z

MODERATE F^+ MODERATE SW^+ SLIGHT A^+	SLIGHT F^+ NEUTRAL SW SLIGHT A^-
LARGE TO MODERATE F^+ MODERATE SW^+ LARGE TO MODERATE A^+	MODERATE F^- LARGE TO MODERATE SW^- MODERATE A^+

FIG. 6.12

(SEE TEXT FOR EXPLATION)

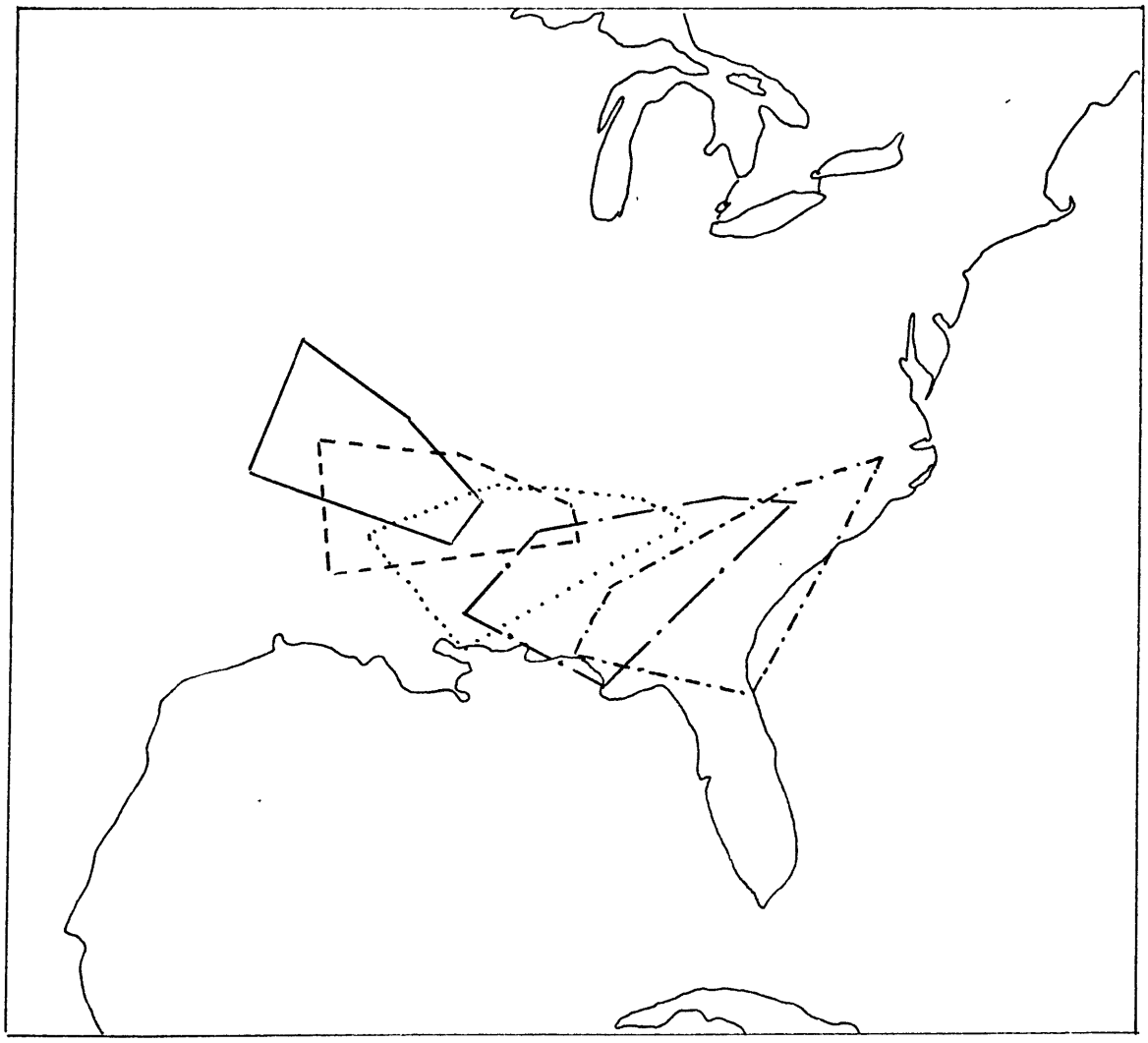

	AREA	θ = 295
——— 2/19/64 12Z	416	AREAS ENCLOSED BY
- - - - - - 2/19/64 15Z	438	TRAJECTORY POSITIONS
. . . . . 2/19/64 18Z	479	ENCOMPASSING BAROCLINIC
—·—·— 2/19/64 21Z	543	ZONE
-·-·-·-·- 2/20/64 00Z	613	

FIG. 6.13

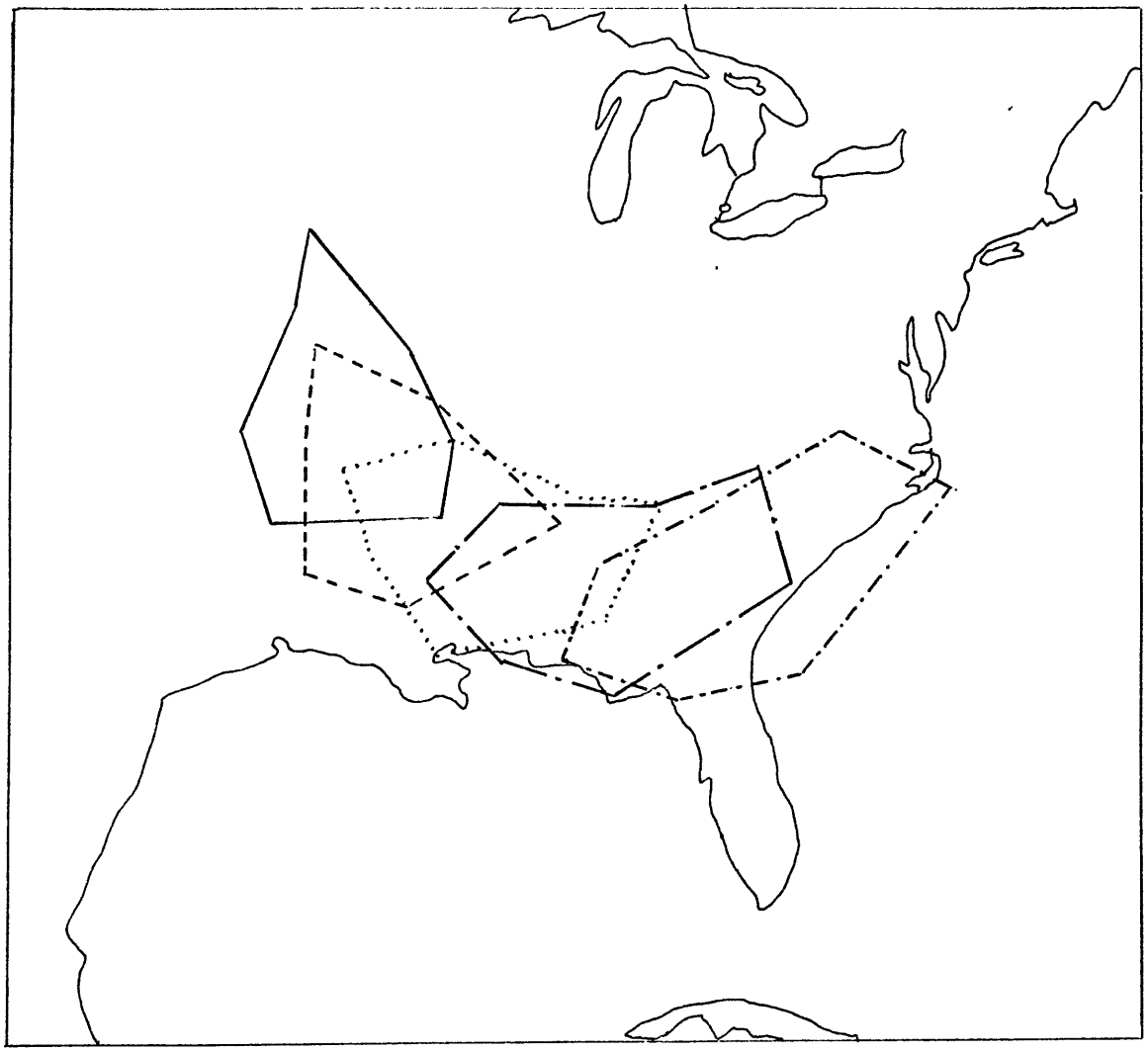

LEGEND IDENTICAL TO FIG. 6.13

θ = 303

AREA		
696	2/19/64	12Z
709	2/19/64	15Z
682	2/19/64	18Z
890	2/19/64	21Z
988	2/20/64	00Z

FIG. 6.14

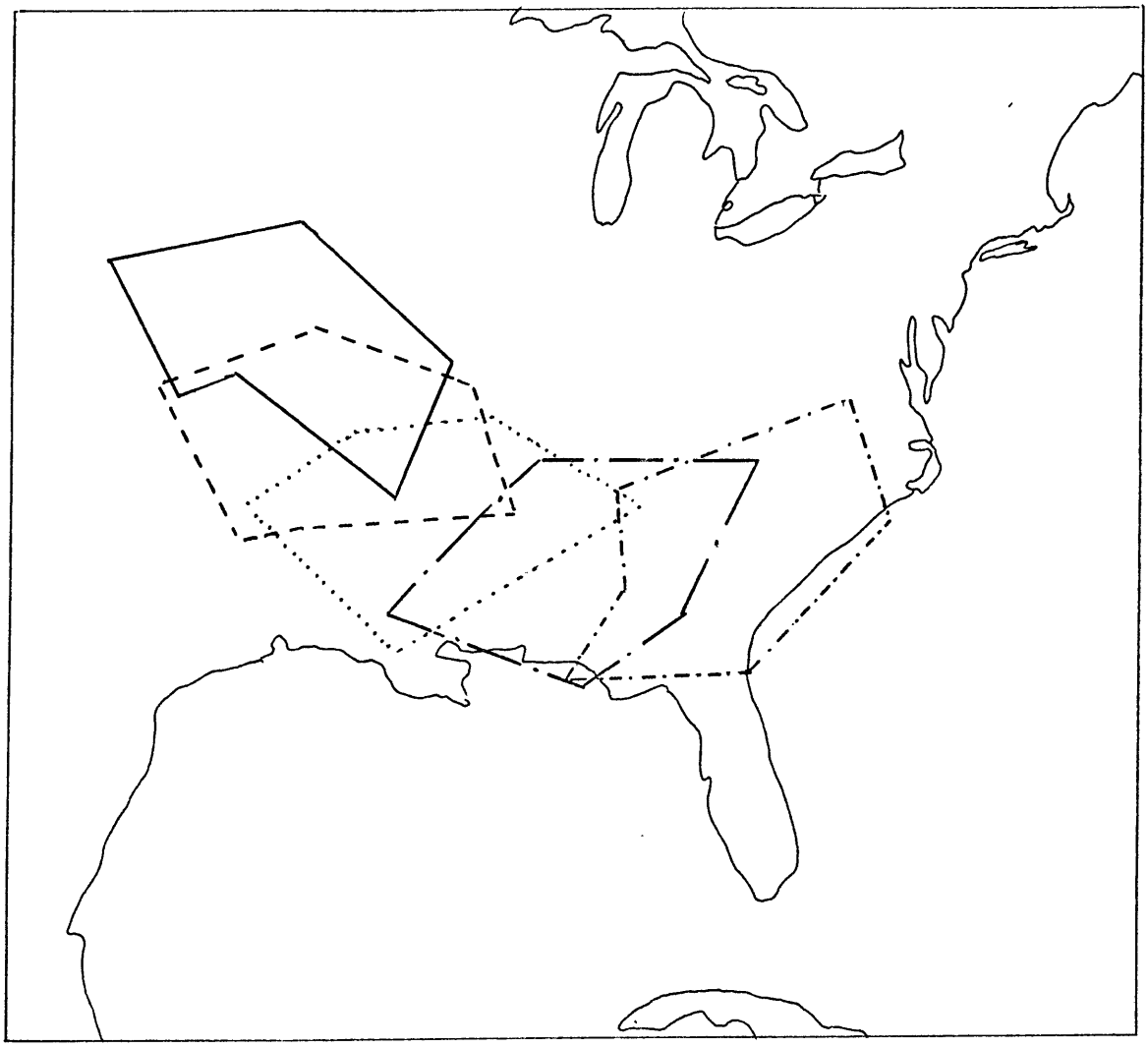

LEGEND IDENTICAL TO FIG. 6.13

θ = 311

AREA		
864	2/19/64	12Z
883	2/19/64	15Z
896	2/19/64	18Z
897	2/19/64	21Z
920	2/20/64	00Z

FIG. 6.15

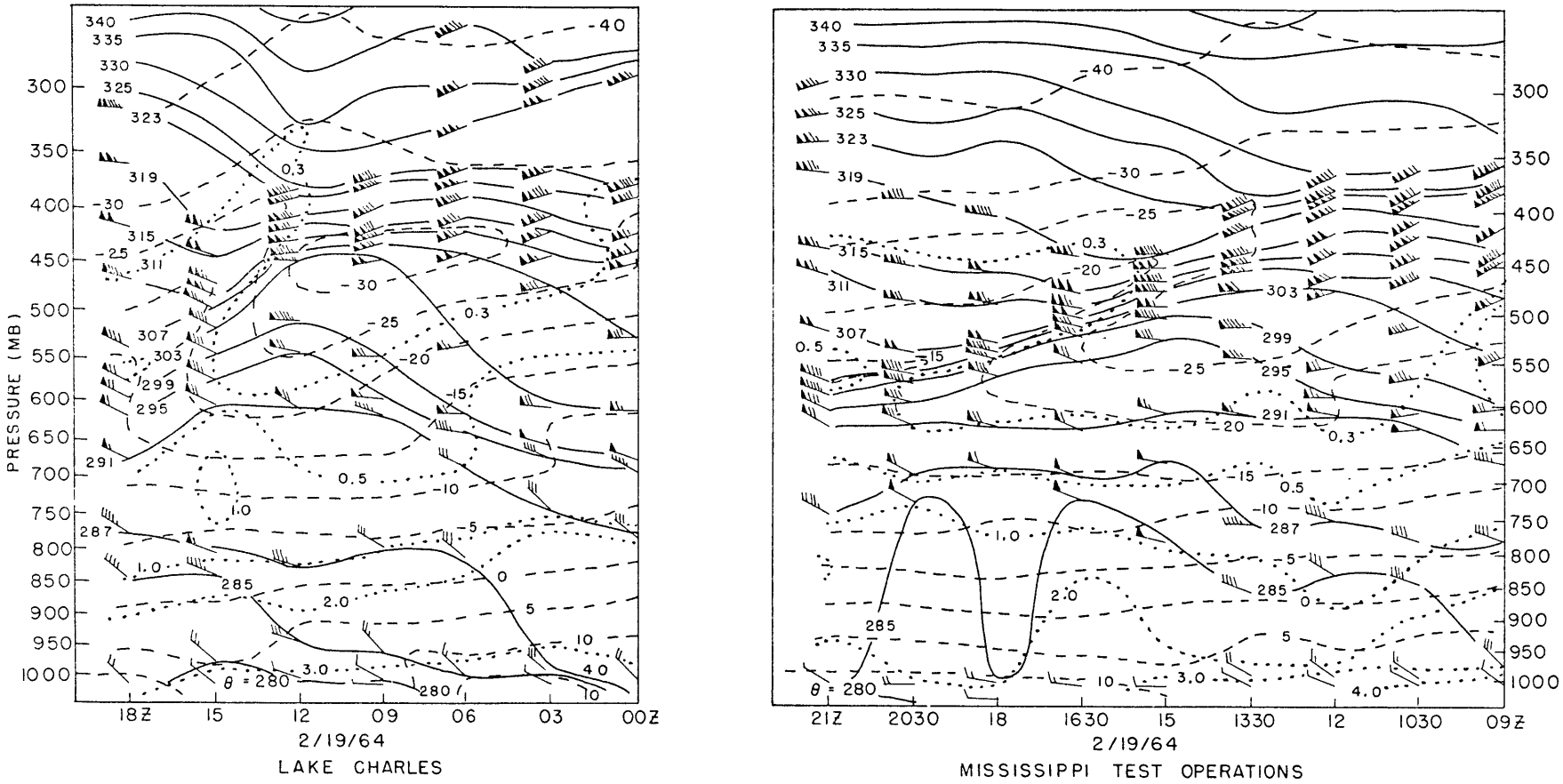

STATION TIME SECTIONS ILLUSTRATING PASSAGE OF BAROCLINIC ZONE

—— POTENTIAL TEMPERATURE IN °K
– – – TEMPERATURE IN °C
••••• WATER VAPOR MIXING RATIO IN G KG^{-1}

= 50 KNOTS
= 10 KNOTS (EXPLANATION IN TEXT)
= 5 KNOTS

FIG. 6.16

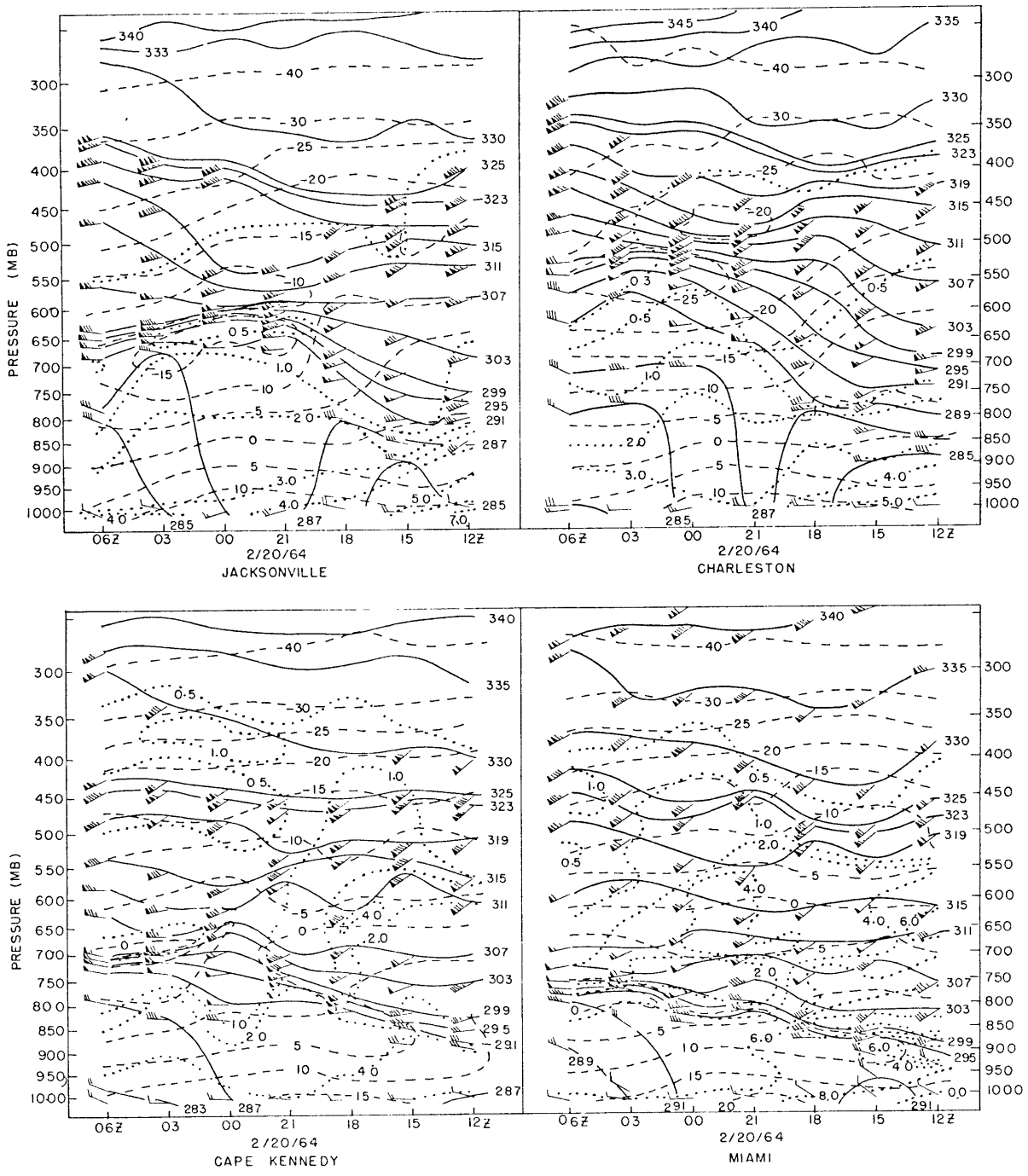
PRESSURE (MB)
JACKSONVILLE
2/20/64
CHARLESTON
2/20/64
CAPE KENNEDY
2/20/64
MIAMI
2/20/64
06Z 03 00 21 18 15 12Z
STATION TIME SECTIONS ALONG APPROXIMATELY 80° W
POTENTIAL TEMPERATURE IN °K
TEMPERATURE IN °C
WATER VAPOR MIXING RATIO IN G KG⁻¹
= 50 KNOTS
= 10 KNOTS
= 5 KNOTS
(EXPLANATION IN TEXT)

FIG. 6.17

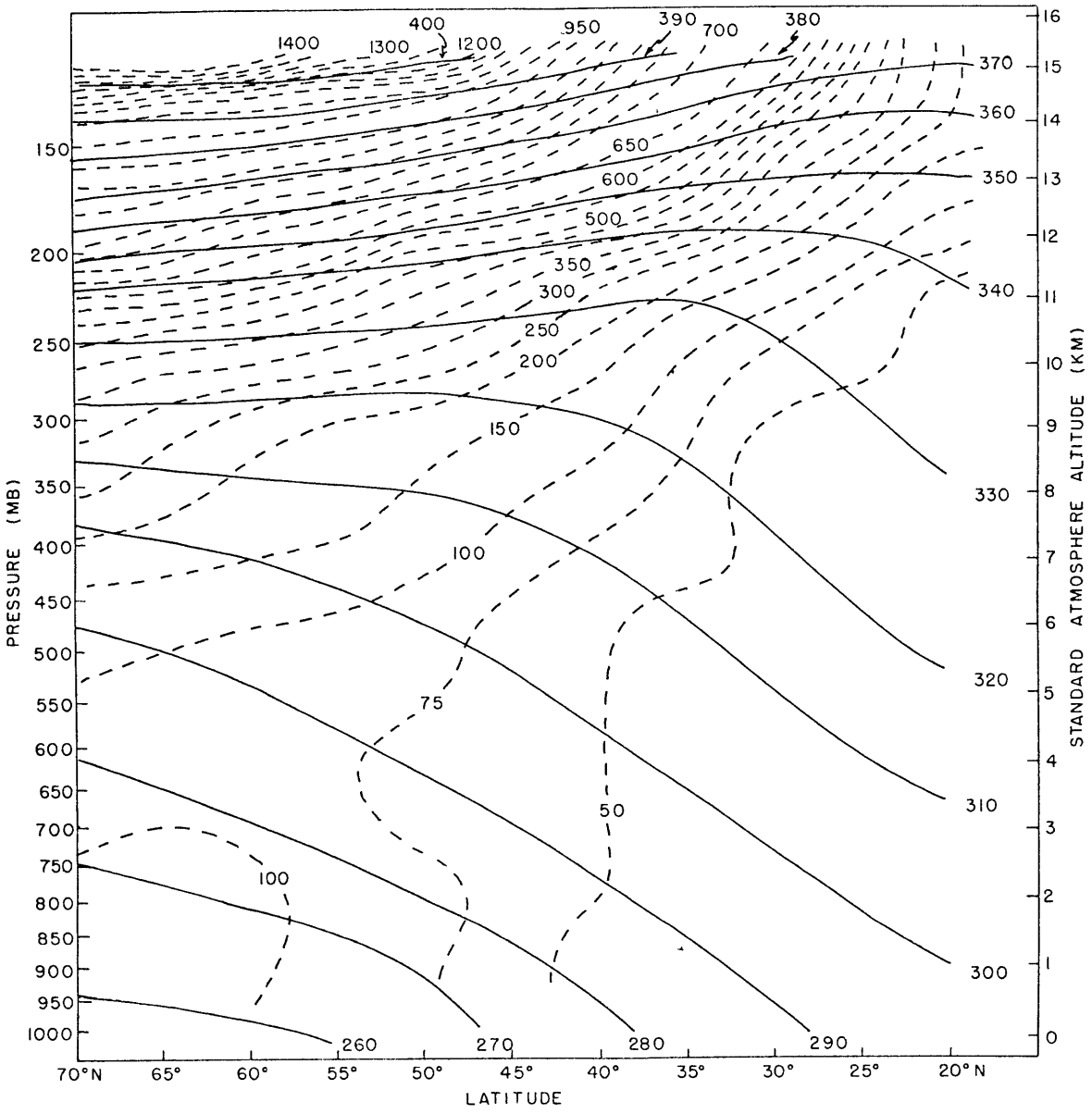

CROSS SECTION OF POTENTIAL VORTICITY AND POTENTIAL TEMPERATURE CALCULATED FROM LONGITUDINALLY AVERAGED DATA GIVEN BY PETTERSSEN (1950).

– – – – POTENTIAL VORTICITY x 10^{-7} °C $mb^{-1}sec^{-1}$

——— POTENTIAL TEMPERATURE °K

FIG. 7.1

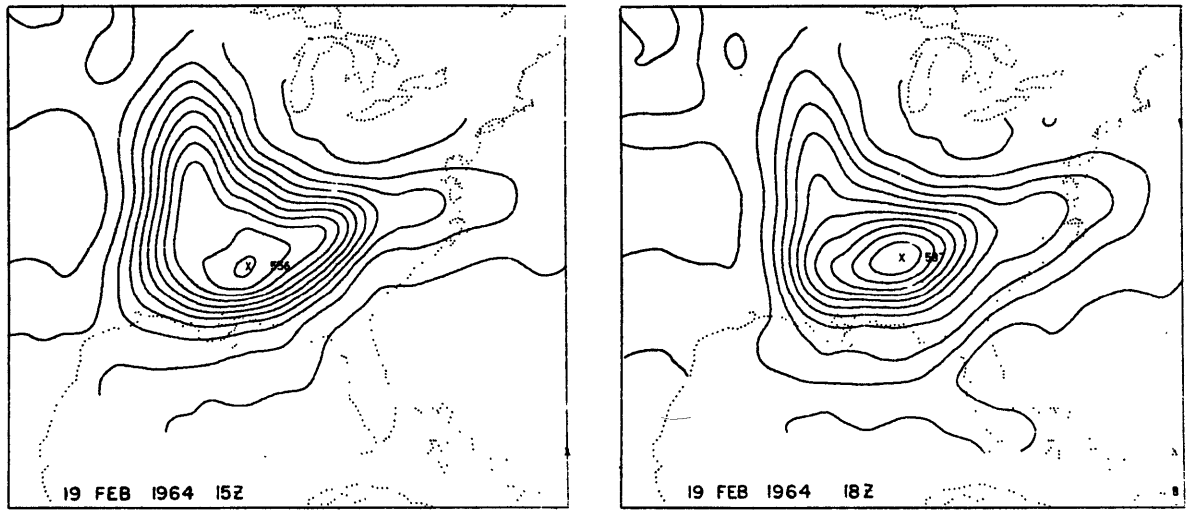

CONTOURS EVERY 50 X 10^{-7} °C mb^{-1} sec^{-1}

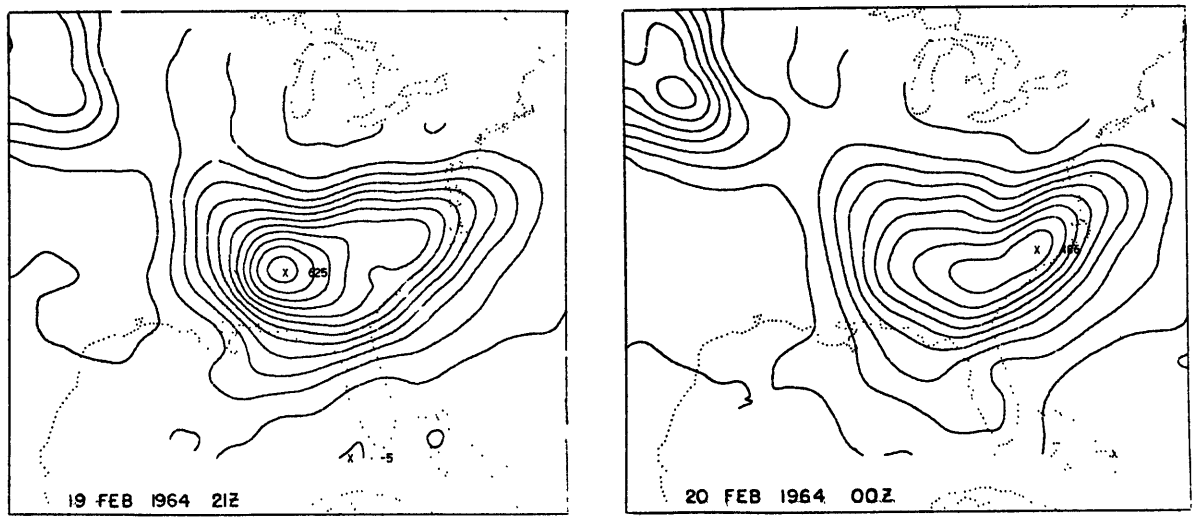

POTENTIAL VORTICITY x 10^{-7} °C mb^{-1} sec^{-1} on θ = 303 °K

FIG. 7.2

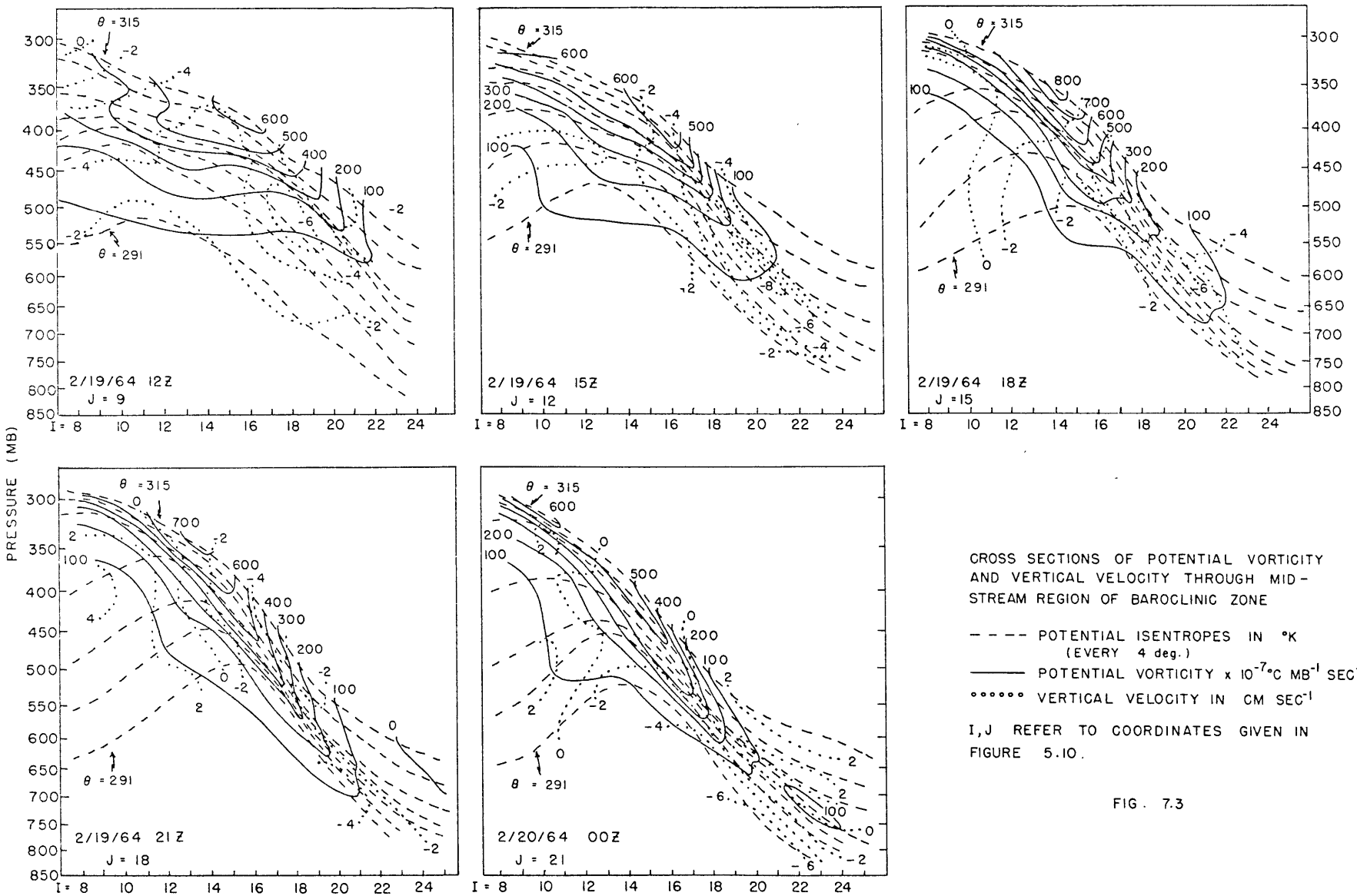

CROSS SECTIONS OF POTENTIAL VORTICITY AND VERTICAL VELOCITY THROUGH MID-STREAM REGION OF BAROCLINIC ZONE

– – – – POTENTIAL ISENTROPES IN °K (EVERY 4 deg.)

——— POTENTIAL VORTICITY x 10^{-7} °C MB^{-1} SEC^{-1}

°°°°°° VERTICAL VELOCITY IN CM SEC^{-1}

I,J REFER TO COORDINATES GIVEN IN FIGURE 5.10.

FIG. 7.3

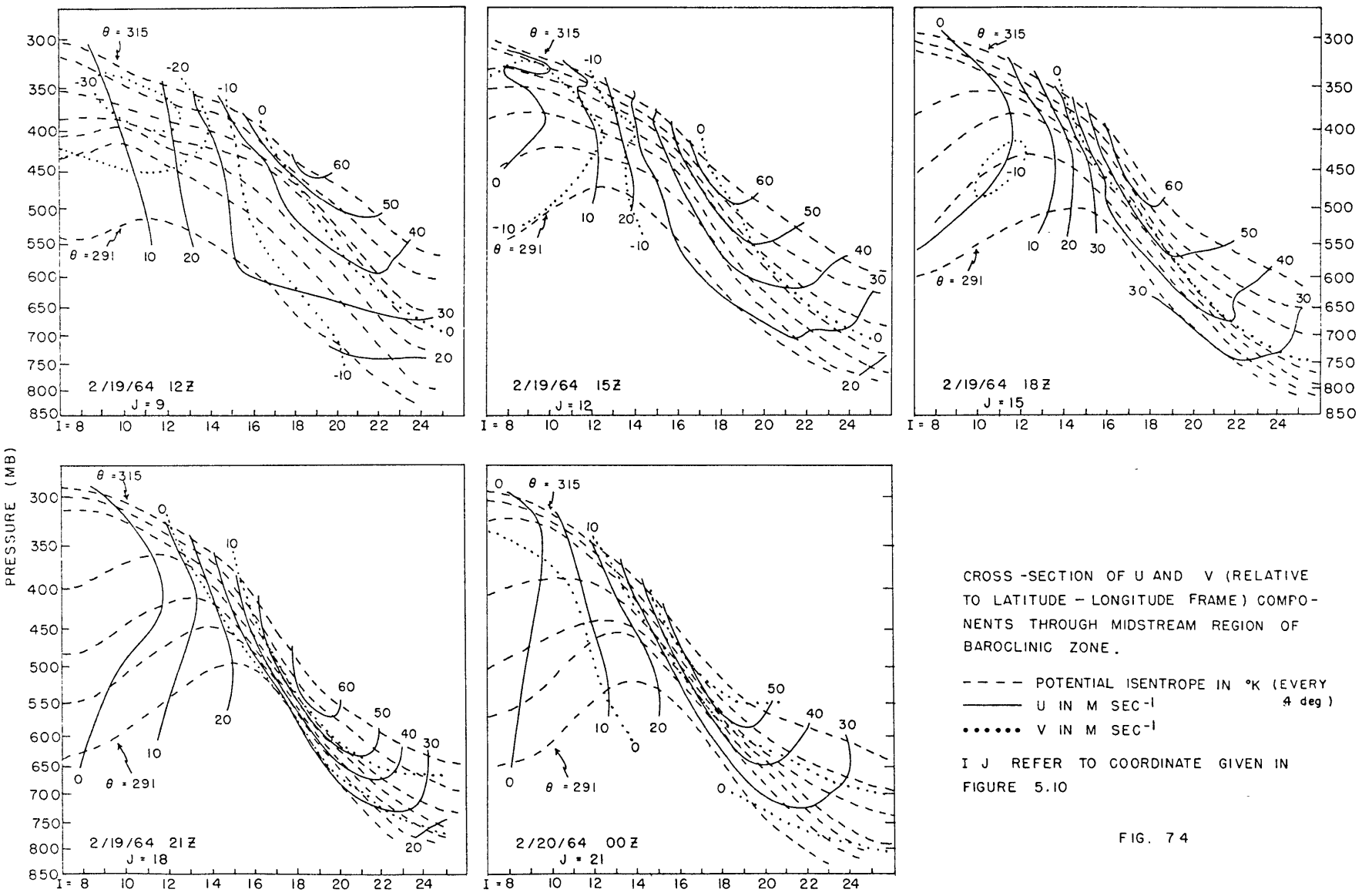

CROSS-SECTION OF U AND V (RELATIVE TO LATITUDE – LONGITUDE FRAME) COMPONENTS THROUGH MIDSTREAM REGION OF BAROCLINIC ZONE.

– – – – POTENTIAL ISENTROPE IN °K (EVERY 4 deg)
——— U IN M SEC^{-1}
••••• V IN M SEC^{-1}

I J REFER TO COORDINATE GIVEN IN FIGURE 5.10

FIG. 74

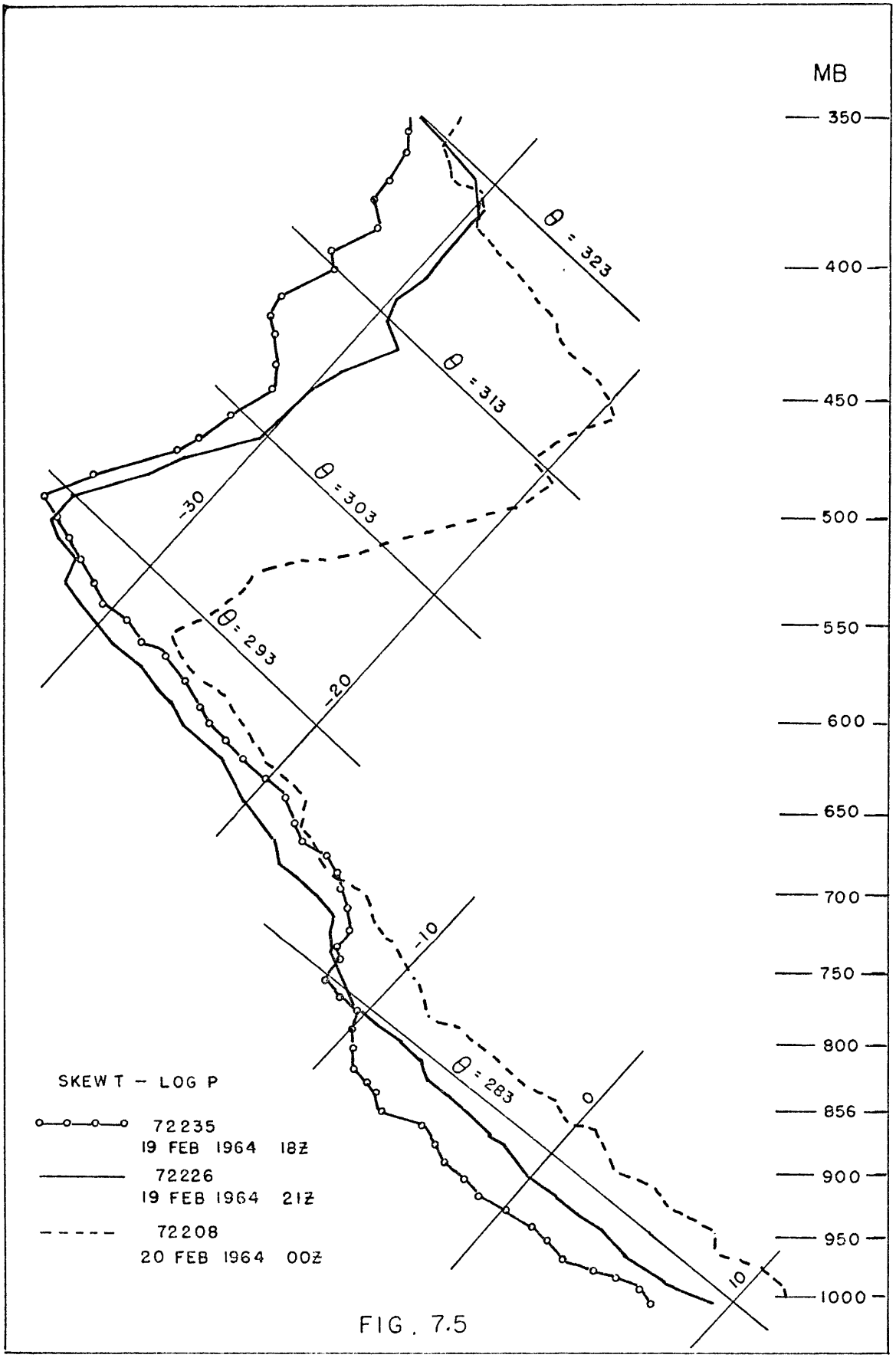
MB
350
400
450
500
550
600
650
700
750
800
856
900
950
1000
θ = 323
θ = 313
θ = 303
θ = 293
θ = 283
-30
-20
-10
0
10
SKEW T – LOG P
72235
19 FEB 1964 18Z
72226
19 FEB 1964 21Z
72208
20 FEB 1964 00Z

FIG. 7.5

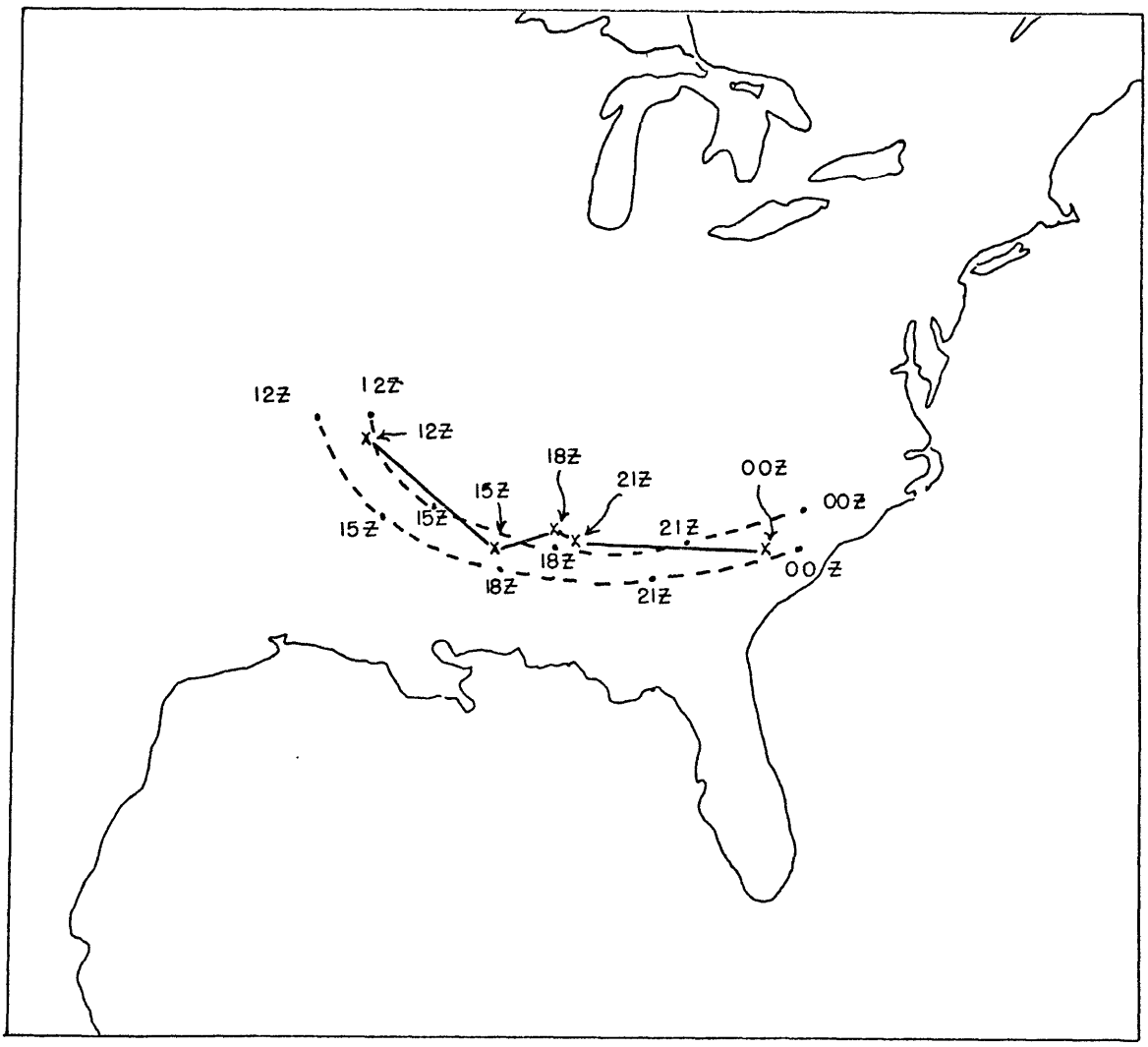

$\theta = 303$

• = TRAJECTORY POSITION EVERY 3 HOURS

x = POTENTIAL VORTICITY MAXIMUM POSITION EVERY 3 HOURS

FIG. 7.6

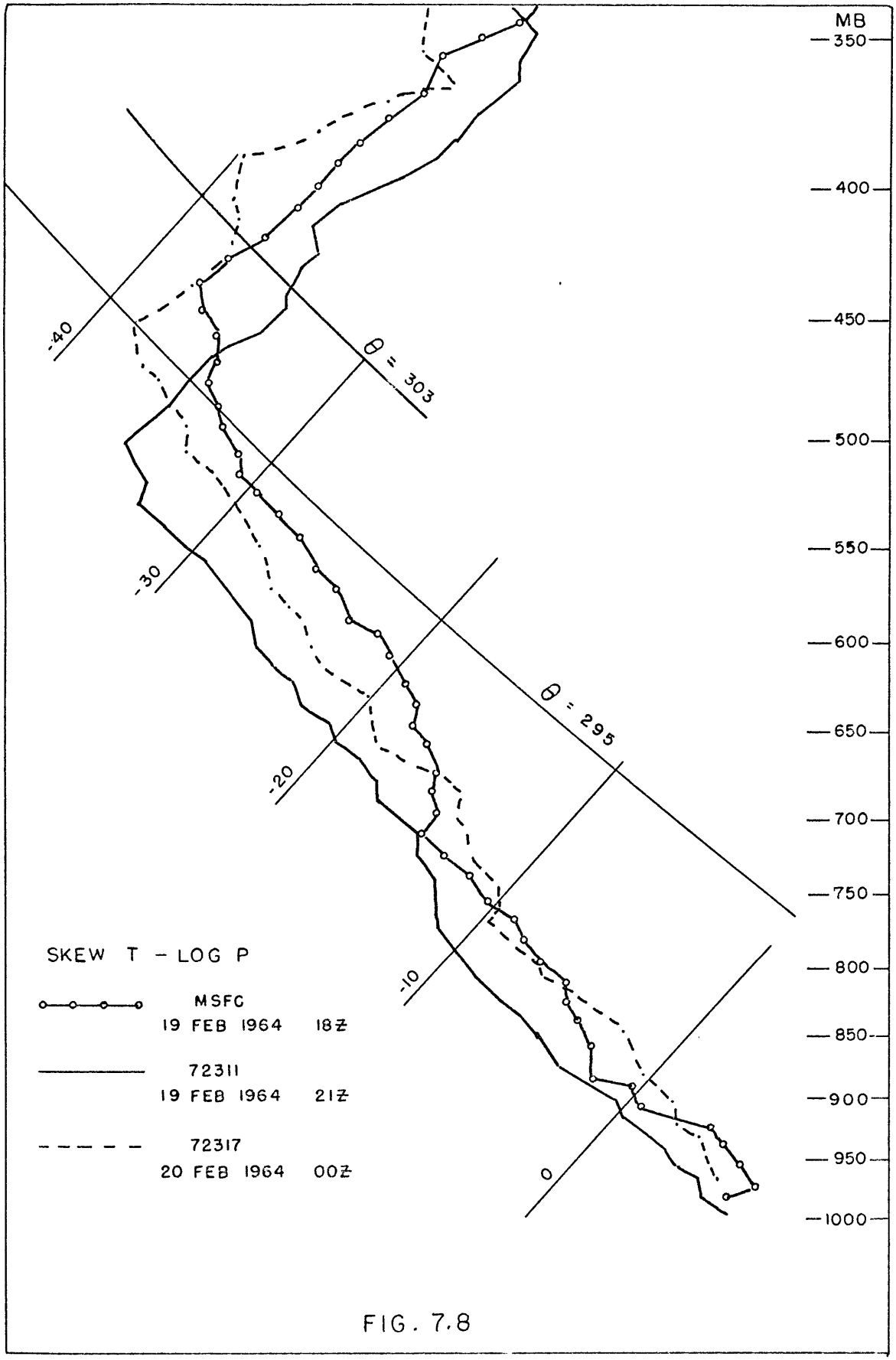
MB
350
400
450
500
550
600
650
700
750
800
850
900
950
1000
-40
-30
-20
-10
0
θ = 303
θ = 295
SKEW T - LOG P
MSFC
19 FEB 1964 18Z
72311
19 FEB 1964 21Z
72317
20 FEB 1964 00Z

FIG. 7.8

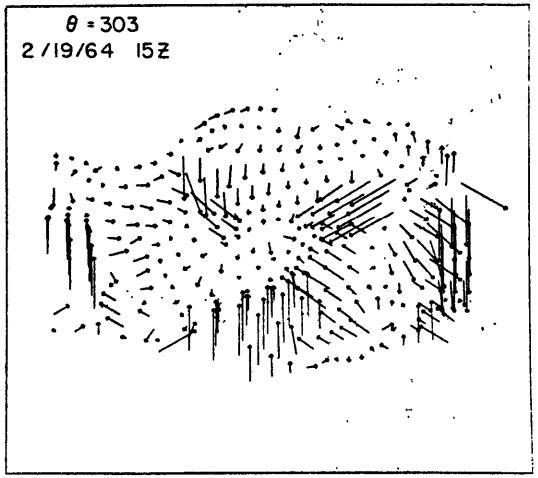

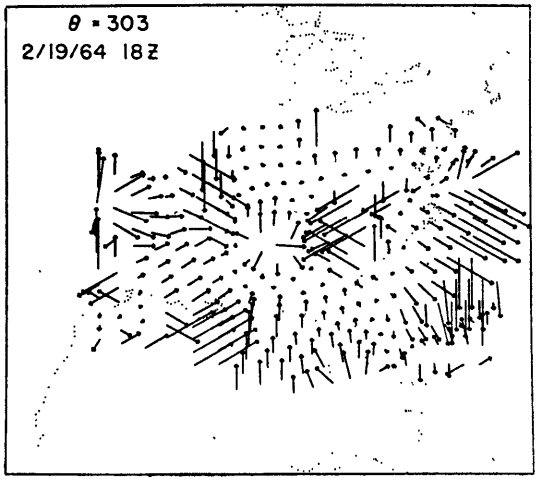

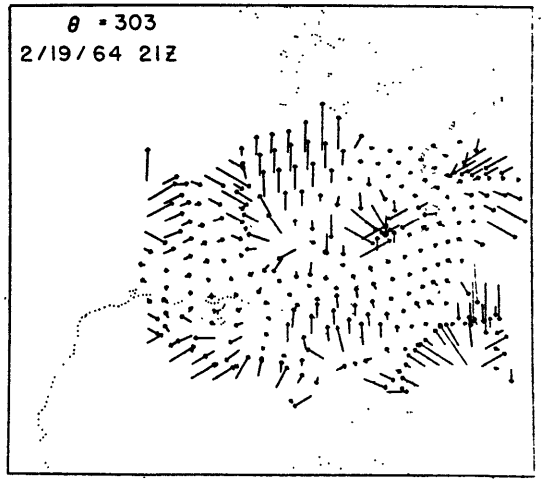

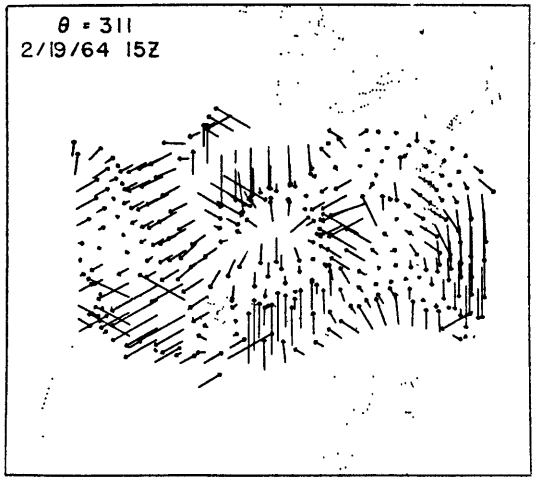

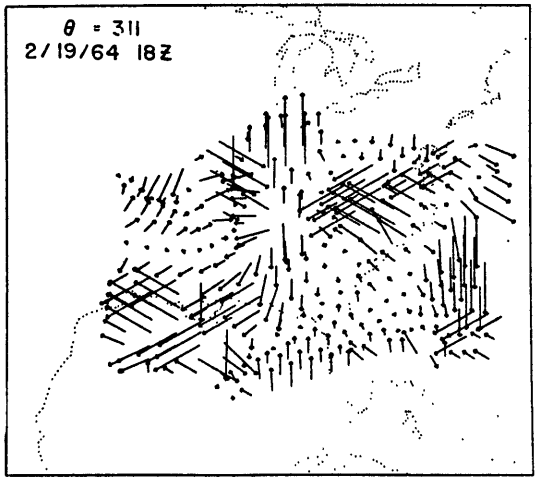

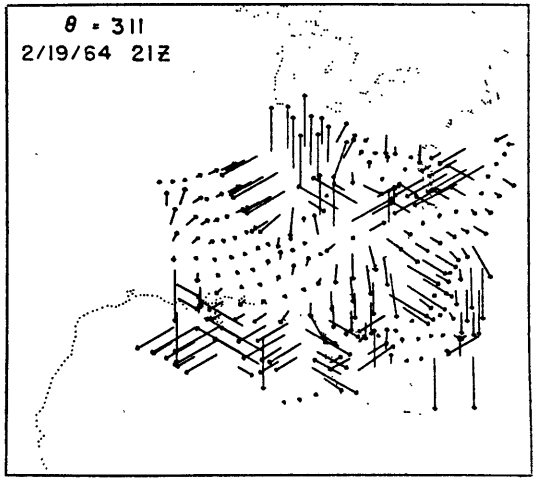

FIG. 7.9

POTENTIAL VORTICITY DEVIATION VECTORS

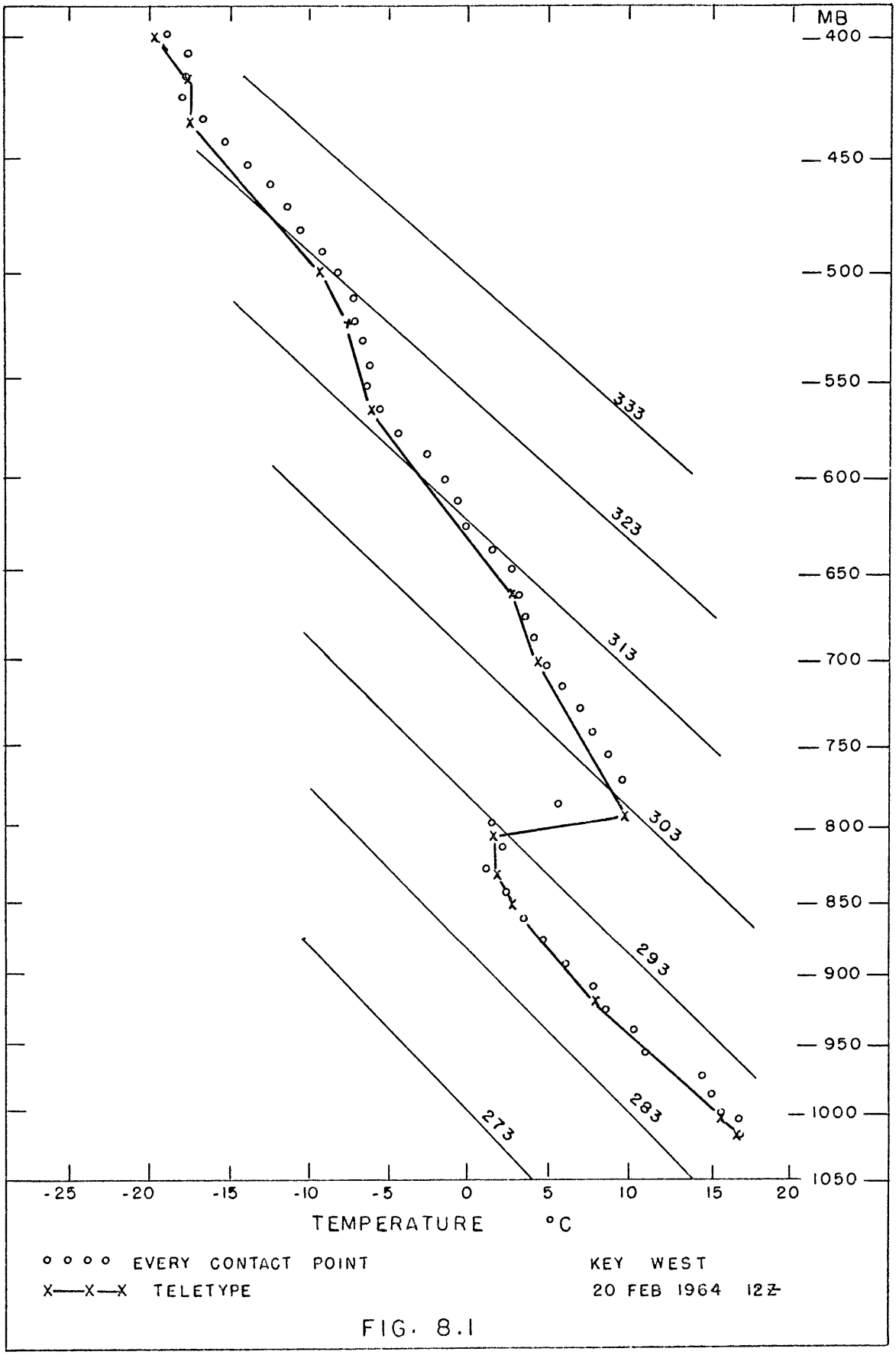
MB
400
450
500
550
600
650
700
750
800
850
900
950
1000
1050
333
323
313
303
293
283
273
-25
-20
-15
-10
-5
0
5
10
15
20
TEMPERATURE °C
o o o o EVERY CONTACT POINT
X—X—X TELETYPE
KEY WEST
20 FEB 1964 12Z

FIG. 8.1

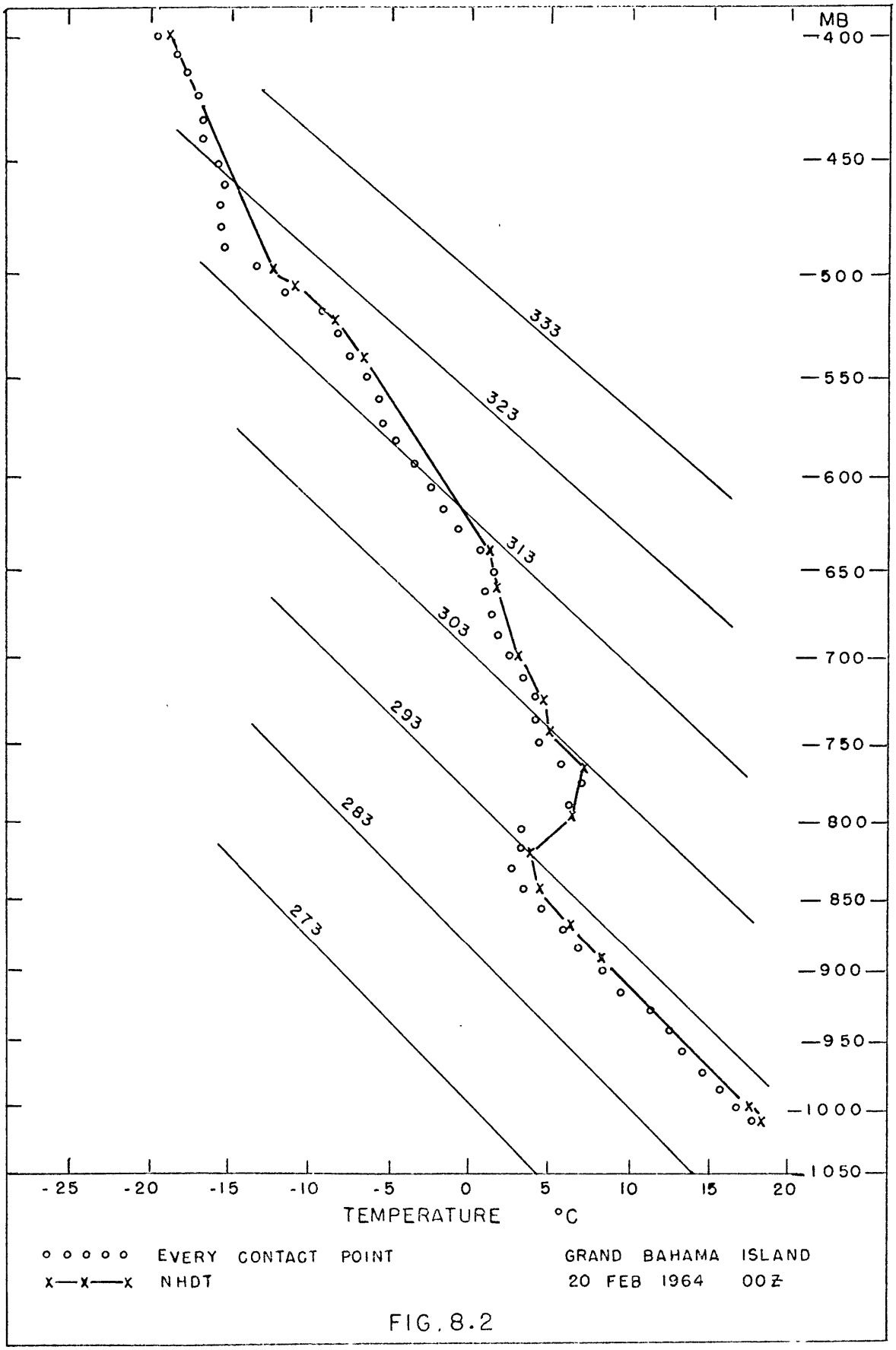
MB
400
450
500
550
600
650
700
750
800
850
900
950
1000
1050
333
323
313
303
293
283
273
-25
-20
-15
-10
-5
0
5
10
15
20
TEMPERATURE °C
o o o o o EVERY CONTACT POINT
x—x—x NHDT
GRAND BAHAMA ISLAND
20 FEB 1964 00Z

FIG. 8.2

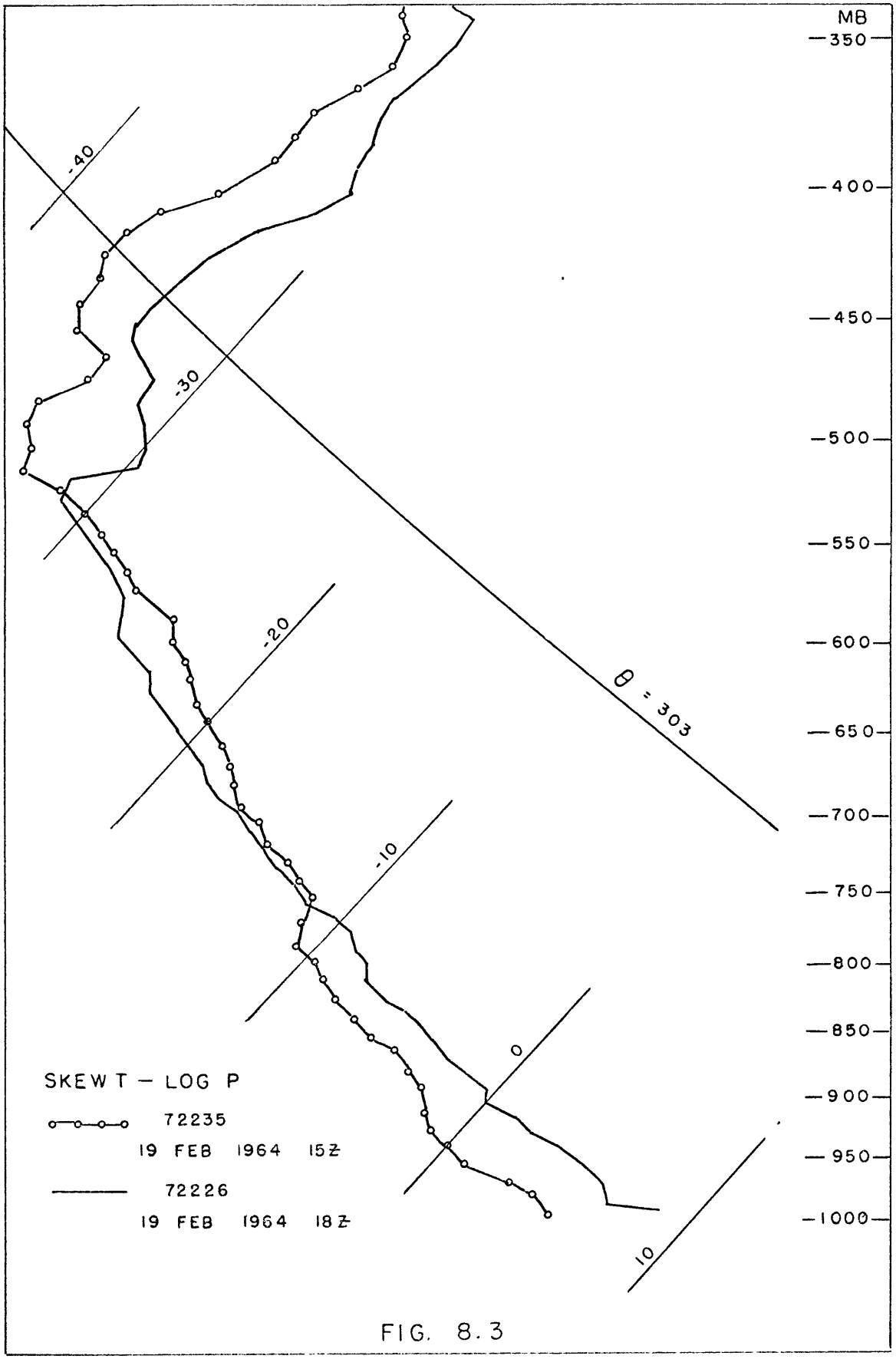
MB
350
400
450
500
550
600
650
700
750
800
850
900
950
1000
-40
-30
-20
-10
0
10
θ = 303
SKEW T – LOG P
72235
19 FEB 1964 15Z
72226
19 FEB 1964 18Z

FIG. 8.3

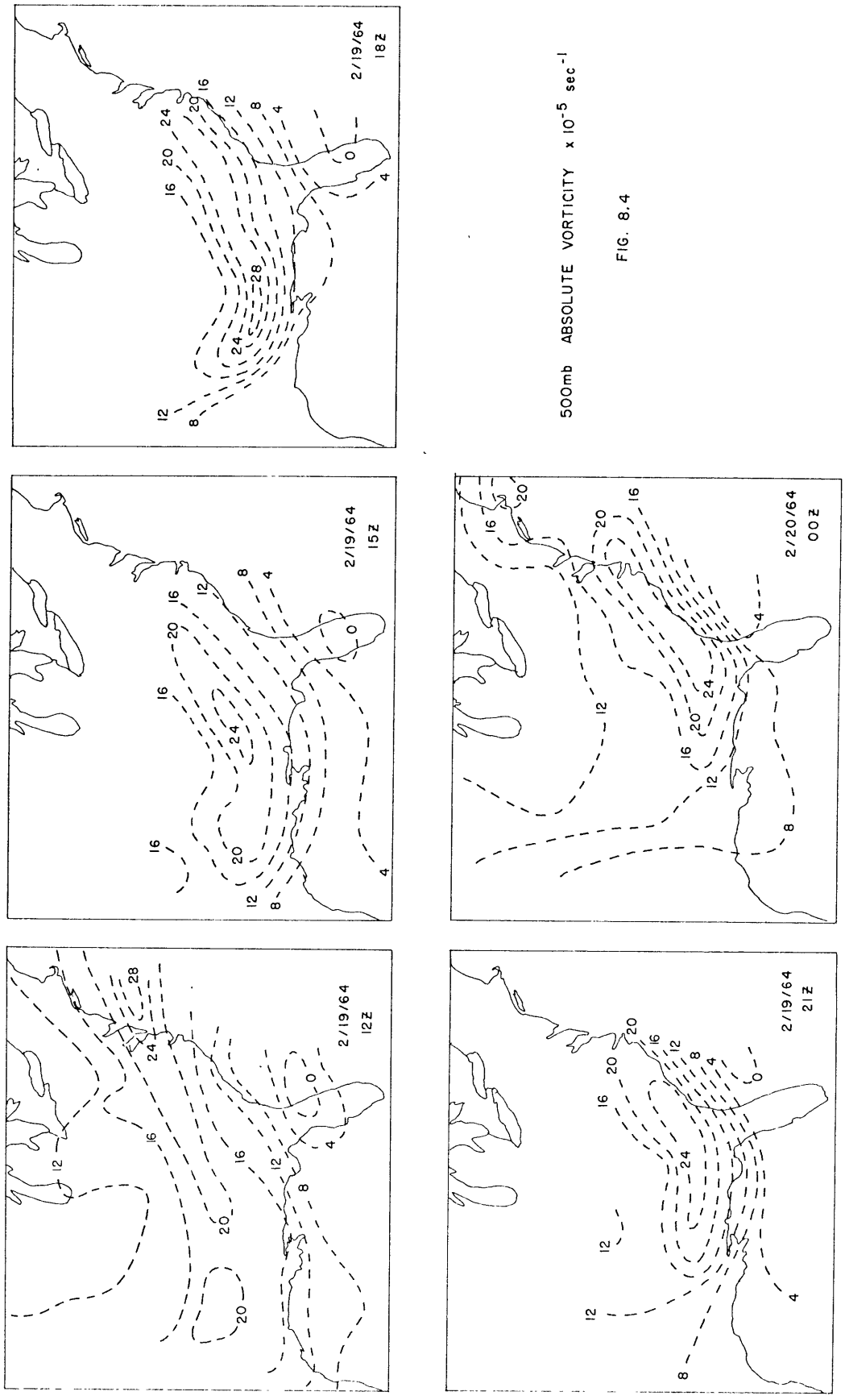

500mb ABSOLUTE VORTICITY $\times 10^{-5}$ sec^{-1}

FIG. 8.4

TRANSVERSE MOTION IN AN IDEALIZED FRONTAL ZONE WHERE $\partial v/\partial y = 0$, $\partial v/\partial p > 0$
(AFTER ELIASSEN (1962))

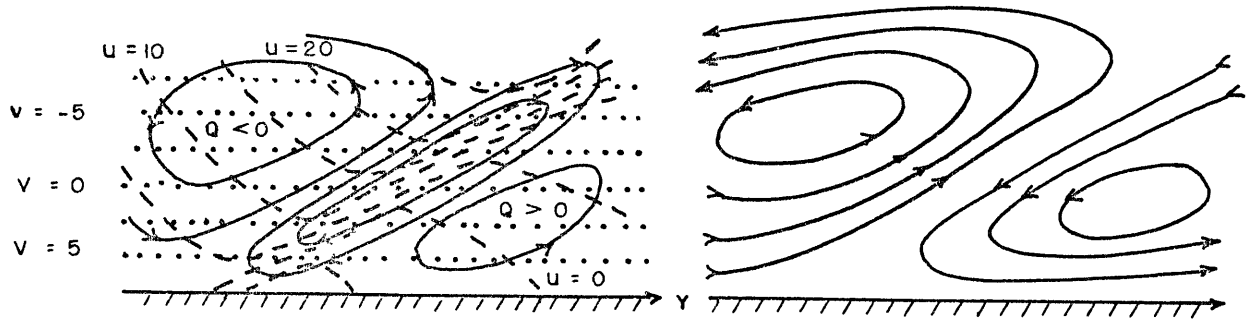

A) U , V ARE GEOSTROPHIC
DASHED: U (M SEC^{-1})
DOTTED: V (M SEC^{-1})
SOLID : STREAMLINES OF TRANSVERSE NON GEOSTROPHIC CIRCULATION

B) STREAMLINES OF TOTAL (GEOSTROPHIC AND NON GEOSTROPHIC) TRANSVERSE MOTION , RELATIVE TO THE MOTION OF THE FRONT.

FIG. 8.5

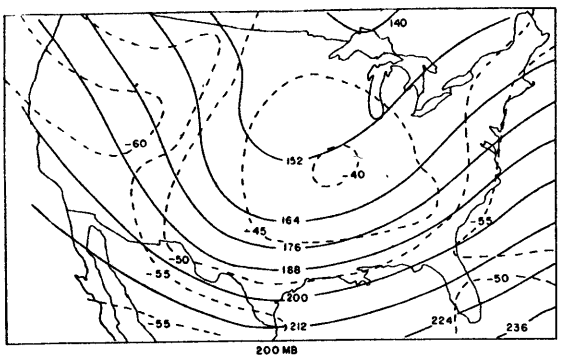

200MB
19 FEB 1964 00Z

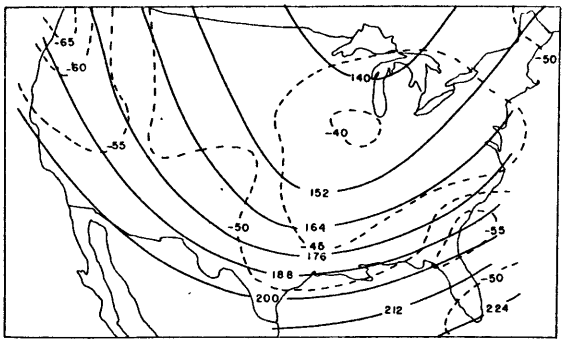

200MB
19 FEB 1964 12Z

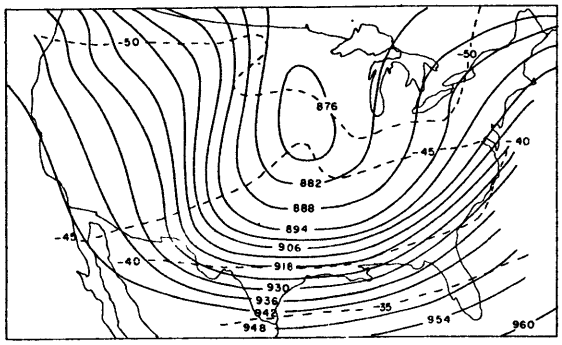

300MB
19 FEB 1964 00Z

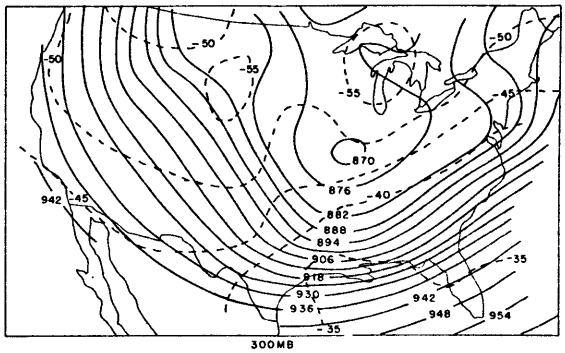

300MB
19 FEB 1964 12Z

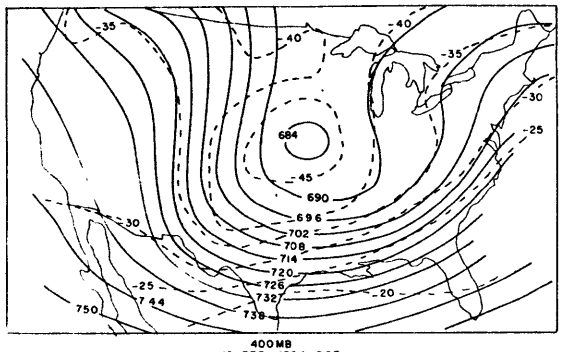

400MB
19 FEB 1964 00Z

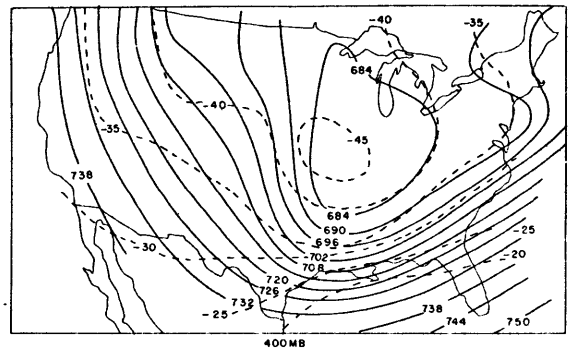

400MB
19 FEB 1964 12Z

HEIGHT CONTOURS AND TEMPERATURE ON 200MB, 300MB AND 400MB, 19 FEB 1964 00Z AND 12Z

—— HEIGHT CONTOURS IN DECAMETERS (Except at 200mb)

– – – TEMPERATURE °C

FIG 86

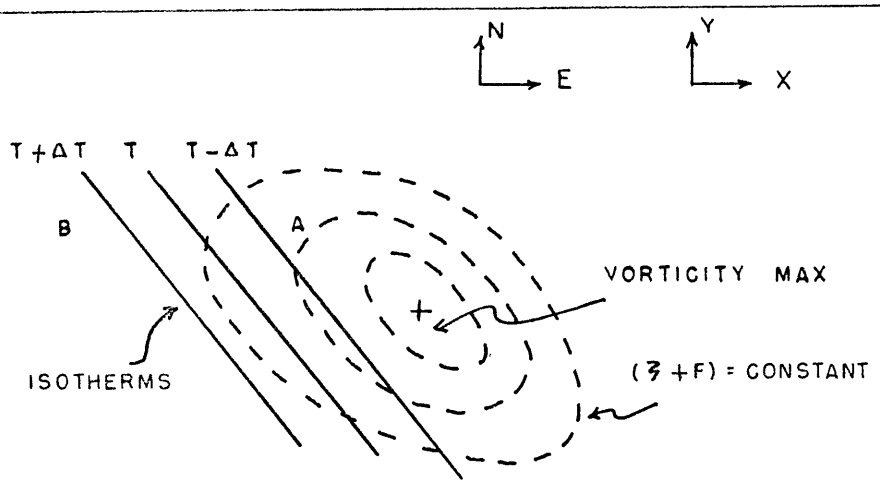

FIG. 8.7a

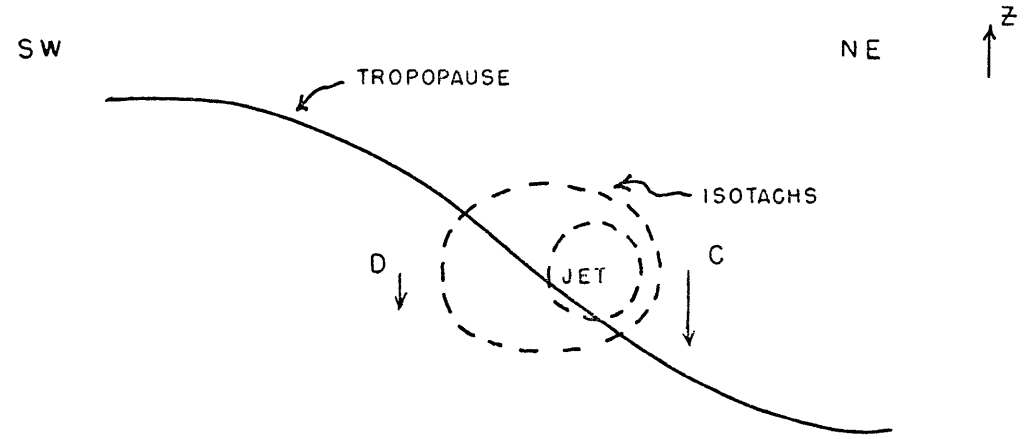

FIG. 8.7b

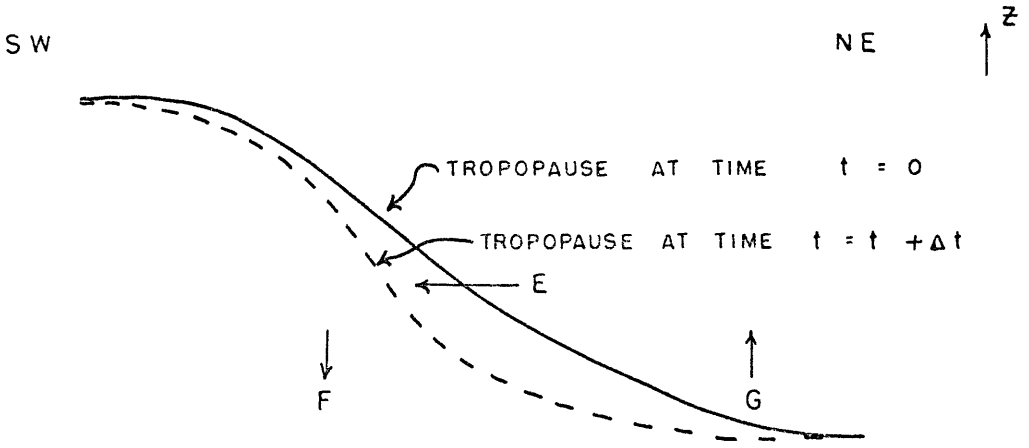

FIG. 8.7c

SCHEMATIC: TROPOPAUSE STEEPENING DUE TO PASSAGE OF SHEAR VORTICITY MAXIMUM IN NW FLOW ALOFT

TRANSVERSE MOTION IN AN IDEALIZED MID-TROPOSPHERIC BAROCLINIC ZONE CASE WHERE $\partial v / \partial y = 0$, $\partial v / \partial p < 0$

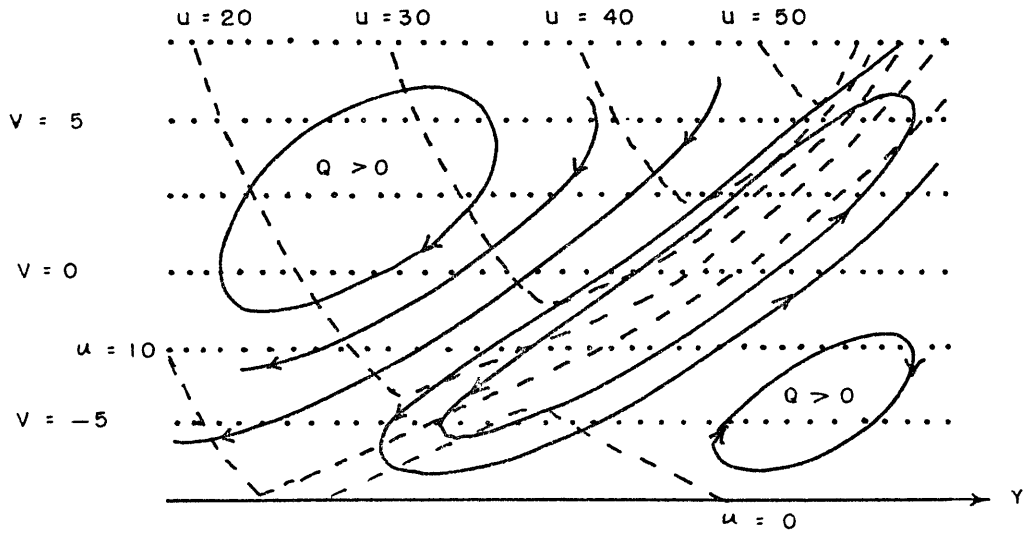

DASHED : u (M SEC^{-1}) } GEOSTROPHIC
DOTTED : V (M SEC^{-1}) }
SOLID : STREAMLINES OF TRANSVERSE NON GEOSTROPHIC CIRCULATION

FIG. 8.8

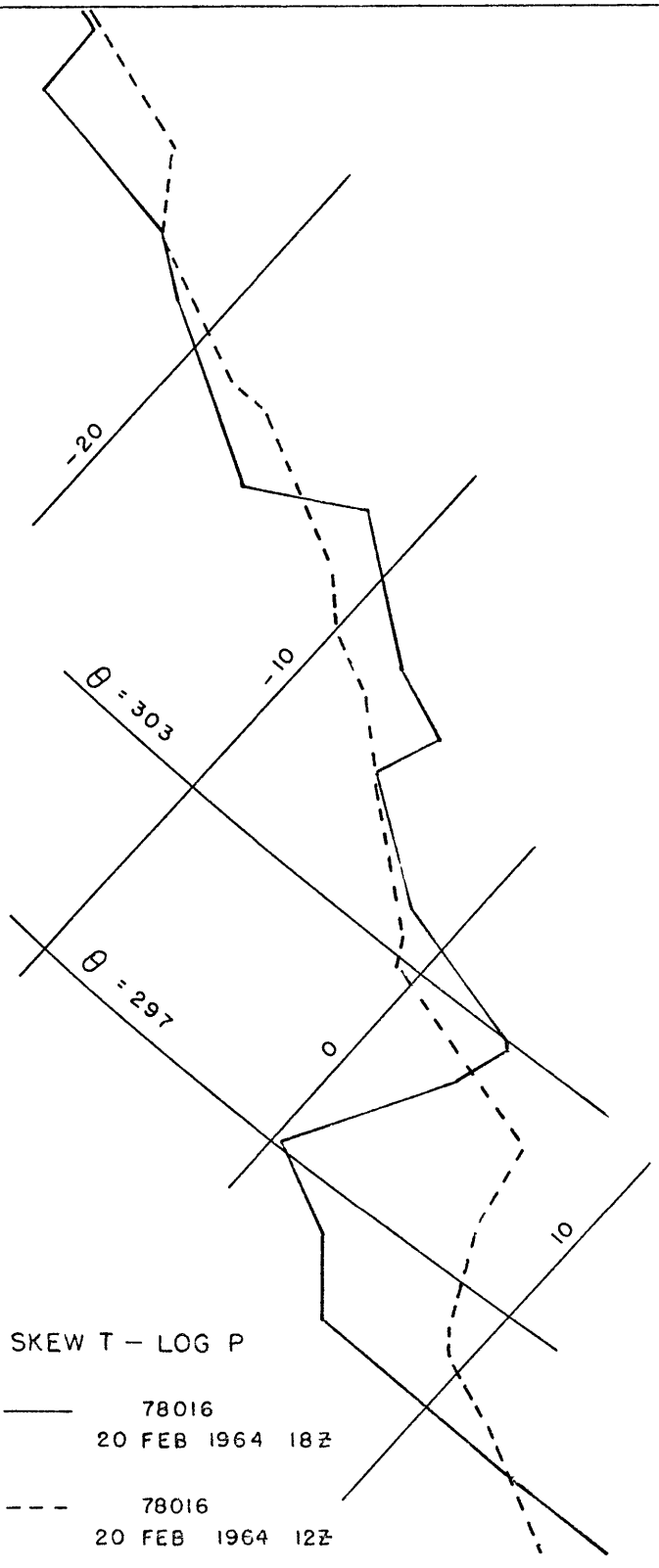

12Z %RH	18Z %RH	MB
		MB
	20	
MB		
MB		
	40	400
	35	
MB		
	33	450
	30	
	60	
MB	46	500
MB		
	10	
MB	MB	550
	MB	
	MB	
MB	MB	600
	MB	
MB	MB	650
80		
85	MB	700
	MB	
	10	
86	53	750
86	55	800
85	60	850
83		
84	56	900
73	51	950
65	48	1000

78016

FIG. 8.9

REFERENCES

Adler, R. F., 1967: A derivation and case study of the theorem of average potential vorticity. S.M. Thesis, Penn. State U., Dept. of Meteor., 45 pp.

Bjerknes, J., 1919: On the structure of moving cyclones. Geofys. Publ., Vol. 1, No. 2.

Bjerknes, J., 1932: Exploration des perturbations atmosphériques à l'aide de sondages rapprochés dans le temps. Geofys. Publ., Vol. 9, No. 9.

Bjerknes, J., and E. Palmén, 1937: Investigations of selected European cyclones by means of serial ascents. Geofys. Publ., Vol. 12, No. 2.

Bleck, R., 1965: Lineare Approximationsmethoden zur Bestimmung ein-und zweidimensionaler numerischer Filter des dynamischen Meteorologie, Institut für Theoretische Meteorologie der Freien Universität Berlin.

Bleck, R., 1968: A numerical technique for calculating dry- and moist-adiabatic trajectories in the atmosphere. Ph.D. Thesis, Penn. State U., Dept. of Meteor., 102 pp.

Briggs, J., and W. T. Roach, 1963: Aircraft observations near jet streams. Quart. J. R. Met. Soc., Vol. 98, No. 380, 225-247.

Campana, K. A., 1967: Frontal structure and the dynamics of frontogenesis, Appendix 6, F. Sanders principal investigator, M.I.T., Dept. of Meteor., GP-1508.

Cressman, G. P., 1959: An operational objective analysis system. Mon. Wea. Rev., Vol. 87, No. 10, 367-374.

Danielsen, E. F., 1959: The laminar structure of the atmosphere and its relation to the concept of a tropopause. Arch. Met. Geoph. Biolk., Ser. A, Band II, 3 Heft, 294-332.

Danielsen, E. F., 1961: Trajectories: isobaric, isentropic and actual. J. Met., Vol. 18, No. 4, 479-486.

Danielsen, E. F., 1964: Project Springfield report. Headquarters, Defense Atomic Support Agency, Wash., D. C., 97 pp.

Danielsen, E. F., 1966a: Research in four-dimensional diagnosis of cyclonic storm cloud systems. Scientific report No. 1, Contract No. AF19(628)-4762, Penn. State U., 53 pp.

Danielsen, E. F., 1966b: Research in four-dimensional diagnosis of cyclonic storm cloud systems. Scientific report No. 2, Contract No. AF19(628)-4762, Penn. State U., 52 pp.

Danielsen, E. F., 1967: Transport and diffusion of stratospheric radioactivity based on synoptic hemispheric analyses of potential vorticity. NYO-3317-1, Penn. State U., 91 pp.

Danielsen, E. F., 1968: Stratospheric-tropospheric exchange based on radioactivity, ozone and potential vorticity. J. Atmos. Sci., Vol. 25, No. 3, 502-518.

Danielsen, E. F., and J. Diercks, 1967: A study of the tropopause based on numerical integration of the potential vorticity equation. NYO-3317-1, Penn. State U., 43 pp.

Danielsen, E. F., and R. T. Duquet, 1967: A comparison of FPS-16 and GMD-1 measurements and methods for processing wind data. J. Appl. Met., Vol. 6, No. 5, 824-836.

de Jong, H. M., 1958: Errors in upper-level wind computations. J. Met., Vol. 15, No. 2, 131-137.

Duquet, R. T., 1964: Data processing for isentropic analyses. Tech. rep. No. 1, Contract AF(30-1)-3317, Penn. State U., 18 pp.

Eddy, A., 1967a: Two-dimensional statistical objective analysis of isotropic scalar data fields. U. of Texas Atmos. Sci. Group, Publ. No. 5, 100 pp.

Eddy, A., 1967b: The statistical objective analysis of scalar data fields. J. Appl. Met., Vol. 6, No. 4, 597-609.

Eliassen, A., 1962: On the vertical circulation in frontal zones. Geofys. Publ., Vol. 24, 147-160.

Ertel, H., 1942: Ein Neuer Hydrodynamic Wirbelsatz. Meteorologische Zeitung, Vol. 79, 227-282.

Hering, W. S., and T. R. Borden, 1964: Ozonesonde observations over North America, Vol. 3, AFCRL-64-30(II), 280 pp.

Hering, W. S., 1966: Ozone and atmospheric transport processes. Tellus, Vol. 18, No. 3, 329-336.

History and catalogue of upper air data for the period 1946-1960, 1963: Key to Meteorological Records Documentation, No. 5.21, 352 pp.

Kidson, J. W., 1968: The general circulation of the tropics. Ph.D. Thesis, M.I.T., Dept. of Meteor., 205 pp.

Kidson, J. W., D. G. Vincent and R. E. Newell, 1969: Observational studies of the general circulation of the tropics, I. 'Long term mean values.' Quart. J. R. Met. Soc., Vol. 95, No. 404, to be published.

Kousky, V. E., 1967: A case study of frontogenetic and frontolytic processes. S. M. Thesis, Penn. State U., 32 pp.

Krishnamurti, T. N., 1961a: The subtropical jet stream of winter. J. Met., Vol. 18, No. 2, 172-191.

Krishnamurti, T. N., 1961b: On the role of the subtropical jet stream of winter in the atmospheric general circulation. J. Met., Vol. 18, No. 5, 657-670.

Miller, J. E., 1948: On the concept of frontogenesis. J. Met., Vol. 5, No. 4, 169-171.

Namias, J., and P. Clapp, 1949: Confluence theory of the high tropospheric jet stream. J. Met., Vol. 6, No. 2, 330-336.

Newell, R. E., 1965: A review of studies of eddy fluxes in the stratosphere and mesosphere. Report No. 12, Planetary Circulations Project, M.I.T. Dept. of Meteor., MIT-2241-3.

Newell, R. E., J. R. Mahoney and R. W. Lenhard, Jr., 1966: A pilot study of small-scale wind variations in the stratosphere and mesosphere. Quart. J. R. Met. Soc., Vol. 92, No. 391, 41-53.

Newton, C. W., 1954: Frontogenesis and frontolysis as a three-dimensional process. J. Met., Vol. 11, No. 6, 449-461.

Paine, D. A., 1966: Decreases of potential vorticity and radioactivity produced by mixing across the lower boundary of a stratospheric extrusion. S.M. Thesis, Penn. State U., 33 pp.

Palmén, E., 1933: Aerologische Untersuchungen der Atmosphärischen Störungen. Commentationes Physico-Mathematicae, Soc. Scient. Fennica, Vol. 7, No. 6.

Petterssen, S., 1950: Some aspects of the general circulation of the atmosphere. Roy. Met. Soc. Centenary Proceedings, 120-155.

Poppe, H. M., 1964: A study of the ageostrophic transverse motions in frontal zones. M. S. Thesis, M.I.T., Dept. of Meteor., 117 pp.

Priestley, C. H. B., 1967: On the importance of variability in the planetary boundary layer. Appendix VI, Report of the study conference held at Stockholm, 28 June -- July 1967. The Global Atmospheric Research Program. WMO-ICSU/IUGG.

Reed, R., 1955: A study of a characteristic type of upper-level frontogenesis. J. Met., Vol. 12, No. 3, 226-237.

Reed, R., and E. F. Danielsen, 1959: Fronts in the vicinity of the tropopause. Arch. Met. Geoph. Biokl. Ser. A, Band II, 1 Heft, 1-17.

Reed, R., and F. Sanders, 1953: An investigation of the development of a mid-tropospheric frontal zone and its associated vorticity field. J. Met., Vol. 10, No. 5, 338-350.

Sanders, F., 1954: An investigation of atmospheric frontal zones. Ph.D. Thesis. M.I.T., Dept. of Meteor., 90 pp.

Sanders, F., 1967: Frontal structure and the dynamics of frontogenesis, GP-1508, M.I.T., Dept. of Meteor.

Sawyer, J. S., 1956: The vertical circulation at meteorological fronts and its relation to frontogenesis. Proc. Roy. Soc., A, Vol. 234, 346-362.

Staley, D. O., 1960: Evaluation of potential vorticity changes near the tropopause and the related vertical motions, vertical advection of vorticity, and transfer of radioactive debris from stratosphere to troposphere. J. Met., Vol. 17, No. 6, 591-620.

Staley, D. O., 1965: Radiative cooling in the vicinity of inversions and the tropopause. Quart. J. R. Met. Soc., Vol. 91, No. 389, 282-301.

Staley, D. O., and P. M. Kuhn, 1961: Measurements of radiative cooling through two intense baroclinic zones in the middle troposphere. J. Met., Vol. 18, No. 2, 208-215.

Staley, D. O., and G. M. Jurica, 1968: Radiative modification of selected vertical temperature distributions. Quart. J. R. Met. Soc., Vol. 94, No. 401, 310-317.

Stuart, D. W., G. P. Watson and N. E. LaSeur, 1967: Aquisition, reduction and analysis of project AVE data. Final report, Contract No. 8-11146, Florida State U., 83 pp.

Wagner, N. K., 1961: The effect of the time constant of radiosonde sensors on the measurement of temperature and humidity discontinuities in the atmosphere. Bull. Amer. Met. Soc., Vol. 42, No. 5, 317-321.

Willett, H. C., and F. Sanders, 1959: Descriptive Meteorology. Academic Press, 355 pp.

VITA

Lance F. Bosart was born in New York City on August 24, 1942. He attended Mamaroneck High School, Manaroneck, New York and entered M.I.T. in September 1960. He gained his B.Sc. Degree in Aeronautics in 1964 and was awarded the M.Sc. Degree in Meteorology by M.I.T. in 1966. His graduate studies were aided by research and teaching assistantships under the direction of Professors Frederick Sanders, Victor P. Starr and James M. Austin. He was married to Helen J. Haskell on June 28th, 1969.

He is a member of the American Meteorological Society, the Royal Meteorological Society and Sigma Xi.